THE ROLE OF MICROVASCULAR CLEARANCE IN THE PROGRESSION OF OSTEOARTHRITIS

A Dissertation
Presented to
The Academic Faculty

by

Fabrice Christopher Bernard

In Partial Fulfillment
of the Requirements for the degree
Doctor of Philosophy in the
Wallace H. Coulter Department of Biomedical Engineering in the College of Engineering

Georgia Institute of Technology & Emory University
August 2021

THE ROLE OF MICROVASCULAR CLEARANCE IN THE PROGRESSION OF OSTEOARTHRITIS

Approved by:

Dr. J. Brandon Dixon
George W. Woodruff School of Mechanical Engineering
Georgia Institute of Technology

Dr. Susan N. Thomas
George W. Woodruff School of Mechanical Engineering
Georgia Institute of Technology

Dr. Nick J. Willett
Department of Orthopaedics
Emory University

Dr. James E. Dahlman
Wallace H. Coulter Department of Biomedical Engineering
Georgia Institute of Technology

Dr. Andres J. Garcia
George W. Woodruff School of Mechanical Engineering
Georgia Institute of Technology

Dr. Kyle D. Allen
J. Crayton Pruitt Family Department of Biomedical Engineering
University of Florida

Date Approved: April 2021

To my mom, Michaël, who raised me always to do the right thing.

ACKNOWLEDGEMENTS

Fifteen years ago, I could not have imagined that a Ph.D. in Biomedical Engineering from Georgia Tech and Emory University would be my terminal degree. My journey started at NYU, where Dr. Charles Martucci took me into his lab to complete my senior research project. I had no idea what I was doing in hindsight, but Dr. Martucci was so generous and reassuring, so I will always be grateful for his support. Dr. Steven Nicoll at the City College of New York and Dr. Mitch Schaffler was instrumental in laying a foundation for which I built my Ph.D.

I would first like to thank God for giving me the strength and keeping me grounded while I undertook this massive task. There are many people who do not receive enough praise, such as the custodial staff that kept the IBB facilities spotless every day to allow us to work in a clean, efficient place. In addition, the animal facility and vets at the VA and IBB allowed us to do this fantastic animal research. Additionally, I must thank the support staff at the VA and IBB for ensuring that all cylinders were running. Finally, I would like to thank a few people, specifically Michelle Wong, Shannon Sullivan, Kyla Ross, Susan Margulies, and Laura Paige. These people went above and beyond their job description to ensure that I made it through, and I cannot thank them enough for treating me as if I were their family member.

My thesis advisors Nick J. Willett and Brandon Dixon took me on as a student in a new area of research. The project was not well funded initially, but it was well-mentored, and their ability to push me and support me has grown into many unique areas of research to be continued when I am gone. I took just as much of a leap of faith in

joining this new project, and I am pleased with the results. Brandon taught me how to keep thinking about pushing the envelope, while Nick taught me how to focus on the immediate task at hand. Now, there were some tears shed, mainly because I wanted to impress them all the time. I learned that their success was just as incremental as mine. Thanks to you both for continuing to be an excellent example of what consistency and balance look like. I wish tremendous success on both of you as you continue to carve out new research and career paths because you both deserve it.

My thesis committee consisted of unique researchers from the Georgia Tech, Emory, and University of Florida communities. Dr. Andres Garcia was one of the biggest advocates in my Georgia Tech recruitment, recommended me for the biomaterials training grant, and became a very integral part of my project with monthly meetings. I am grateful for his mentorship and technical expertise, attitude towards life, and dedication to making sure my science was airtight. To Dr. Susan Thomas, she has been incredibly supportive from day one. There were times when I did not feel that I was worthy of this opportunity, but Susan continued to celebrate my intelligence and ideas. To Dr. James Dahlman, I feel as though we started here together. It has been exceptional to watch you become incredibly successful. You have contributed so much to my perspective of what a healthy relationship with work and balance was, and you continue to remind me that life is not a sprint, but it is a marathon. Finally, to Dr. Kyle Allen, as someone who did not interact with me daily like the rest of my committee members, I still felt your presence as you are an expert in OA, and your commitment to excellence and sharing knowledge allows us to all make strides in OA. Thank you for being resourceful and allowing me to pick your brain when needed.

To my Dixon labmates (Anish, Iris, Josh, Matt, Mohammad, Ria, Yarelis, Young Jae, Tyler, Yanina, Lauren, Alexandra, Swetha, and Zhanna), the number of laughs and tears that we have shared (more laughs than tears) has made this experience more than bearable. To my Willett lab mates (Jarred, Thanh, Jay, Julia, Toma, Natasja, Brett, Marissa, Shannon, Hyunhee, Travis, Ananthu). Thank you for struggling with me, always being critical of the science, and finding time to kick back and just be like a lab family. Being in two labs was difficult at times, which sometimes double meetings and double responsibilities. However, the people made it worth every second.

It is amazing how at every stage of life, I have found amazing people. I met Jason Denis, Michael Colavito, and John Barraco (Twin, Chewy, and B-Rocks) in high school, who became a pretty good support system when they were not forcing me to play video games with them. At that same time, I met Marvin LaRoche and Bibin Thomas, who continue to be my life-long friends who have become like brothers. While in college, I met Rahul Anthony in class and James Scott and Andre Grier while engaging in my second passion, music. During my extension of education and simultaneous hiatus from music, these people have become family. I am excited to be moving back to New York, where those roots began.

While in Atlanta, I have met some truly exceptional people, some of whom have become my terrific friends. Bailey, we clicked from day one, and I'm so happy I got to see you grow into an excellent scientist and now wife. Simone and Arman Green, you had my back every step of the way, and I am still trying to be half the academics you are. The McKinneys, Jay and Allyson, thank you for inviting us into your home and being so supportive for us. The black girl magic crew, I'm so thankful for sometimes being an

honorary member and finding ways to crush racial injustice and inequity at the collegiate level. The 5:30 am lifting crew, Nico, Jay, and Matt, thank you for staving on my 60-pound weight gain for two years. To the BEAM crew, thank you for helping to create a support system for people like me in this BME program, and thank you for showing up when no one else did. Lastly, thank you to Neil Breen's Dream Team (Matt, David, Thomas) for teaching me how to make the most of a terrible situation and how to see the beauty in all things.

Leah Elizabeth Anderson, you have been a remarkable person by my side through this whole process, and I know for a fact that I would have struggled through this process even more if it were not for your strength, support, and love. I want to travel the world and life with you and be by your side as you finish your journey. To Leah's parents, Ada and Daryl Anderson, you not only invited me into your home but treated me as a son, and for that, I will eternally be grateful.

My mother, Michael Vallery, you have given me a lifetime of support, courage, strength, resilience, prayer, food, headaches, love, and purpose. I have made some decisions in my life to try to find a way to financially repay you for the things that you have done for me, but the older I get, the more I realize that there is no price tag on being an exceptional mother. The only way I can ever repay you is by being an exceptional son (I'm working on it). To my dad Joseph Francois Bernard, my transition through adulthood has brought on its fair share of challenges. I am very thankful for the opportunity to tackle adulthood with you by my side and to find ways to celebrate life with you even if an ocean divides us. To my sister and brothers Jenny, Reginald, and Bryan, I am so proud of the work you have accomplished so far and the work we have yet to do.

Last but not least, to my Mamia and Papia (grandparents). My grandfather Stevens Bernard passed in Haiti while I was finishing this document. I know he is super proud and continues to live on through stories and my grandma. I regret not having the time or money to say goodbye adequately or to visit, but I will ensure that part of your legacy lives on through me here in America.

TABLE OF CONTENTS

LIST OF FIGURES

LIST OF SYMBOLS AND ABBREVIATIONS

ACL	Anterior Cruciate Ligament
BECs	Blood Endothelial Cells
ECM	Extracellular Matrix
ET-1	Endothelin-1
FGF	Fibroblast Growth Factor
FOXC2	Forkhead box protein C2
GAGs	Glycosaminoglycans
HA	Hyaluronic Acid
IA	Intra-articular
IAP	Intra-articular Pressure
ICG	Indocyanine Green
IL-1B	Interleukin 1 Beta
LECs	Lymphatic Endothelial Cells
LMCs	Lymphatic Muscle Cells
LV	Lymphatic Vessel
LYVE-1	Lymphatic vessel endothelial hyaluronan receptor 1 (LYVE1)
MCL	Medial Collateral Ligament
MMPs	Matrix Metalloproteinases
MMT	Medial Menscial Transection
NIR	Near Infrared
OA	Osteoarthritis
OASF	Osteoarthritic Synovial Fluid
PEG	Polyethylene Glycol
PRG4 or Lubricin	Proteoglycan-4
PROX-1	Prospero Homeobox Protein 1
PRP	Platelet-rich plasma
PTOA	Post-Traumatic OA
QOL	Quality of Life
RA	Rheumatoid Arthritis
RFLV	Rat Femoral Lymphatic Vessel
SAPLs	Surface Active Phospholipids
SF	Synovial Fluid
SMC	Smooth Muscle Cell
TGFB	Transforming Growth Factor beta
TNFa	Tumor Necrosis Factor Alpha
VEGF-A	Vascular Endothelial Growth Factor A
VEGF-C	Vascular Endothelial Growth Factor C
VEGFR2	Vascular Endothelial Growth Factor Receptor 2
VEGFR3	Vascular Endothelial Growth Factor Receptor 3

SUMMARY

Osteoarthritis (OA) is the most common disease of the knee. OA is characterized by damage to the articular cartilage, underlying bone, and chronic inflammation of the joint tissues, leading to the progressive loss of joint function, increased disability, and reduced quality of life. In OA, the role of chronic low-grade inflammation has been implicated in disease progression. In wound healing, lymphangiogenesis, or the formation of new lymphatic vessels, is central to inflammation resolution. However, in the osteoarthritic synovium, lymphatic vessel density is decreased in later stages of OA, and changes in the microcirculatory environment may be responsible for joint dysfunction. Blood vessels and lymphatic vessels (the microvasculature) play a critical role in tissue maintenance and may impact OA development and treatment strategies. Therefore, our main objective was to understand joint clearance mechanisms under normal and diseased conditions. This thesis's long-term goal was to establish biomolecular engineering strategies to assess microvascular function in normal and OA joints and assess *ex vivo* lymphatic function using lymphatic tissue culture devices.

In Aim 1, we used near-infrared (NIR) imaging techniques to non-invasively evaluate venous and lymphatic drainage in the naïve knee joint in vivo. We then perturbed joint homeostasis using exercise or endothelin-1(ET-1), a cytokine elevated in human OA with strong vascular tonic activity and investigated the effects on microvascular function and clearance mechanisms. In Aim 2, we used these techniques to determine how microvascular clearance changes during OA progression in a post-traumatic OA model in the rat. Finally, in Aim 3, we used two *ex vivo* systems to study

two aspects of lymphatic physiology. In the first application, we used a lymphatic pressurization device to study the effect of post-traumatic and simulated OA microenvironment on femoral lymphatic contractility. In the second application, we used an *ex* vivo polyethylene glycol (PEG) hydrogel culture platform to investigate mature collecting vessel collateralization 1) in a simulated OA environment and 2) in an inducible knockout of epsins 1, 2, which regulate receptor internalization in lymphangiogenesis.

Collectively, we found that exercise or ET-1 can alter joint clearance and that OA induction in the rat has differential effects on venous and lymphatic clearance. Additionally, we found that treatment with human OA synovial fluid reduces lymphatic collecting vessel function and collecting vessel growth *ex vivo* and that epsin deletion decreases lymphatic collecting vessel sprouting. Thus, these studies increased the fundamental knowledge about the role of the microvasculature, specifically lymphatics, in normal and diseased joint function and provided some *ex vivo* context on how dysfunction may persist *in vivo*.

CHAPTER 1. INTRODUCTION

1.1 Motivation

Osteoarthritis (OA) is the most common disease of the joints. It is characterized by damage to the articular cartilage, underlying bone, and chronic inflammation of the joint tissues, leading to the progressive loss of joint function, increased disability, and reduced quality of life[1,2]. OA's current standard of treatment is rehabilitation and exercise to maintain joint mobility, palliative treatment to manage pain, or in severe cases, joint replacement surgery for late-stage disease[3]. In OA, the role of chronic low-grade inflammation has been implicated disease progression. In wound healing, lymphangiogenesis, the formation of new lymphatic vessels, is central to inflammation resolution[4,5]. However, in the osteoarthritic synovium, lymphatic vessel density decreases, which may be involved in the observed reduction in fluid and macromolecule clearance from the joint and sustained inflammation[6]. Thus, blood vessels and lymphatics play a critical role in joint maintenance and could potentially affect OA development, progression, therapies, and rehabilitation[7–9]; therefore, it is necessary to understand clearance mechanisms under normal and diseased conditions.

The long-term goal of this work is to establish bioengineering strategies to assess and modulate microvascular function in the context of OA. The objective of this thesis was to determine the role of microvascular function in OA progression. The central hypothesis was that microvascular (lymphatic and venous) clearance, central to the resolution of inflammation, is reduced in later stages of OA. In this thesis, we established

techniques to measure tracer clearance in rat knee joints using near-infrared imaging (NIR), quantitatively assessed microvascular clearance in a clinically relevant rat model of OA, studied lymphatic contractility *ex vivo*, and utilized a polymer-based biomaterial scaffold to study lymphangiogenesis *ex vivo*. Using these techniques, we furthered our understanding of the potential role of microvascular function in osteoarthritis progression.

Specific Aims

1.1.1 Specific Aim 1: Quantify microvascular clearance in naïve rat joints

The primary objective of this aim was to assess microvascular clearance in the joint. Size is a significant determinant of how materials clear interstitial spaces *in vivo*; therefore, we validated that we could engineer NIR tracers to target venous uptake with a small 1-2 kDa NIR dye and lymphatic uptake with a 40 kDa polyethylene glycol (PEG) conjugated NIR dye and utilized the size-dependent nature of venous and lymphatic uptake. We then utilized this approach to assess the effects of endothelin 1 (ET-1), a vasoactive compound chronically elevated in OA, on joint clearance. Lastly, we further assessed the role of exercise in joint clearance. We hypothesized that ET-1 would significantly reduce lymphatic clearance. Additionally, we hypothesized that venous and lymphatic clearance would increase with exercise.

1.1.2 Specific Aim 2: Determine the effect of OA on microvascular function

A growing body of literature has implicated lymphatic dysfunction in OA[6,10–14] and the positive effect of exercise on patient outcomes[15–18]. However, no groups have directly investigated: 1) venous and lymphatic drainage simultaneously in a clinically relevant model of OA, 2) the effect of exercise on venous and lymphatic drainage during OA progression. Given this, we investigated the effect of OA on microvascular function via clearance. OA was induced via a post-traumatic rat model of OA, the medial meniscus transection (MMT) surgery, and *in vivo* microvascular clearance was assessed. After we assessed joint clearance longitudinally as a function of surgery, we evaluated the effect of exercise on clearance during MMT surgery. We quantified the clearance of tracers. Our working hypotheses were that microvascular mediated clearance would decrease over time in the MMT and that exercise would increase the clearance of tracers from the joint space in OA.

1.1.3 Specific Aim 3: Using ex vivo platforms to assess lymphatic contractility and lymphangiogenesis

Ex vivo platforms have previously allowed groups to study the factors that affect lymphatic collecting vessel contractility and lymphatic collecting vessel segment growth[19–24]. In this aim, we used these two platforms to study lymphatic collecting vessel function and lymphangiogenesis in the context of OA. We used a custom *ex vivo* functional testing setup to assess rat femoral lymphatic collecting vessel contractility after MMT surgery or after perfusion with human OA synovial fluid (OASF). Additionally, we used a PEG hydrogel platform to study OA synovial fluid's effect on lymphangiogenesis with rat femoral collecting lymphatic vessel segments. Lastly, we

used the PEG hydrogel platform to understand how endothelial epsins regulate lymphangiogenesis using mouse flank collecting vessel segments. Our working hypotheses were that lymphatic vessel pumping function would decrease in MMT isolated vessels and OASF treated vessels and that OASF would reduce lymphatic collecting vessel growth. Additionally, we hypothesized that OA synovial fluid would decrease lymphangiogenesis, while epsin deletion would increase collecting vessel lymphangiogenesis.

1.2 Significance and innovation

1.2.1 Biomaterials-based diagnostic approach to determining joint health

Classically lymphoscintigraphy (the identification and imaging of lymphatics via tracers) has been executed via radiolabeled dyes used in the joint to observe albumin or dextran clearance. ICG is currently used clinically for sentinel node biopsy procedures *in vivo*. However, given its propensity to non-specifically bind to proteins, indocyanine green (ICG) effects on lymphatic function are unknown. In this thesis, we showed that PEG NIR tracers, which do not exert long-term effects on lymphatic contractility[25], can be used to assess venous and lymphatic clearance from joint space simultaneously. This work is innovative because it couples NIR imaging with the simultaneous assessment of venous and lymphatic drainage in various joint health states and interventions.

1.2.2 Ex vivo lymphatic model to study the effect of OA on lymphatic contractility

The MMT model and other relevant pre-clinical models have uncovered various aspects of OA's pathogenesis and investigated the efficacy of therapeutics on OA progression[26,27]. However, the effects of OA on lymphatic collecting vessel function and the contribution of lymphatic collecting vessels to joint health. We know there may be proliferative changes or loss of lymphatics in OA. To isolate the effect of altered lymphatic function on OA, we assessed how a lymphatic collecting vessel treatment affects contractility. This work is novel because no one has isolated lymphatics from arthritic animals and tested their capacity to pump. Additionally, no groups have assessed the effects of human synovial fluid on lymphatic contractility *ex vivo*.

1.2.3 PEG-based platform to study collecting vessel lymphangiogenesis

Maleimide terminated multi-arm PEG hydrogels can help elucidate the effects of materials stiffness and soluble factors on angiogenesis *in vitro*[28,29]. Here used this platform to study the effects of synovial fluid extracted from human OA patients on lymphangiogenesis and to study how epsins regulate collecting vessel lymphangiogenesis. This work is different from other approaches because it seeks to understand how synovial fluid from OA patients affects mature collecting vessel lymphangiogenesis and remodeling. Additionally, this work is different from most lymphangiogenesis studies as most of them are performed using LECs or *in vivo* at initial lymphatic beds using the mouse ear or zebrafish[30–36]. Furthermore, mature collecting vessels may respond differently to inflammatory cues, and these interactions are understudied[37–39].

1.2.4 Summary

Overall, this thesis sought to further our understanding of clearance mechanisms of healthy and diseased joints. Aim 1 established NIR imaging's utility and sensitivity to capture the clearance of sized tracers from the joint space and determined that exogenous vasoactive factors could decrease outflow from the joint. In Aim 2, we used our pre-clinical OA model to quantify the dynamic longitudinal changes in venous and lymphatic uptake with the techniques established in Aim 1. In Aim 3, we used *ex vivo* tissue mechanical testing to investigate how OA affects tissue and *ex vivo* tissue culture to assess the effect of epsin deletion and a simulated OA environment on collecting lymphatic vessel lymphangiogenesis. This body of work can serve as multiple platforms capable of investigating detectable changes in clearance in human OA and screening candidates for combatting adverse effects of the inflammatory OA environment on the microvasculature.

CHAPTER 2. BACKGROUND AND LITERATURE REVIEW

2.1 Osteoarthritis Epidemiology and Impact

Osteoarthritis (OA) is the most common form of arthritis affecting millions of people worldwide, with notably more than 3 million additional cases diagnosed per year in the US [40–42]. While OA can affect all joints, the hands, knees, hips, feet, and spine are the most commonly affected areas[43]. OA symptoms include pain, joint dysfunction, and deformity, while gender, age, obesity, and biomechanical predisposing factors seem to affect the development of OA[41,44–47]. OA is characterized by the gradual degradation of the articular cartilage, along with changes in the subchondral bone, synovium, meniscus, tendons, and muscles[48–51]. The current understanding of the pathophysiology of OA is evolving from what was initially thought to be only a mechanical disease caused by cartilage degradation progressed to a multi-factorial process mediated by the immunological response and abnormal mechanics[47,51].

OA was historically associated with increasing age as OA's manifestations were primarily reported in older populations[52,53]. As life expectancy increases, the number of people affected with OA will likely increase with time. Additionally, a recent systematic review of OA prevalence within tactical athletes (e.g., the military, firefighters, law enforcement, first responders) revealed that OA incidence was significantly higher in these exposed athletes when compared to non-exposed controls, which was likely due to increased and repetitive bending, squatting, lifting, and kneeling associated with these jobs[54]. Give tremendous sacrifice of military personal, identifying the mechanisms of

dysfunction, and identifying population-specific risk factors will allow for the development and implementation of strategies that reduce OA incidence.

OA has devastating effects on physical and mental health[2,55,56] as well as social support and social function[1]. This disease reduces the quality of life of hundreds of millions globally and substantially burdens the global healthcare system. Behind back/neck pain, osteoarthritis is the leading cause of musculoskeletal disability globally[57]. In terms of joints affected by OA, knee OA accounts for a large percentage of OA diagnoses precisely because of the knee's load-bearing nature and its association with obesity[58]. Those with knee injuries of particular interest to the OA community carry a high risk for post-traumatic OA (PTOA) development. For example, those with an ACL injury are 13% likely to develop PTOA[59], while those with a combined ACL meniscal injury are 21-48% likely to develop PTOA 10 years post-injury[60]. Destabilization of the joints leads to aberrant mechanical loading, propagating tissue damage, leading to PTOA[61].

2.2 Joint Anatomy and Physiology

The synovial joint, like the knee, is a specialized collection of tissues that enables joint movement and is a critical part of the musculoskeletal system[62]. Joints are named and aptly characterized by the movement they allow. For example, synovial (diarthrodial) joints differ from fibrous (amphiarthrodial) and rigid (synarthrodial) due to the synovial membrane and maximal flexibility[62]. The knee joint's main structural components include

the tendons and ligaments, which work in conjunction with the skeletal muscle and cartilage to move the large bones.

2.2.1 Articular Cartilage

Articular cartilage (Figure 1) is a specialized tissue where the extracellular matrix (ECM) is mainly composed of type II collagen and aggrecan (a proteoglycan that binds glycosaminoglycans (GAGs))[63]. GAGs possess carboxyl and sulfate groups that confer a net negative charge to the ECM; due to this negative charge, articular cartilage imbibes

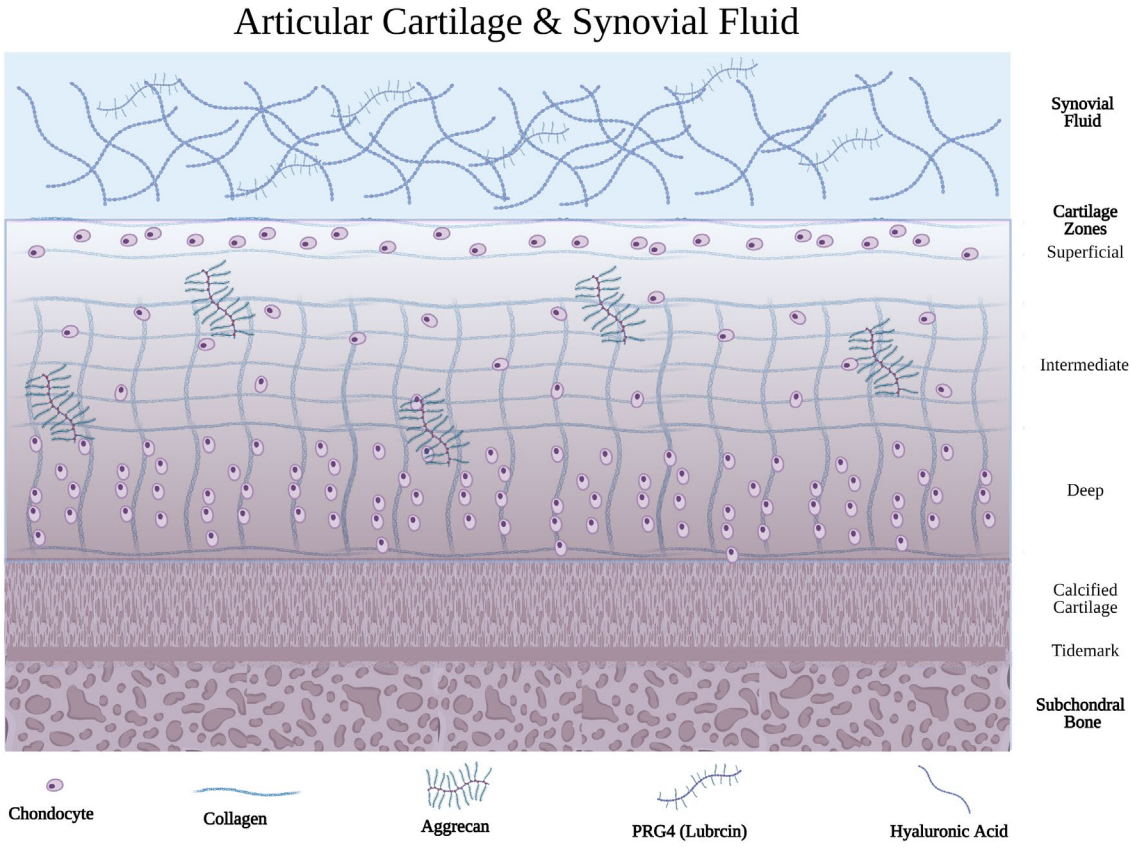

Figure 1 Articular Cartilage Composition and Structure.

water and is well hydrated[64,65]. Distinct layers characterize the tibia and femur's articular cartilage: the superficial zone, intermediate zone, deep zone, and transitional zones, including tidemark and calcified cartilage[63]. These different zones provide structural support during physiological loading of the cartilage during movement or while stationary. The superficial zone is responsible for providing structural support to the shear loading of articular cartilage and exchanges with the synovial fluid (SF). The intermediate zone is a transitional zone and can resist shear and compressive shear forces[66]. Cartilage's deep zone is responsible for supporting compressive loads[66]. The tidemark and calcified cartilage are structurally more like bone and connect the cartilage to the tibia and femur. Chondrocytes within the intermediate and deep zones are responsible for ECM synthesis and maintenance of the tissue[67]. The meniscus is a fibrocartilaginous structure between the medial and lateral bone surfaces and allows shock absorption[68]. External forces generated from daily activities result in a complex combination of shear, tensile and compressive stresses in cartilage. The unique composition and structure of collagen within the different cartilage zones allow for the tissue's adequate response to external forces. Like most tissues, cartilage is viscoelastic, and its behavior is strain rate dependent[69]. For viscoelastic materials, the application of stress causes temporary deformation if the stress is quickly removed, like elastic materials, but permanent deformation if it is maintained, like a fluid[70]. The articular cartilage is avascular and exchanges nutrients via the vascularized subchondral bone and synovial fluid[71].

2.2.2 Tendons and Ligaments

Multiple ligaments have insertion sites within the joint and outside the joint to stabilize the joint (Figure 2). Some of the main ligaments include the anterior cruciate ligament (ACL) and posterior cruciate ligament (PCL), preventing posterior-anterior

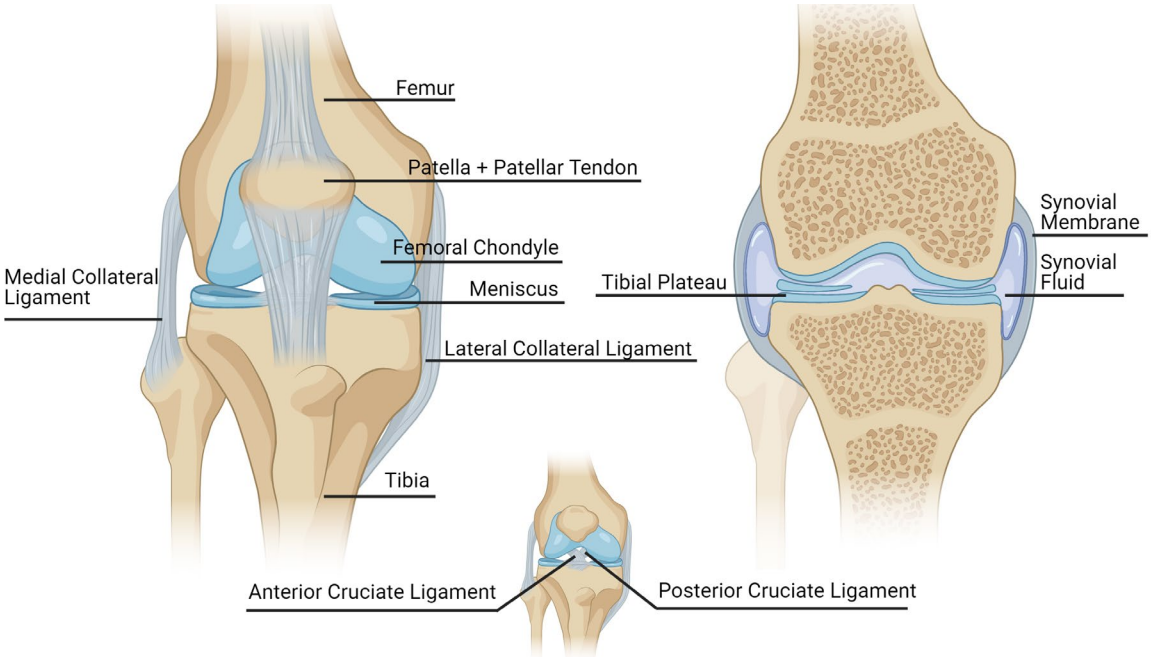

Figure 2 Knee Joint Anatomy.

displacement of the joint. The transverse ligament (not pictured) connects the two lateral and medial meniscal surfaces. Outside of the joint capsule, the patellar ligament/tendon connects the patella to the tibia and femur and primarily functions as a pully for the quadricep. Lastly, the medial collateral and lateral collateral ligaments (MCL & LCL) prevent the knee joint from bending in the medial and lateral directions. Most of the joint tissues like the cartilage surfaces, tendons, and ligaments have limited regenerative capacity, attributed to lack of vascular supply and inadequate repair mechanisms[72].

Therefore, all these tissues work in conjunction to reduce the likelihood of joint hyperflexion or tendon and ligament tears[73].

2.2.3 Synovial Membrane

The synovial membrane is another specialized tissue that serves many functions with the joint: 1) synoviocytes line the membrane and are in contact with the synovial fluid to synthesize hyaluronic acid (HA) and lubricin and keep critical components from leaving the joint space 2) the synovial membrane house the vasculature that participates in fluid exchange, namely the lymphatic and blood capillaries, and 3) the synovial membrane houses resident immune cells and participates in immune surveillance[74–77]. The synovial membrane and joint capsule make up connective tissues that form a sleeve around the synovial membrane's lateral aspects[78]. The synovial lining's intimal surface contains two synoviocytes, type A synoviocytes from macrophage lineage and type B synoviocytes, derived from fibroblasts[74,79]. The intimal layer of the synovium is generally 1-2 cells in thickness, while the subintimal layer contains scattered blood vessels, lymphatic vessels, lymphocytes, and macrophages[80]. The vascularized subintimal layers allow for fluid and molecule balance and mediating immune cell surveillance. Synoviocytes synthesize and secrete HA in a mechanosensitive manner[81]. Increased synoviocyte loading through joint motion leads to increased HA production and secretion into the synovial fluid matrix. Proteoglycan 4 (PRG4 or lubricin) is synthesized by superficial chondrocytes and synoviocytes[82–84]. The mechanical regulators of lubricin synthesis are not as well-known as HA; however, chondrocytes exposed to an injury can upregulate lubricin production[83,85].

2.2.4 Synovial Fluid

Synovial fluid is a viscous lubricative fluid within the joint space integral to the function of cartilage and the transport of solutes to different joint tissues[86]. The primary function of synovial fluid is to lubricate the joint surfaces and reduce friction between articular cartilage[77]. Due to the limited capacity for cartilage to repair, maintenance of the synovial fluid composition is essential[72]. Synovial fluid contains lubricin, HA, surface-active phospholipids (SAPLs), and albumin, all of which work to lubricate the joint surfaces, maintain oncotic pressure, and serve as a medium for nutrients, waste, and cytokines to traffic through. Lubricin, a 0.25 MDa glycoprotein that is a critical component of the joint lubrication process, was believed to participate directly in boundary lubrication[87,88]. However, later it was discovered that the primary function of lubricin was to transport SAPLs to the cartilage surface, and these SAPLs account for roughly 10% of the weight of lubricin and directly lubricate the cartilage surfaces[89–91]. Albumin is a 66 kDa protein that serves as a ubiquitous carrier molecule in the bloodstream, and interstitium also helps increase synovial interstitial fluid viscosity and exerts interstitial oncotic pressure[92]. Albumin also binds lipids, anions, peptides and thus can help drive the lubricative role of SAPLs by helping to carry them into the joint space from the synovium[92,93].

A net imbalance in the Starling forces drives the ultrafiltration of plasma into the joint space[9,94]. Oncotic pressure drives fluid flow and materials within that fluid out of capillary fenestrations and into the joint space[8]. The net negative charge of the synovial fluid constituents leads to significant hydration. One of the main functions of the synovial

fluid is to help maintain hydrostatic pressure within the joints. Without SF, joint loading would force water to escape due to a large favorable hydrostatic pressure gradient rapidly[95]. However, due to the electrostatic interactions and considerable osmotic pressure generated by SF, this is averted. The reflection of the large SF constituents by the synovial membrane is a vital contribution to joint maintenance[96]. Additionally, HA polymer entanglements result in significant HA and water retention in the joint, leading to consistent and adequate lubrication of the cartilage surfaces[97].

2.3 Joint Fluid Transport

Interstitial volume and protein concentrations are maintained in tissues via microvascular filtration, lymphatic return, and interstitial storage[98]. Due to the favoring of capillary filtration (movement from the blood vessels into the tissues), fluid would accumulate in the tissues resulting in pathologies like lymphedema without the appropriate vascular machinery[99]. Each tissue within the joint has its intrinsic sieving capacity/pore size/hydraulic conductance, which dictates which molecules can be present within the tissue and how quickly they move through them[100,101]. Additionally, our lack of understanding of how things can enter and exit tissue spaces in health and disease complicates our ability to understand disease mechanisms and appropriate treatment strategies.

2.3.1 Cartilage, synovial fluid, and synovial membrane transport

Due to its avascularity and small pore size (6 nm), cartilage relies on diffusion to transport growth factors and nutrients[102]. However, advection can assist the transport of

growth factors during joint motion, with larger molecules affected more by cyclical mechanical loading than small ones[103,104]. Load-induced interstitial fluid pressure changes and diffusion transports molecules within the matrix. These loads can are induced by sliding (shear) or compression on the cartilage surfaces[105,106]. The synovial fluid, like the cartilage, is an extracellular compartment that serves as a medium for the movement of nutrients and growth factors. The pore size of synovial fluid has not been studied extensively; however, solutions crosslinked HA solutions at physiological concentrations have pore sizes between 30 to 500 μm[107]. Like cartilage, small solute movement through the synovial fluid via diffusion is dominant[86]. Synovial fluid is in constant exchange with the surrounding synovial membrane and cartilage.

The synovial membrane is the first or final extracellular space that a solute entering or leaving the joint must traverse. The synovial membrane's intimal and subintimal layer contains an interstitial matrix composed of collagens, GAGs, proteoglycans, fibronectin, and laminin[75]. Interstitial matrix proteins significantly affect the synovium's permeability, as demonstrated by increased hydraulic conductance of the synovium in the presence of collagen sparing protease[108]. The pore size of the synovial membrane is approximated to be between 20–90 nm[109,110]. Once in the synovial matrix, there are two vascular routes by which materials can clear. Radiolabeled iodine and albumin drainage from the joint has demonstrated the size-based clearance of tracers, as iodine and albumin cleared through circulatory and lymphatic uptake, respectively[111]. Small molecules (< 5 nm)are cleared mostly through venous capillary uptake due to fenestrations that exclude larger

molecules[112]. Large molecules (> 10 nm) cannot leave through venous circulation in most tissue beds and are cleared mostly via lymphatic circulation[113–115].

2.3.2 Effect of intra-articular pressure and hydraulic conductance on joint transport

Intra-articular pressure (IAP) is dictated by various factors in the healthy joint, including joint position, synovial fluid composition, and activity levels. With the increased extension of the leg, the joint pressure decreases in humans, demonstrating that joint angle changes hydrostatic pressure within the joint. IAP is negative when not in motion and becomes momentarily positive with active joint motion[116]. Additionally, increases in IAP increase the hydraulic conductance of the synovium, likely mediated by increased extracellular gaps[117].

Colloid osmotic pressure has a more negligible contribution from HA than from albumin in the joint; however, hydraulic conductance is affected by HA concentration[118,119]. The viscosity of HA concentrations below 1.35 mg/mL behaves linearly, however above 1.35 mg/mL, the effects of HA chain interactions increase the linear rate at which viscosity increases with concentration and serves as a mechanism to improve HA retention[118]. As HA chain length decreases, its ability to buffer flow significantly decreases[119]. Experimentally, the reflection of HA is size-dependent as the synovium entirely reflects 2 MDa HA while smaller HA chains are cleared increasingly as their size decreases[109,110].

While exercise is an essential determinant of human health, exercise's effect on joint balance remains elusive. Exercise is known to increase blood flow to the synovium

and menicsus[120]. Increases in IAP via injection experimentally have shown increased downstream femoral lymphatic flow by 16%, showing that downstream lymphatic function could be increased by modulating IAP[121]. However, little is known about the contribution of exercise to flow from the joint. To date, few have shown the effect of exercise on synovial fluid transport[84,120,122–124]. These studies have assessed the effect of joint motion or exercise on material distribution or biomolecule synthesis but not downstream transport. Exercise has been shown in other tissues to increase blood and lymphatic flow to and from the tissue[125–127]. However, given the unique chemical composition of the synovial fluid and synovial membrane, the effect of exercise on joint clearance is a significant knowledge gap that must be addressed to further our understanding of how synovial joints function, given that exercise is a critical component of overall human health.

2.4 Circulatory System Anatomy and Physiology

In mammals, the circulatory system involves two interconnected systems that manage the transport of fluids through the body. The cardiovascular and lymphatic systems and their functions are reviewed in great detail by Miller et al.[128]. The cardiovascular system provides nutrients to tissues in the body via the blood and uses this same highway to transport waste materials away from the tissues[128]. Once materials reach the tissues, the lymphatic system is responsible for three main functions: 1) remaining interstitial fluid transport, 2) immune cell trafficking, and 3) intestinal lipid absorption and overall lipid homeostasis[129]. In addition to the circulatory system's essential nutrient and fluid homeostasis functions, the cardiovascular and lymphatic systems allow for the

long-range communication of tissues through cytokine/hormone signaling and immune cell surveillance by providing conduits by which these interactions occur[130,131].

The cardiovascular system is composed of hierarchical vessel networks with a centralized pump, the heart. The largest is the artery (0.1-20 mm in diameter) which transports blood out of the heart into smaller arterioles (< 100 μm in diameter)[128]. Arterioles propagate the blood into smaller capillaries (5 to 10 μm in diameter) where nutrient and fluid exchange occurs at the tissues[128]. The venules (10-100 μm) transport the deoxygenated blood away from the tissue and return it to the heart via the veins, which have valves (millimeters in diameter)[128]. At rest, the mean velocity of blood flow in the larger blood vessels is approximately 10 cm/sec[132], while in the capillaries, the average blood velocity is roughly $1/10^{th}$ of that in the larger vessels[133]. The intimal layer of large and medium-sized blood vessels contains blood endothelial cells (BECs). The medial layer contains support cells and ECM that support the vessel's contractility functions and provide structural rigidity. Finally, arterioles contain smooth muscle cells which contract to tightly regulate blood pressure and blood flow to the appropriate tissues[128]. The mechanisms that regulate vascular tone in blood vessels have been reviewed in great detail by Sandoo et al.[134].

The lymphatic system is the other circulatory system and originates from the tissues at the capillary level, aptly named initial lymphatics[135]. Initial lymphatics (10-60 μm in diameter) collect lymph from the interstitial spaces to more mature pre-collecting vessels, which are intermittently lined with smooth muscle cells, larger than lymphatic capillaries, and may contain valves[136]. Pre-collecting vessels merge into the collecting

vessels (1-2 mm in diameter), which have complete smooth muscle cell coverage and valves that help transport lymph against an adverse pressure gradient back to the systemic circulation via lymph node venous exchange and emptying the thoracic duct into the left subclavian vein[129,137]. Thus, collecting vessels transport lymph through lymph nodes which serves two main functions: 1)lymph nodes return 4L of the 8L of interstitial fluid that remains from capillary filtration back to the venous circulation[138] 2)lymph nodes are where antigen-presenting cells and naïve lymphocytes communicate and initiate immune responses[139].

The lymphangion is the segmental unit that encompasses the space between two valves in a mature collecting lymphatic vessel[22,140]. The pumping activity of lymphatics requires valves and specialized lymphatic smooth muscle-lined collecting vessels that, contrary to vascular smooth muscle cells, exhibit strong intrinsic phasic contractions to drive lymph downstream[23]. Lymphatic pumping is controlled by a variety of intrinsic and extrinsic factors. Lymphatic vessels have their intrinsic pacemaking activity controlled by the smooth muscle cells[141]. Fluid shear and transmural pressure can modulate this intrinsic pacemaking activity. *Ex vivo* perfusion and pressurization systems have been used to control flow and transmural pressure across isolated lymphatic vessels[21,142–147]. Under conditions of low flow, as the lymphangion fills with lymph, transmural pressure increases. The strength and frequency of the following lymphatic contractions are dictated by the rate at which the lymphangion fills[148]. In the cases of high filling and high fluid shear stress, lymphatics become more like a conduit and decrease contractility, and this pump-conduit duality allows lymphatics to adapt to changes in fluid flow[21]. Extrinsic

mechanical stimuli can also drive increased fluid flow in lymphatics and veins. These vessels can be located in or near the skeletal muscle, and they are subjected to external forces when muscles contract and relax; therefore, skeletal or smooth muscle pumps can improve lymph flow[149].

2.4.1 Angiogenesis

Angiogenesis is the process by which blood vessels grow from existing vessels[150]. Classically angiogenesis occurs in response to a lack of oxygenation in tissues[151152]. Sprouting capillary angiogenesis is part of the normal response to injury and changing tissue demands *in vivo*. A significant number of factors exist that promote angiogenesis. The most well-known factor is vascular endothelial growth factor A (VEGF-A or VEGF). VEGF works in conjunction with a variety of factors to stimulate capillary angiogenesis. VEGFR2, the receptor for which VEGF-A has the highest affinity, is expressed by blood vessels and lymphatic vessels.

A stable blood vessel is characterized by an inner endothelial monolayer called the tunica intima, which contains blood endothelial cells (BECs)[128]. The following layer is the tunica media, which contains smooth muscle cells, pericytes, and basement membrane. The tunica adventitia consists of connective tissue and elastin. Angiogenesis is initiated when growth factors interact with the endothelial cell cells. Growth factor signaling results in cell mitosis, increased migration, and proteolysis, which increases the permeability of the vasculature[153]. After disrupting the subintimal vessel layers, the endothelial cells can now extravasate into the matrix and grow towards chemical

gradients. BECs extend out into the matrix, degrade the matrix, and form tubular networks through vacuolar and pinocytic events[154]. Some of the most potent pro-angiogenic regulators have been reviewed in great detail[151] and include VEGF-A, fibroblast growth factor (FGF), angiotensin 1 and 2 (ANG-1 and ANG-2), transforming growth factor-beta (TGF-β), tumor necrosis factor-alpha (TNF-α). To eventually turn off the cellular cues, direct angiogenesis, arrestin, canstatin, and high molecular weight kininogen initiate vessel stabilization and terminate angiogenesis[151].

2.4.2 Lymphangiogenesis

Lymphangiogenesis is the process by which lymphatic vessels grow from existing vessels. A stable lymphatic collecting vessel is defined by a tunica intima consisting of lymphatic endothelial cells, a tunica media consisting of lymphatic muscle cells and elastic fibers, and a tunica adventitia consisting of collagen and elastin, which help connect the lymphatic vessels to the surrounding tissue[128]. During embryonic development, lymphatic vessels originate from the cardinal veins (the pre-natal venous system)[93]. VEGF-C signaling is the primary driver of lymphatic growth from budding and initiates lymphatic sprouting from embryonic veins[155]. Vascular endothelial cells bud off the cardinal vein and, through PROX-1 signaling, differentiate into lymphatic endothelial cells that form collecting vessels, and ultimately smaller lymphatic capillaries grow in the mesenchymal tissue[156]. Lymphatic valves are formed as lymphatic collecting and precollecting vessels mature[157,158]. LECs in the collecting vessels downregulate PROX1, VEGFR3, and LYVE-1, except for valve-forming cells, and FOXC2 is another critical transcription factor shown to regulate lymphatic valve formation[159]. As collecting

vessels mature, LECs secrete reelin into the extracellular matrix, which helps drive the recruitment of smooth muscle cells (SMCs) to collecting lymphatic vessels[160]. Postnatally, in response to growth factors like VEGF-C, LECs destabilize lymphatic vessels, extend long filaments into the extraluminal space that sample the ECM, and these cellular processes lead to the tunneling of thin vacuolized lymphatic sprouts through the ECM. As these groups of LECs tunnel through the ECM, intracellular vacuoles coalesce and form an intraluminal space, leading to a capillary lumen formation, as demonstrated in BECs[37].

In response to injury or inflammatory stimuli, capillary lymphangiogenesis can be stimulated: this process occurs through many of the same factors that drive angiogenesis (reviewed in detail by Aebischer et al.[4]) and include VEGF-C/D, IGF-1, IGF-2, PDGF-BB, HGF, ANG-1, ANG-2, and FGF-2[161]. VEGF-C and VEGFR3 are the main lymphatic growth factor and receptors studied, and VEGF-C is mainly produced by inflammatory cells postnatally. The most abundant source of VEGF-A and VEGF-C *in vivo* is macrophages[4]. VEGF-C increases lymphatic vessel size *in vivo*, while VEGF-A increases lymphatic vessel proliferation and migration[162]. VEGF-D, another variant in the VEGF family, is the most potent regulator of lymphangiogenesis and, in its most post-translationally modified form, has a high affinity for VEGFR2 and VEGFR3[163].

After VEGF-A and VEGF-C interact with their receptors, endocytosis or internalization of the receptor helps to modulate the signaling process. Epsins are endocytic adaptor proteins that regulate the internalization of VEGF receptors. EGFR protein tyrosine kinase substrate #15 (Eps15) was discovered in the clathrin-coated pits of

synaptic vesicles in the brain and crucial in the receptor internalization process[164]. Eps15 interacting protein, better known as epsin, was discovered with precipitate proteins from that endocytic machinery[165,166]. Epsins bind to membranes with specific cargo and connect them with the endocytosis machinery, and Epsin 1 and 2 are present in all tissues[167,168]. In the context of two inflammatory diseases, epsin function has been shown to be dysregulated. Several genetic models of epsin mice have been created to understand the role of epsins in the embryonic patterning and development of blood and lymphatic vessels. Researchers discovered that epsin 1 and 2 deletion in vascular endothelial cells during gestation results in death and highly disorganized vascular networks[169]. When a LEC-specific variant of these double knockout mice was generated, the mice are viable but have a series of abnormalities, including enlarged lymphatics, delayed or defective lymphatic valve formation, abnormal VEGFR3, and PROX1 signaling[157]. LECs from LEC-iDKO are more responsive to VEGF-C as assessed by tube formation assay *in vitro,* and *in vivo* corneal lymphatic vessels are more responsive to VEGF-C treatment[157]. Postnatal epsin deletion in LEC-iDKO lymphatics vessels does not affect the size and shape of lymphatic collecting vessels.

Epsins have also been investigated as potential therapeutic targets in a variety of diseases. For example, in diabetes, epsins are also upregulated, leading to increased VEGFR3 degradation through oxidative stress[157]. In addition, LEC-specific deletions of epsin 1 and 2 lead to improved VEGF-C mediated lymphangiogenesis and the recovery of normal lymphangiogenesis *in vivo*. Another disease where epsins are augmented is atherosclerosis[170]. Myeloid epsins promote the generation of atherosclerotic plaques by

facilitating pro-inflammatory macrophage recruitment and downregulating low-density lipoprotein receptor-related protein 1, which has anti-sclerotic properties. Therefore the myeloid-specific deletion of epsins reduces plaque formation via the upregulation of LRP-1 and generally led to decreased pro-inflammatory cytokines and an increase in an anti-inflammatory phenotype.

Unlike angiogenesis, the growth and remodeling of mature lymphatic vessels after an injury has not been well-studied. Models in mice have provided some context and information about how lymphatic remodeling occurs post-natally[171]. In response to lymphatic obstruction or ligation, lymphatic pre-collecting vessels and capillaries form to help bypass the injury site to restore flow, demonstrating the regenerative capacity for lymphatics[172136]. Additionally, collateralization, or the formation of initial and precollecting lymphatics to restore fluid flow, has also been shown in the context of lymphatic obstruction or insufficiency[173]. However, the effect of inflammation on the capacity for collateral vessels to form from mature lymphatic vessels is not well established. Given the established link between OA and inflammation, it is unknown to which extent OA affects this process. To study the effect of individual cytokines and growth factors on lymphangiogenesis from mature collecting vessels, Bruyere et al. used a lymphatic ring assay in a collagen gel[38]. Building off this type of ring assay, we can investigate the direct role of clinical OA samples in collecting vessels in growth and remodeling. This thesis will report the use of PEG hydrogel to investigate how a simulated OA environment affects mature vessel sprouting and collateralization.

2.5 Pre-clinical models of OA

To study the complex pathophysiological events in OA, several animal models have been developed. The three categories of animal models include naturally occurring, mechanical insult, and surgical insult and reviewed in great detail[174]. Spontaneously occurring animal models have the advantage of simulating spontaneous age-related OA. Dunkin Hartley guinea pigs have been the most widely used naturally occurring OA due to their rapid maturity to adults, size, and how OA manifests in human OA[175]. Spontaneous models are advantageous in some cases because they mimic the progressive loss of joint function in humans and can be used for studying early therapeutic intervention[176,177]. Additionally, they are fewer confounding effects such as surgeon technique and institutional differences in animal care[178].

The progressive joint destruction following post-traumatic injury is demonstrated *in vivo* in various animal models and *ex vivo* with whole joint studies or cartilage explants[179]. Additionally, different targets include the meniscus, the cartilage, and the ligaments of the surgically induced insults. Some mouse models include the destabilization of the medial meniscus, partial medial meniscectomy, and media meniscectomy. PTOA models are advantageous because they mimic OA's risk factors, which is a previous injury.

In this thesis, we used the medial meniscal transection (MMT) induced model of PTOA due to its ability to rapidly develop pathological OA joint damage. The MMT model proceeds with a skin incision, blunt dissection of the muscle above the joint, transection of the MCL, and complete transection of the medial meniscus. This model has been characterized in various contexts, including delivering treatments[180,181], gait

analysis[182], and pain assessment[26]. Histologically, this model has been evaluated from 3-12 weeks, with the early timepoints being used to evaluate the ability to prevent OA onset and with the later timepoints evaluating the ability to attenuate OA progression or evaluate the secondary effects of OA development. In this thesis, we evaluate the MMT model characteristics that have not to be established, including the venous clearance, the effect of exercise on clearance, and longitudinal lymphatic drainage over nine weeks.

2.6 Osteoarthritis Pathophysiology

OA's current standard of treatment is rehabilitation to maintain mobility, palliative treatments to manage pain, and joint replacement surgery for end-stage disease[183]. Low-grade chronic inflammation is a crucial driver of OA, and it is well-documented that OA tissue and synovial fluid have increased serum proteins, complement components, and pro-and anti-inflammatory cytokines, immune cells,[18,184–191]. OA was considered a disease of wear and tear in the past, and the potential immune effects were not of significant interest. However, given that rheumatoid arthritis is associated with inflammation. The following section will discuss some of the pathological changes in OA and the degree to which they may affect fluid balance.

2.6.1 Pathological changes in cartilage in OA

The abnormal loading of cartilage through traumatic injury, altered biomechanics, or repetitive loading results in the destruction of the cartilage architecture[69]. The loss of the articular cartilage structure integrity changes its lubricative and fluid retention capabilities and leads to proteoglycan loss[27,192–194]. Swelling is followed by cartilage

fibrillation and roughening cartilage defects[195,196]. Aside from the biomechanical function, there are changes in the chemical interaction. Cartilage degradation is mediated by pro-inflammatory cytokines, aggrecanases, matrix metalloproteinases, and nitric oxide[195,197]. Pro-inflammatory cytokines including interleukin-1β (IL-1β) and tumor necrosis factor α (TNFα) have been shown to promote cartilage degradation by stimulating the production of matrix metalloproteinases (MMPs)[198,199]. Ultimately cartilage fluid flow is likely to increase during OA progression due to the loss of structural integrity and proteoglycans[70,200].

2.6.2 Synovitis in OA

Within the synovium, the innate immune system is the first line of defense against foreign materials. In OA, tissue damage is a feedforward process that drives the activation of the innate immune response, the release of pro-inflammatory cytokines, and the recruitment of inflammatory cells, resulting in inflammation of the synovium (synovitis)[51,71,191,201–204].

Functionally synovitis is associated with palpable joint swelling, sudden increases in pain as well as morning stiffness[13,205]. In the clinic, MRI and ultrasound are the primary imaging modalities by which synovitis is assessed[206–209]. Pathologically, synovitis presents cell hypertrophy and hyperplasia, the infiltration of immune cells (T-cells, B-cells, macrophages), and increased angiogenesis and lymphangiogenesis[210]. While the immune cell contributions to OA development and synovitis have been explored, the

relationship between synovitis and lymphatic function in terms of initial lymphatic uptake and downstream lymphatic function is significantly understudied.

2.6.3 Synovial Fluid Changes in OA

Changes within the synovial fluid matrix may also be responsible for OA progression in humans. Human synovial fluid samples assessed as a function of age in non-OA patients demonstrated an inverse relationship with patient age and the concentration of HA[211]. The mean size of HA within the joint in rheumatic diseases is significantly decreased[212]. Additionally, compared to non-OA synovial fluid, the lubricating ability of HA was not significantly lower, but the mean size was much lower ($p = 0.1$)[213]. The superficial cartilage boundary roughness and decreased synovial fluid quality likely lead to the insufficient lubrication of the cartilage surface in OA[213]. Changes in HA integrity (concentration and size) may also change the rate at which materials flow through the synovial fluid matrix, affecting overall joint homeostasis; however, the flow of materials through osteoarthritic synovium has not been extensively studied, and this a gap in knowledge[211,214–217].

2.6.4 Clearance Changes in Osteoarthritis

Given the role of clearance in the maintenance of joint fluid balance, joint clearance is of great interest to understand the physiology of the joint during disease and understand if lymphatics may be a therapeutic target in OA. The body of research investigating the effect of OA on microvascular anatomy and physiology is a small subset of OA research. Simkin et al. observed differences in clearance between rheumatoid arthritis (RA) and

OA patients[205]. When clearance in OA patients was compared to RA patients, the study showed that clearance of proteins ranging from 6 – 18 nm in hydrodynamic diameter and determined that the synovial permeance, clearance, and flux were lower in OA to RA patients[218]. However, this seminal study was limited due to the lack of adequate non-OA controls, and these differences could only speculatively be attributed to decreased clearance in OA or increased clearance in RA. These *in vivo* clinical studies implicate critical changes in microvascular clearance in humans, but studying this in a rigorous and highly controlled manner has been challenging clinically. Thus researchers have utilized pre-clinical models to investigate various aspects of OA progression more precisely.

A variety of pre-clinical models have been used to study the effect of OA on lymphatic clearance previously. Albumin clearance from the knee joint was increased 12 weeks post-OA induction in an ACL-induced joint injury in the canine[219]. In normal healthy tissues, albumin is cleared primarily by lymphatics[220]; therefore, increased albumin clearance could be mediated by increased lymphatic drainage or synovial or venous integrity changes, either of which would lead to increased flow. Additionally, this study was a small study with no histological evidence to explain the increased albumin clearance. More recently, rodents have been used as a model to investigate the effect of OA surgery on ICG clearance[11,14]. In the mouse meniscal/ligamentous injury (MLI) model, ICG clearance was slower than Sham at 6, 12, and 20 weeks post-surgery[11,14]. In other studies utilizing a rat knee joint model, dextran at two molecular weights, 10 kDa and 500 kDa were used to determine MMT surgery's effect on joint clearance. Three weeks post-injury, 10 kDa Dextran cleared slightly faster while 500 kDa dextran was

slower than their respective naïve joints[221]. Significantly synovial retention of the Dextran was noted in this study by MMT rats compared to naïve age-matched rats, suggesting that synovial permeability is decreased during OA development. While these studies provided critical insight into clearance rates, clearance and microvascular transport routes remain unknown.

While most studies have focused on functional transport measurements in the joint, a few studies have begun to investigate structural lymphatic changes in the synovium during disease. Recently clinical human synovial samples have been assessed for the presence of lymphatic vessels. In osteoarthritic synovium, there is decreased lymphatic vessel size and vessel number compared to cadaveric non-OA controls[6,11]. Additionally, joint effusion (swelling) was associated with decreased lymphatic vessel density and lymphatic endothelial cell fractional area. These data together suggest that lymphatic clearance changes may be responsible for joint effusion in OA[6].

Recently clinical human synovial samples have been assessed for the presence of lymphatic vessels. In osteoarthritic synovium, there is decreased lymphatic vessel size and vessel number compared to cadaveric non-OA controls[6,11]. Additionally, joint effusion (swelling) was associated with decreased lymphatic vessel density and lymphatic endothelial cell fractional area, suggesting that lymphatic clearance changes may be responsible for joint effusion in OA[6].

2.7 Osteoarthritis Treatment

2.7.1 Clinical Treatments for OA

OA's current standard of treatment is rehabilitation to maintain mobility, palliative treatment to manage pain, and joint replacement surgery for end-stage disease. Over 600,000 hip replacement surgeries and 300,000 knee joint replacement surgeries result in over 200 billion dollars in health expenditures every year[183,222,223]. Given current heterogeneity in treatment, there is an unmet scientific need in disease pathogenesis and an unmet clinical need for disease-modifying therapies for OA.

A study recently conducted by the department of human health and services researchers looked at the efficacy of various therapies, including cell-based therapies, oral supplements, viscosupplementation, transcutaneous electrical stimulation, strength and agility training, aerobic exercise, and weight-loss diets. Exercise and physical therapy have the potential to serve as a baseline practice for those with OA to improve and alleviate their symptoms and outcome. Strength training, in general, has been shown self-reported measures of pain and physical function in over 50–75%[224]. Except for weight loss, general exercise, and agility training, most treatments demonstrated short-term benefits on pain and function[3]. Exercise and increased movement may improve disease outcomes through the increased clearance of inflammatory cytokines[122]. Additionally, cyclical joint movement may improve disease outcomes through the increased secretion of HA, which helps make the synovial fluid more viscous to lubricate and prevent the outflow of synovial fluid[84].

The delivery of HA-like molecules to the joint space is of clinical significance[225–227]. Viscosupplementation with exogenous HA has been a long-explored strategy in OA, and they have been previously recommended to AAOS and ACR; however, they are no

longer recommended due to lack of efficacy[228]. HA clearance has been studied in various animal models, and the articular half-life was in the range of 12-24 hours[229,230]. The residence time for larger viscosupplements vary and is mediated mainly by size and chemical modifications[100]. The food and drug administration has approved a variety of products which include Hyalgan (1997), Euflexxa (2004), Synvisc-One (2009), and most recently, Durolane (2017)[231]. One of the main reasons why viscosupplementation as a singular strategy for OA treatment has failed may be ignoring the multiple underlying causes of the disease. These treatments, in most cases, require multiple injections of HA; however, increased HA catabolism is one of the hallmarks of OA[232,233]. Viscosupplementation continues to be explored via alternative approaches that improve lubrication and residence time within the joints[234]. Durolane has shown increased residence time in the joint compared to other HA-based injectable viscosupplements[235–237].

Platelet-rich plasma (PRP), a concentrated blood product containing high concentrations of factors that drive angiogenesis and cell recruitment, has recently been investigated as a potential therapeutic option for people with OA, with the ultimate goal of creating repair tissue in the cartilage[238]. A meta-analysis conducted has shown that in comparison to saline or HA injections, PRP improves self-reported outcomes 12 months post-injection and provides additional relief for patients with significant joint degeneration[225].

Total hip and knee arthroplasty are the standard of care for patients with end-stage OA[1]. They are relatively safe and effective and improves patient mobility and pain, and

increase life quality. One of the burdens of total knee replacement or total hip replacements is the costs associated with them, the burden they add, and the associated costs of adverse effects such as revision surgeries[239]. However, in some cases, the QOL indicators matched those without OA, suggesting that these methods are effective. However, many factors control patient outcomes, including patient age, weight, lifestyle, and surgery wait times which all are involved in the likelihood that arthroplasty would be successful[240–242]. In addition, the residence time of intra-articularly delivered therapeutics modulates their bioavailability and likely their efficacy of the pain treatment. Given current heterogeneity in treatments, there is an unmet scientific need to understand the involvement of lymphatics and clearance mechanisms of endogenous and exogenous viscosupplements in disease pathogenesis and progression.

2.7.2 Targeting Lymphatics for Joint Diseases

The two most common joint diseases are rheumatoid arthritis and osteoarthritis—RA and OA symptomatically present with pain, stiffness, and decreased range of motion. RA differs in etiology from OA because auto-immunity is the main precipitating event, rather than biomechanical drivers. OA tends to develop unilaterally or in one place, whereas RA tends to be symmetrical and present in multiple joints. Synovial inflammation is one of the hallmarks of RA. This immune overactivity in RA leads to flairs that can be predicted and controlled therapeutically. Unlike OA, RA has various disease-modifying antirheumatic drugs, ranging from biologics like anti-TNFα and non-biologicals with a variety of targets and many unknown targets[243]. Based on recent

clinical and pre-clinical success in treating RA, modulating lymphatic function is of interest in OA.

A variety of biologics and pharmaceuticals have been used to try to modulate lymphatic function in rheumatic diseases. In the context of an inflammatory model of RA in mice, Wang et al. showed that blocking VEGFR3 activity could reduce synovial lymphatic function[14]. Additionally, they showed that Bortezomib (BTZ), an anti-cancer medication used to treat multiple myeloma and mantle cell lymphoma, inhibits pro-inflammatory cytokines in the T cells of RA patients, reduces inflammation in RA in rats, and suppresses TNF-a inflammatory effects in human chondrocytes[244,245]. BTZ has also been shown to improve lymphatic drainage and attenuate OA progression in rodents showing enhanced lymphatic drainage. Additionally, in the case of an RA-like model in the mouse, the overexpression of VEGF-C in the joint leads to improved clearance and articular cartilage health[246]. While it has been shown that VEGF-C can rescue lymphatic function in RA *in vivo,* critical gaps in knowledge remain, including what is the effect of the OA milieu on lymphatic collateralization. These data together demonstrate the potential of targeting lymphatics and lymphatic function as a therapeutic for joint diseases; however, critical gaps in knowledge remain both about the fundamental role of lymphatics in joint disease and how to target the lymphatics as a long term functional therapeutic approach.

CHAPTER 3. QUANTIFYING MICROVASCULAR CLEARANCE USING NIR IMAGING

3.1 Introduction

This chapter has been adapted from the following manuscript: Doan, T. N., Bernard, F. C., McKinney, J. M., Dixon, J. B. & Willett, N. J. Endothelin-1 inhibits size dependent lymphatic clearance of PEG-based conjugates after intra-articular injection into the rat knee. Acta Biomater. 93, 270–281 (2019).

The homeostatic maintenance of joint tissues and synovial fluid is regulated by multiple mechanisms, including blood flow, synovial permeability, capillary uptake, and lymphatic clearance[9,101]. Recent evidence has suggested that proper lymphatic function is critical to joint health and inflammation resolution[100]. During joint diseases, such as osteoarthritis, the production and consumption of various metabolites, including proteins, cytokines, and proteoglycans within the joints, are altered; understanding the clearance kinetics and mechanisms inform potential therapeutic delivery strategies as well as therapeutic targets. Cytokines and degraded ECM during joint disease diffuse passively through hyaluronan lattices, the synovial matrix, and then into capillaries of the synovium. Low-molecular-weight molecules diffuse along their concentration gradients and are dominantly taken up into venous vessels[247]. On the other hand, high-molecular-weight molecules and cells are cleared primarily through the synovium's initial lymphatic vessels[248].

Much of our understanding of joint physiology and clearance relies on observations from several decades ago—molecules above specific molecular weights appear to clear at rates independent of their size, suggesting that the lymphatics are the primary route of clearance of large molecules from the joint[220,249]. Pioneering work by Simkin and colleagues simultaneously measured the clearance of two different sized-tracers from the joint to provide an indirect measurement of plasma flow and lymphatic drainage from knee effusions of patients with rheumatoid arthritis (RA) or osteoarthritis (OA); they found that clearance of proteins from the joint space is significantly slower in OA compared to RA[218]. However, all of these differential isotope studies were conducted in late-stage diseased patients, and 30 years later, we still do not know how these measurements compare to early-stage disease or healthy patients[112]. Recent work in human patients has demonstrated a decrease in lymphatic capillary density in the synovia of OA patients, suggesting an impairment of lymphangiogenesis[6]. However, in pre-clinical studies using an injury-induced OA model in mice, lymphatic capillary density increased in OA animals, while the number of mature collecting vessels was markedly decreased in severe OA cases. More importantly, functional drainage from the knee space was reduced, consistent with reduced collecting vessel density and reduced drainage in OA[11]. A follow-up study found that systemic delivery of therapeutic to promote lymphangiogenesis could attenuate OA disease progression in this model, suggesting that lymphatics function and clearance mechanisms may be a promising therapeutic target [14].

Traditionally, tools used to assess in vivo clearance kinetics from joints have relied on radioactive-labeled materials[112,250–253] and, in some instances, euthanizing animals for

measurement at various time points[254]. More recently, near-infrared dyes, such as indocyanine green (ICG)[255]and Cyanine 5.5, have proven to be alternatives when paired with sophisticated imaging hardware[256]. When ICG is unbound, it binds to native proteins and preferentially drains into lymphatics when delivered intradermally [257,258]. However, Weiler et al.[259] recently showed that repeat injections of ICG caused a reduction in lymphatic pump function and an enlargement of the downstream draining lymph nodes, while the dye itself is retained at detectable levels within the injection site for up to 2 weeks. We have recently developed methods to quantify lymphatic pump function and transport non-invasively in the context of various lymphatic and inflammatory insults using rodent models[25,257,259].

Lymphatic vessels are known to be regulated by vasoactive peptides such as angiotensin, serotonin, and endothelin. Endothelin-1 (ET-1) is a soluble secreted protein that is a potent vasoconstrictor of blood and lymphatic vessels. For lymphatic regulation, ET-1 is a potent constrictor of lymphatic vessels isolated from the human thoracic duct[22] and rat mesentery[260]. In addition, ET_b receptors are expressed by lymphatic endothelial cells[261]. Clinical evidence has shown elevated ET-1 levels in synovial fluid and is correlated with the severity of knee osteoarthritis[262,263]. Within the synovium, ET-1 can be expressed by synoviocytes [264].

Articular chondrocytes can express ET receptors, and levels are increased during aging[265,266]. Further, upregulation of ET-1[267] can lead to increased expression of metalloproteinases and thus degradation of cartilage matrix, which occurs in arthritis[268]. Evidence is building that pharmacological inhibition of ET receptors may ameliorate

arthritis progression[185]. However, the implication for ET-1 has been mainly through a direct effect on chondrocytes, and a potential role in clearance mechanisms remains unknown.

In Chapter 3, we applied NIR imaging technology to quantify the clearance kinetics of nanosized PEG-NIR conjugates from rat knees and demonstrated the effect of ET-1 on lymphatic and venous drainage. We hypothesized that there would be a size-dependent clearance of tracers from the joint space. Additionally, we hypothesized that ET-1 would reduce lymphatic mediated uptake while venous drainage would remain unchanged. Thus, the effects of ET-1 on tracer clearance may elucidate its action during arthritis development.

3.2 Methods

3.2.1 Ethical approval

IACUC committees approved this study at the Georgia Institute of Technology (#A15019) and the Veteran's Administration (#V004-15) in Atlanta, GA. Sasco Sprague Dawley rats (Charles River Laboratories) were used for all studies reported herein. Rats (between 3 and 9 months old) were age-matched for each set of experiments.

3.2.2 Reagents

Endothelin-1 (21 amino acids), bosentan, and BQ-123 were purchased from Sigma-Aldrich. 2 kDa PEG and 40 kDa PEG amine were purchased from JenKem Technology.

3.2.3 Synthesis of PEG-NIR materials

2 or 40 kDa PEG amine was conjugated to IRDye 800CW NHS ester (LI-COR Biosciences) according to the manufacturer's instruction (LI-COR). Briefly, a 1:8 molar ratio of NIR dye to PEG was incubated in Dulbecco's Phosphate-Buffered Saline (PBS; Life Technologies) at pH 8.5 for 24 hours at room temperature with gentle stirring. The mixture was lyophilized and stored at -20ºC. PEG-NIR aliquots were thawed and resuspended with sterile 0.9% NaCl for *in vivo* studies.

Increasing concentrations of 40 kDa amine PEG reacted with a fixed concentration of IRDye 800CW NHS ester overnight to determine the optimal PEG ratio to NIR-dye reaction. The reaction mixtures were separated on 8% SDS-PAGE (Bio-Rad), and fluorescent images were captured using the LI-COR Odyssey Infrared Imaging System. Fluorescence was quantified using ImageJ software[269].

3.2.4 Hydrodynamic radius measurements

ET-1 (Sigma-Aldrich), 2 kDa PEG, or 40 kDa PEG were suspended in PBS to a final concentration of 1 mg/mL. The hydrodynamic diameter was measured using Zetasizer Nano ZS (Malvern Instruments Ltd., United Kingdom).

3.2.5 NIR imaging of joint clearance

Sasco Sprague Dawley rats were anesthetized with isoflurane (SomnoSuite, Kent Scientific), and hind limbs were shaved. Intra-articular injections (anterior approach, 4–5 mm depth) were performed into the knee joints using 0.3 mL insulin syringes (Becton

Dickinson). All reagents were diluted in 0.9% sterile saline and co-injected with a total volume of 50 μL in each knee. NIR images of rat knee joints were captured using an in-house, custom-built NIR imaging system[171,257]. The computer-driven system included a cooled EMCCD camera (Evolve eXcelon, Photometrics) attached to a stereomicroscope (Olympus) equipped with NIR bandpass excitation and long pass emission filters and an automated shutter-controlled xenon arc light-source (Sutter Instrument Company). Fluorescence images were captured at various time points with a fixed camera exposure time of 100 ms using MicroManager software[270]. Animals recovered from anesthesia before the next time point was collected (unless otherwise stated). Animals were left ad libitum from time of injection to time of euthanasia.

With this in vivo NIR imaging technique, we quantified the clearance of materials from the knee space can. Using a custom MATLAB (MathWorks) code, the region of interest (ROI) for each image by isolating the 5% most intense pixels. This ROI visually corresponded with the size and position of the knee space. Those pixels within the ROI were then averaged to obtain the mean fluorescence intensity. Increasing the ROI to 10, 15, 20, 25, and 50% most intense pixels yielded similar changes in fluorescence; however, this also increased the number of background (non-fluorescent) pixels and decreased the signal-to-noise ratio. Data points were fitted to a mono-exponential function (Origin software): $f(t) = y0 + A\ e^{(-t/\tau)}$, where y0 is the offset, t is time, A is normalized fluorescence at $t = 0$, and τ is time constant. At a minimum, 5 data points were collected within the first 24 hours. The R^2 ranged from 0.976 to 0.999 with a mean of 0.990 ± 0.002 for mono-exponential fits of 2 kDa PEG-NIR clearance and from 0.979

to 0.999 with a mean of 0.993 ± 0.002 for mono-exponential fits of 40 kDa PEG-NIR clearance. To verify the intra-articular injection technique, 2 and 40 kDa, PEG-NIR was injected into rat knees, and fluorescence and x-ray images were captured using In-Vivo Extreme (Bruker). Fluorescence was captured using a 730 nm excitation bandpass filter and a 790 nm emission long-pass filter with a camera exposure of 5 min. The overlay of the fluorescence and x-ray images showed the dye location relative to the rat hindlimb's skeletal structures.

3.2.6 Lymphatic and systemic biodistribution of particles in rat

Following intra-articular injection of 2 kDa or 40 kDa PEG-NIR into the left knee, rats were asphyxiated with CO_2 at 4 hours post-injection. The bladder was imaged *in situ*. Lymphatic tissues (i.e., lumbar, popliteal, and inguinal lymph nodes) and other systemic organs (i.e., heart, liver, lungs, spleen, and kidneys) were dissected and placed in 24-well plates. Fluorescence images of tissues and organs were captured using an in-house built NIR imaging system with a camera exposure setting of 2000 msec. Quantification of fluorescence was performed using ImageJ software.

To determine if 40kDa PEG-NIR was metabolized in the lymph node, the isolated tissues were solubilized in RIPA buffer (ThermoFisher Scientific), centrifuged at 14,000 rpm for 10 min, and the supernatant was separated on SDS-PAGE. In addition, urine was collected from the bladder, centrifuged at 14,000 rpm for 10 min, diluted in RIPA buffer, and separated on SDS-PAGE.

3.2.7 Statistical analysis

Data were represented as means ± SE. Unless otherwise stated, a one-way ANOVA was performed with Tukey's honest significant difference test (GraphPad Prism version 6.02). A *p*-value less than 0.05 was considered significant. For biodistribution studies, a one-way ANOVA was performed with a Bonferroni test.

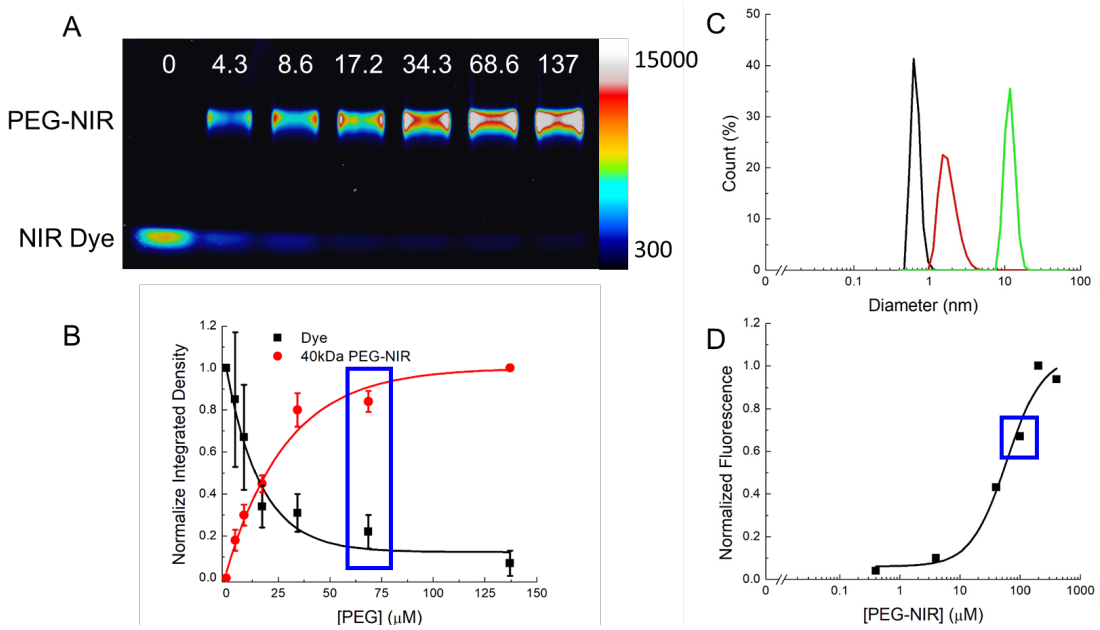

Figure 3 - Synthesis of PEG-NIR conjugates. A: Representative fluorescence image of SDS-PAGE separating IRDye 800CW NHS ester (lower band) and 40 kDa PEG-conjugated NIR dye (upper band). IRDye 800CW NHS ester (8.6 µM) was reacted with differing amounts of 40 kDa PEG and equivalent volume was loaded onto SDS-PAGE. **B:** Integrated density analysis of SDS page gel **C**: Representative measurement of hydrodynamic diameter for ET-1 (black), 2 kDa PEG (red) and 40 kDa PEG (green) using Zetasizer Nano ZS (n = 3). **D**: Representative data of normalized fluorescence for 2 kDa PEG-NIR resuspended in sterile 0.9% NaCl. Data points were fitted to sigmoidal function (solid line). The 100µM concentration (blue square) was used for in vivo studies. Similar profile was found for 40 kDa PEG-NIR.

3.3 Results

3.3.1 Tracer Characterization

To optimize the synthesis of different sized particles from the knee joint, 2 kDa and 40 kDa PEG's were conjugated to near-infrared (NIR) dye via NHS ester reactivity

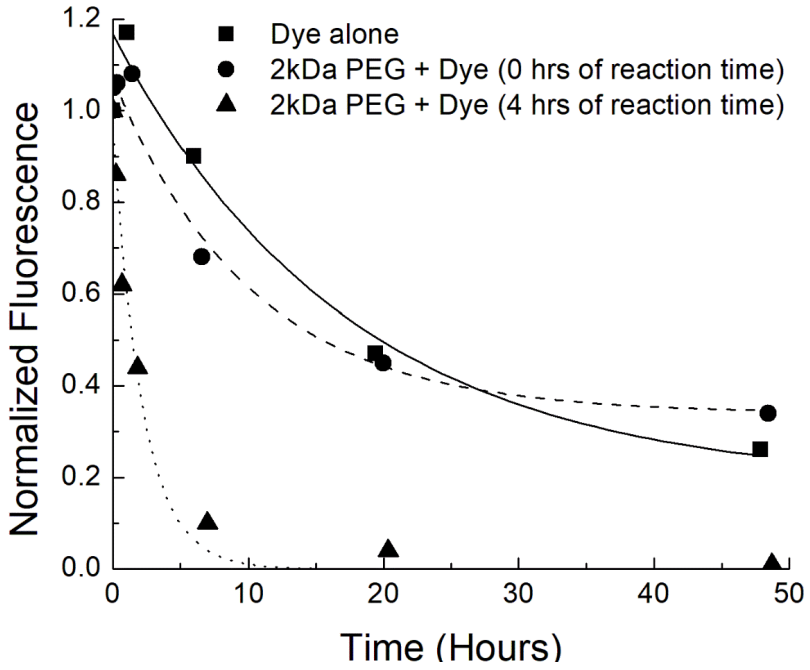

Figure 4 2kDa PEG-NIR clearance was distinct from dye alone clearance rate. Representative data points illustrated the time-dependent clearance of IRDye 800CW NHS ester dye alone (square), IRDye 800CW NHS ester dye in the presence of 2 kDa PEG amine without any reaction time (circle), and IRDye 800CW NHS ester dye in the presence of 2kDa PEG amine after 4 hours of reaction time (triangle). Monoexponential decay fits of the data points are shown for IRDye dye alone (solid line), IRDye dye in the presence of 2 kDa PEG without any reaction time (dashed line), and IRDye dye in the presence of 2kDa PEG after 4 hours of reaction time (dotted line). The conjugation of IRDye 800CW NHS ester dye to 2 kDa PEG amine was a time-dependent reaction and thus, the clearance kinetics of PEG-NIR was altered when conjugation was left for 4 hours. The clearance of dye alone or dye in the presence of 2kDa PEG was similar and thus suggested that free PEG does not alter the dye clearance. Average time constants were 398 min (n = 2), 435 min (n = 3) and 152 (n = 3) for dye alone, for dye with 2 kDa PEG without any reaction time and for dye with 2 kDa PEG after 4 hours of reaction time, respectively.

with the functional amine group. A reaction ratio of 1:8 of IRDye: PEG was found to

maximize PEG-NIR conjugation while minimizing free dye and unconjugated PEG (Figure 3A). The hydrodynamic diameters for 2 kDa PEG and 40 kDa PEG were 2.60 ± 0.18 nm and 11.93 ± 0.33 nm, respectively (Figure 3B). The fluorescence intensities of PEG-NIR dyes were linear within the range of 10 - 200 μM (Figure 3C). At concentrations above 200 μM, the fluorescence intensity of PEG-NIR dyes decreased, which is suggestive of self-quenching (Figure 3D).

3.3.2 Clearance of PEG-NIR from the knee joint

For *in vivo* knee clearance studies, we injected 50 μL of 100 μM PEG-NIR (5 nmol) into rat knees. We captured fluorescence and x-ray images of rat knees before and after intra-articular injection(Figure 5). The dye intensity was highest at the knee joint (immediately after intra-articular injection) and decreased subsequent times. Using our custom-built NIR imaging system, similar changes in fluorescence intensity followed when PEG-NIR particles were injected into rat knee joints. With this system, a camera exposure time of 100 msec was sufficient to assess the fluorescence change of PEG-NIR dyes. When the normalized averaged fluorescence intensity of the top 5% fluorescent pixels were plotted against time(Figure 6), the calculated knee clearance rate (τ) was 170.7 ± 11.0 min for 2 kDa PEG-NIR (n = 10) and 243.2 ± 15.8 min for 40 kDa PEG-NIR (n = 11; $p < 0.005$). The concentration and volume of tracer injected were identical; therefore, the difference in clearance rate was attributed to the difference in size. The clearance kinetics of PEG-NIR was not due to residual free or unbound NIR dye in the mixture. When 2 kDa PEG and NIR dye were not given time to conjugate and injected

into the rat knee immediately (after mixing), the fluorescence signal remained elevated for more than 2 days and exhibited a slower clearance rate (Figure 4). Additionally, 40 kDa PEG-NIR purified through a gravimetric Sephadex column showed similar kinetics as non-purified 40 kDa PEG-NIR. 2 kDa PEG-NIR could not be purified via gravimetric filtration or dialysis; hence for direct comparisons, non-purified NIR tracers were used for this study.

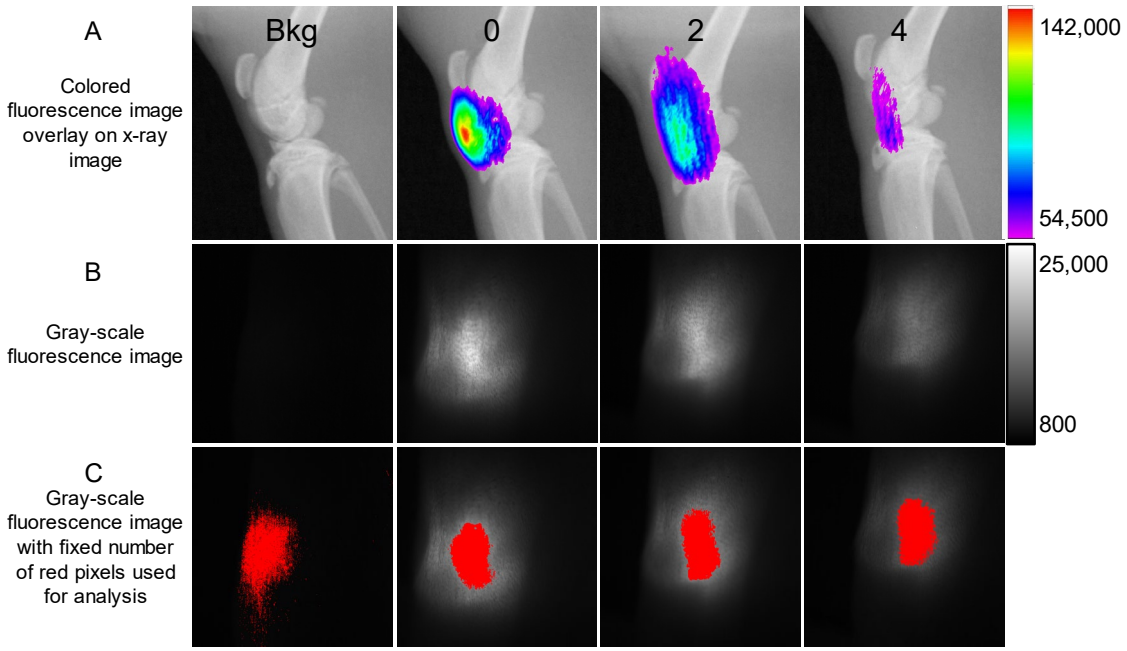

Figure 5 Representative images of near infrared and x-ray images of rat knees with 40 kDa PEG-NIR. Intra-articular injection of 40 kDa PEG-NIR was administered to rat knee. Representative images of rat knee at various time points: before (background, bkg), immediately after 0, 2 and 4 h post dye injection were shown. **A:** X-ray images (black and white) and fluorescence images (pseudo-color) were captured using the In-Vivo Extreme imaging system. **B:** Fluorescence images (gray scale) were captured using a custom- built NIR imaging system. **C:** Same fluorescence images as in B with threshold red region. Threshold region represented the top 5% of pixels with the highest fluorescence intensities.

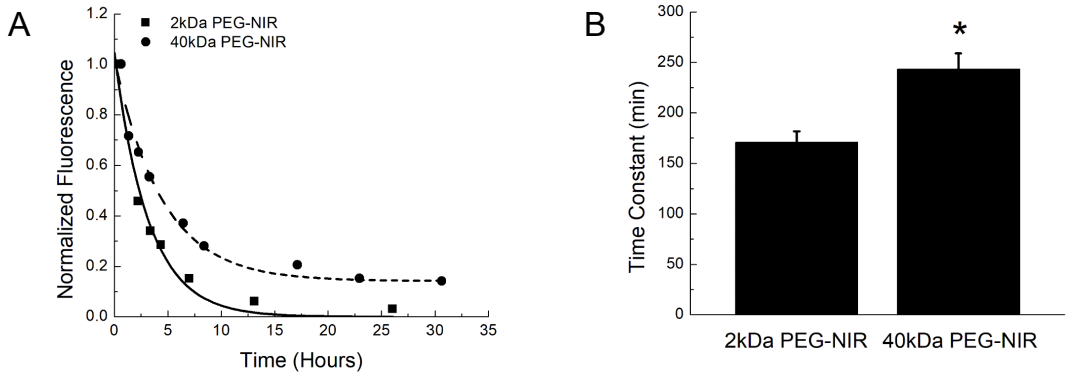

Figure 6 Clearance of conjugates from rat knees. A: A representative clearance curve of 2 kDa (square; 1 representative curve from the 10 animals) and 40 kDa (circle; 1 representative curve from the 11 animals) PEG-NIR from rat knees. Solid and dashed lines were mono-exponential fits to 2 kDa and 40 kDa PEG-NIR data points, respectively. **B:** Average time constant for 2 kDa (n = 10) and 40 kDa PEG-NIR (n = 11; *denoted $p < 0.005$).

3.3.3 Biodistribution of PEG-NIR

Within the synovium, materials may be cleared through capillaries of venous vessels (for particles < 5 nm) and/or through initial lymphatics. Tissues and organs were isolated 4 hours post-injection, a time point where nearly two-third of injected 40 kDa PEG-NIR was cleared from the knee joint to determine clearance pathways of these different sized PEG-NIR conjugate. Fluorescence significantly increased in the left lumbar lymph node of rats injected with 40 kDa PEG-NIR compared to the left lumbar node of naive animals (Figure 7). The lumbar node is known to collect materials drained from the knee joint[137].

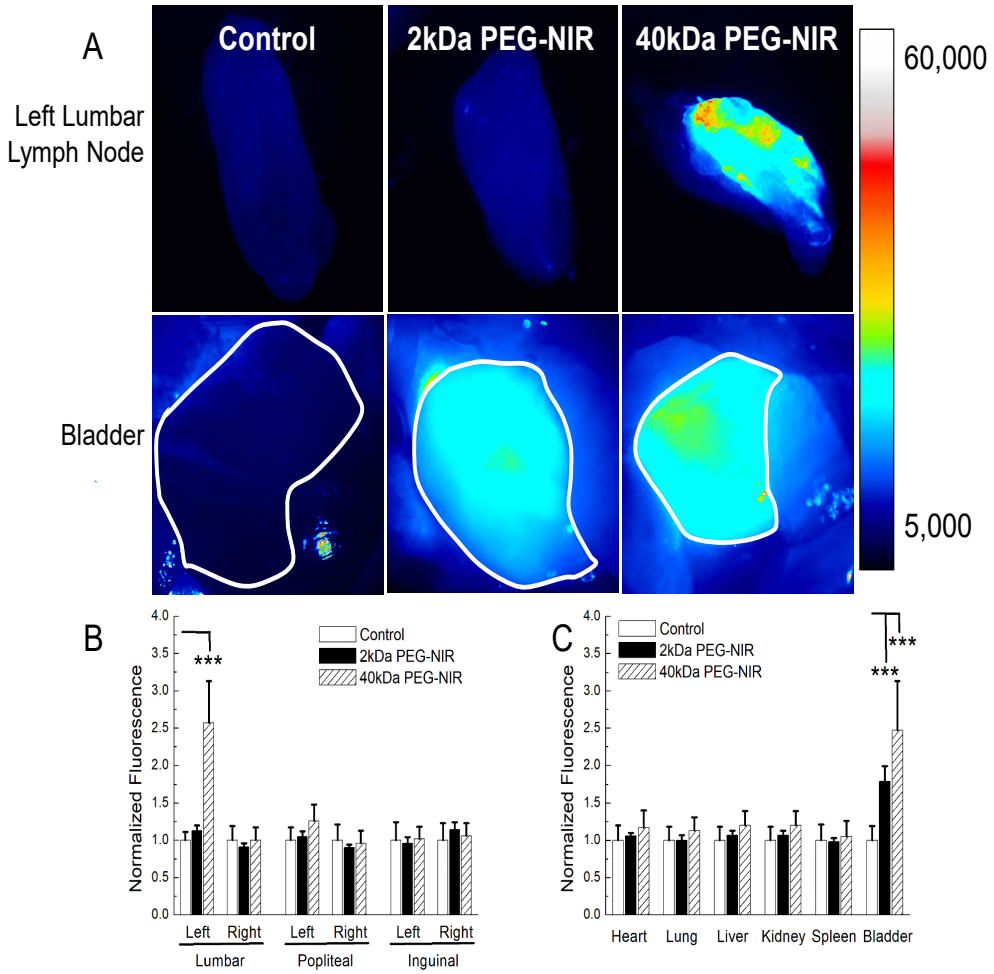

Figure 7 Biodistribution of PEG-NIR from intra-articular injection into rat knees. A: Representative fluorescence images of left lumbar lymph nodes and bladders isolated from rats that were naïve (control) or injected with 2 kDa PEG-NIR or 40 kDa PEG-NIR into left knees. For the bladders, a white border was manually drawn, and this ROI was used to calculate the mean fluorescence intensity for the tissue. Mean fluorescence intensities were calculated for each lymphatic tissues **(B)** and organs **(C)**. Significance was determined using one-way ANOVA and post hoc Bonferroni test with calculated p values to be < 0.001 (***) when compared to respective tissues from naïve animals. **D:** Representative image of SDS-PAGE (n = 4) loaded with solubilized left lumber node (left lane) and urine (right lane) from a rat intra-articularly injected with 40 kDa PEG-NIR into the knee after 4 h.

2 kDa PEG-NIR was not found in the lumbar lymph node, suggesting that this conjugate

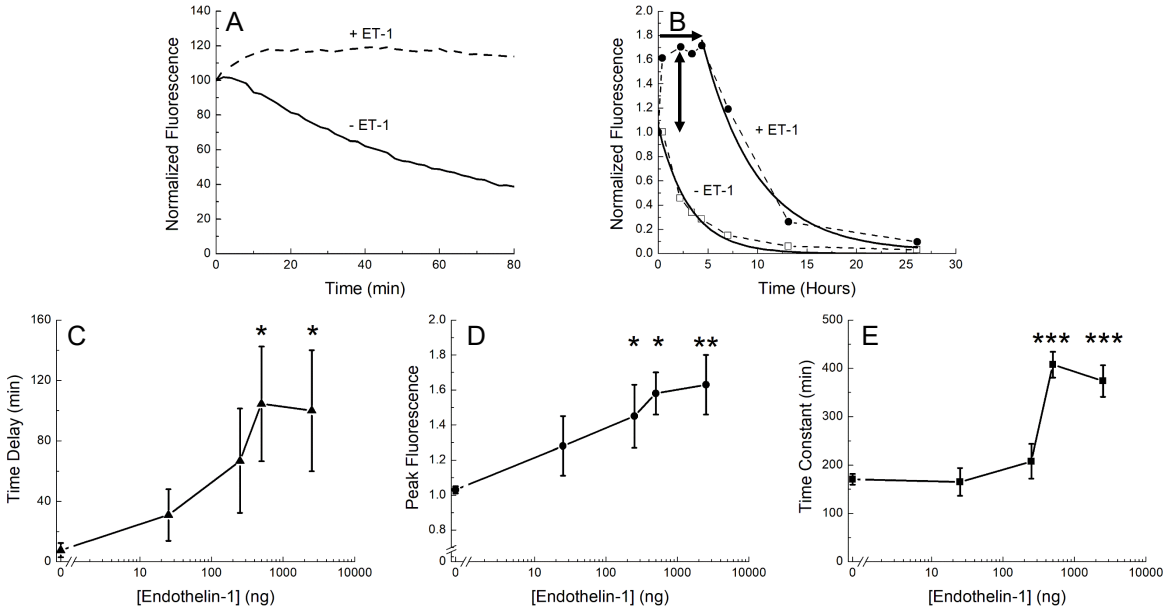

Figure 8 Endothelin-1 dose-dependently inhibited the clearance of 2 kDa PEG-NIR from rat knees. A: Anesthetized rats were injected with 50 µL of 100 µM 2 kDa PEG-NIR in the presence (dashed line) or absence (solid line) of 2.5 lg ET-1. Fluorescence images were taken every 2 min and the rats were kept under anesthesia throughout the 80 min of data collection. **B:** Anaesthetized rats were injected with 50 µL of 100 µM 2 kDa PEG-NIR in the presence (solid circles; 1 representative study from the 6 animals) or absence (open squares; 1 representative study from the 10 animals) of 2.5 lg ET-1. Fluorescence images were taken at each time point and rats recovered from anesthesia in between the time points. Solid lines were mono-exponential fits for the clearance of PEG-NIR. Horizontal arrow (single arrowhead) reflected the measured time delay, and the vertical arrow (double arrowhead) reflected the fold difference in fluorescence. The effect of ET-1 on the time delay **(C)**, peak normalized fluorescence **(D)** and calculated time constant (E) were shown. The number of samples for 0, 25, 250, 500 and 2500 ng ET-1 with 2 kDa PEG-NIR were 10, 6, 6, 4 and 6, respectively. Statistical significance was determined after performing one-way ANOVA with Tukey's test and p values were $<$ 0.05 (*), $\leq$ 0.01 (**) or $\leq$ 0.001 (***).

was not taken up lymphatic vessels or, if so, not retained in the lumbar lymph node. In addition to the lumbar lymph node, increased NIR signals were evident in the bladder for both 2 kDa and 40 kDa PEG-NIR administrations. No change in fluorescence was observed for any other tissues and organs examined, including popliteal lymph nodes,

inguinal lymph nodes, heart, lung, liver, kidney, and spleen. However, for the signal to accumulate in these tissues, the tracer must be retained by some mechanism, either intracellular uptake or retained within the ECM. Therefore the lack of signal does not rule out transport through these tissues.

3.3.4 Endothelin-1 inhibited the clearance of 2 kDa PEG-NIR from the knee joint

ET-1, a potent vasoconstrictor, was co-administered with 2 kDa PEG-NIR (Figure 9). ET-1 (2.5 μg) significantly prevented the clearance of 2 kDa PEG-NIR for up to 100.0 ± 40.0 min ($p < 0.05$). ET-1 caused an increase in fluorescence within the knee space during this initial inhibitory phase with a magnitude of 1.63 ± 0.17 ($p < 0.01$). After the ET-1 induced inhibitory phase, 2 kDa PEG-NIR was cleared with a calculated time constant of 373.7 ± 32.8 min ($p < 0.001$). The effects of ET-1 were dose-dependent *in vivo*. ET-1 effects on peak fluorescence (Figure 8D) were significant at doses as low as 250 ng, suggesting that this parameter may be more sensitive to capturing the biological effects of ET-1 than time delay or time constant.

In a separate group of animals kept continuously under anesthesia after intra-articular injection, the ET-1 effect on peak fluorescence was less pronounced (Figure 8A) than those recovered from anesthesia before collecting the next data point (Figure 8B, E). This finding suggests that joint distention and the subsequent convective transport and diffusion of ET-1 to surrounding tissues may facilitate ET-1 action.

3.3.5 ET-1 inhibited the clearance of 40 kDa PEG-NIR from the knee joint

When ET-1 was co-administered with 40 kDa PEG-NIR, an inhibitory phase

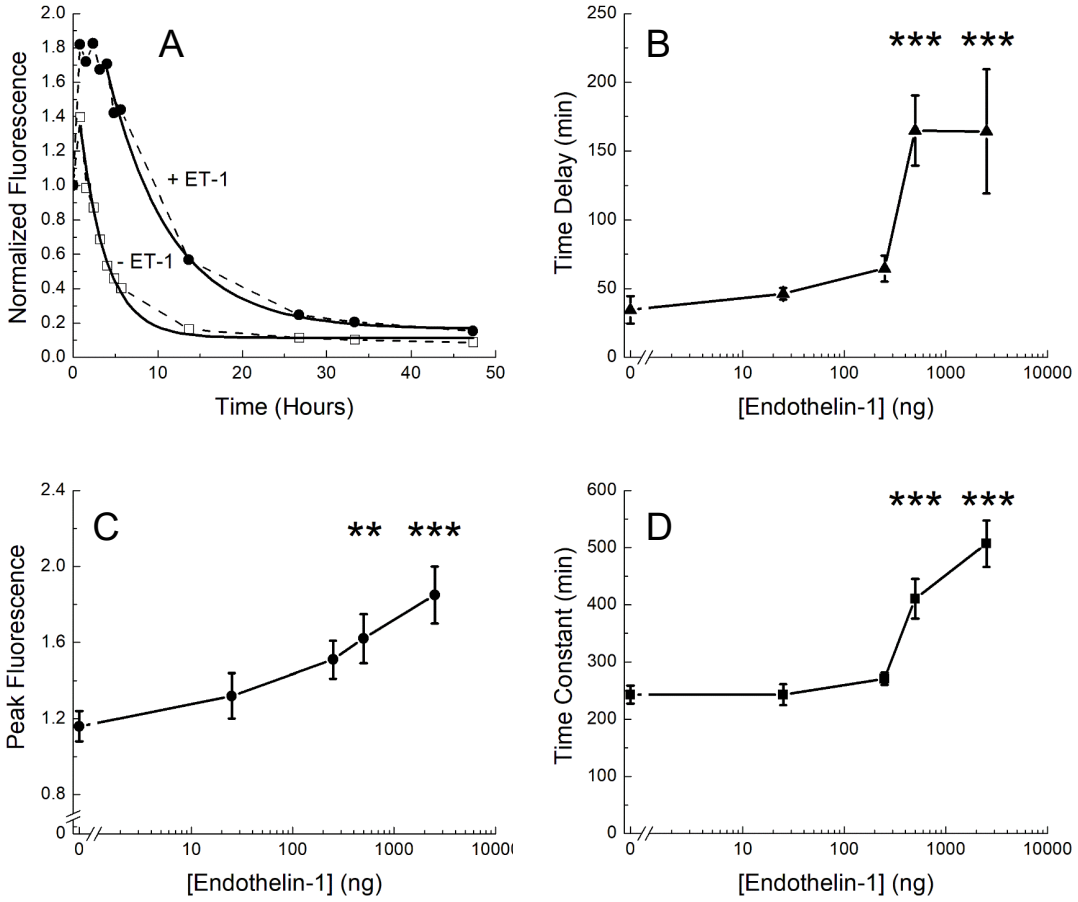

Figure 9 Endothelin-1 dose-dependently inhibited the clearance of 40 kDa PEG-NIR from rat knees. A: Anaesthetized rats were injected intra-articularly with 50 µL of 100 µM 40 kDa PEG-NIR in the presence (solid circles; 1 representative trace from the 6 animals) or absence (open squares; 1 representative trace from the 11 animals) of 2.5 lg ET-1. Fluorescence images of the knee were taken at each time point and rats recovered from anesthesia in between the time points. Solid lines represented mono-exponential fits for the clearance of PEG-NIR. The effect of ET-1 on the time delay (B), peak normalized fluorescence (C) and calculated time constant (D) were shown. The sample size for 0, 25, 250, 500 and 2500 ng ET-1 with 40 kDa PEG-NIR were 11, 6, 6, 7 and 6, respectively. Significance was determined after performing one-way ANOVA and post ad hoc Tukey analysis with calculated p values <0.01 (**) or 0.001 (***).

(Figure 9) was observed for the ET-1 effect on 2 kDa PEG-NIR clearance. The time delay for 40 kDa PEG-NIR with 2.5 µg ET-1 was 164.2 ± 45.2 min, and without ET-1 was 34.5 ± 10.0 min ($p < 0.001$). ET-1 (2.5 µg) significantly increased the peak fluorescence of 40 kDa PEG-NIR from 1.16 ± 0.08 (without ET-1) to 1.85 ± 0.15 ($p < 0.001$). ET-1 co-delivery led to a significantly higher time constant of 506.7 ± 40.6 min for 40 kDa PEG-NIR compared to 40 kDa PEG-NIR alone ($p < 0.001$).

3.4.3 Specificity of ET-1 on knee clearance

To determine the specificity of ET-1, bosentan, a competitive antagonist for both ET_A and ET_B receptors, was co-injected with ET-1 and 2 kDa PEG-NIR (Figure 10). Bosentan blocked the ET-1-induced changes to 2 kDa PEG-NIR clearance. The time constant for 2 kDa PEG-NIR clearance with ET-1 was 408.0 ± 26.7 min, and in the presence of bosentan, it was 153.7 ± 21.7 min ($p < 0.001$), a value that was not significant from the clearance of 2 kDa PEG-NIR alone (164.5 ± 26.9 min). Bosentan did not significantly alter ET-1 effects on time delay and peak fluorescence for 2 kDa PEG-NIR. Co-injection of an antagonist with specificity for the ET_A receptor, BQ-123, also prevented ET-1 induced changes to 2 kDa PEG-NIR clearance.

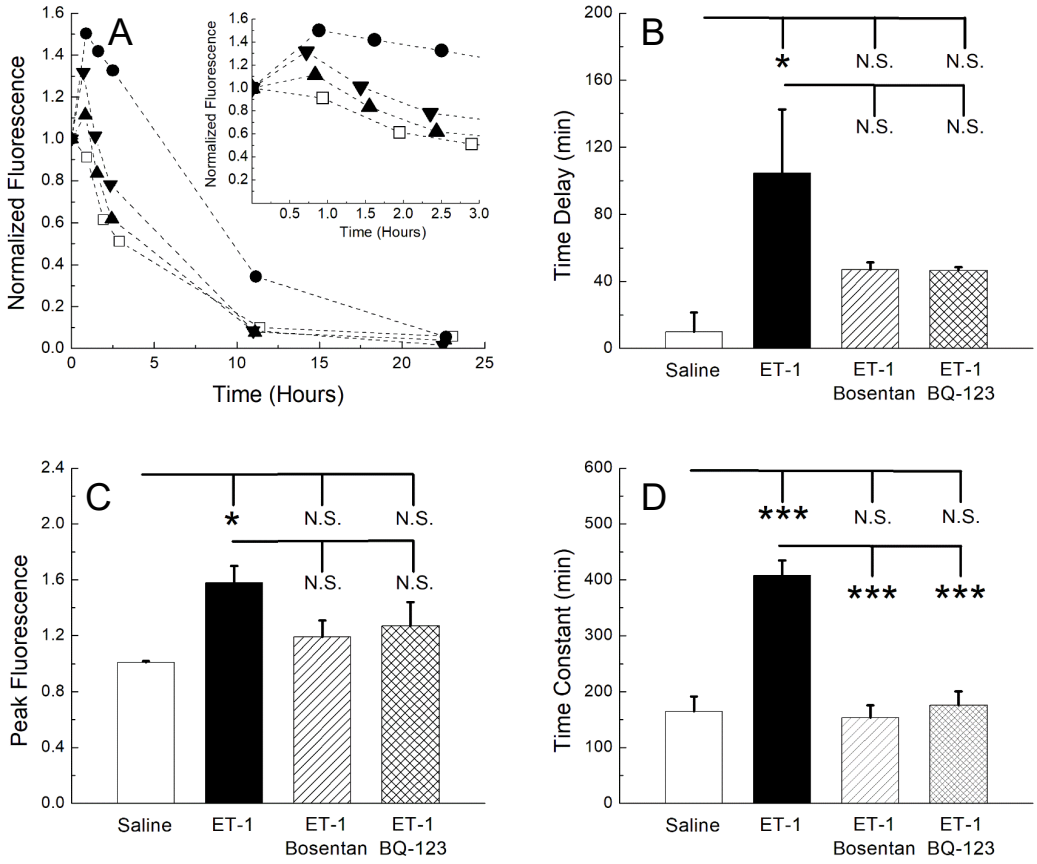

Figure 10 Bosentan and BQ-123 attenuated the effects of ET-1 inhibition of 2 kDa PEG-NIR clearance. A: Data points illustrated the time-dependent clearance of 2 kDa PEG-NIR without (open squares; 1 representative trace from the 4 animals) or with ET-1 (filled circles; 1 representative trace from the 4 animals), with ET-1 and bosentan (solid, upright triangle; 1 representative trace from the 4 animals) and with ET-1 and BQ-123 (solid, inverted triangle; 1 representative trace from the 4 animals). 500 ng ET-1 (0.2 nmol) were challenged with 25 lg bosentan (43.9 nmol) or 5 lg BQ-123 (8.2 nmol). Inset, the effect of ET-1 antagonists on the clearance of 2 kDa PEG-NIR with a reduced time scale (up to 3 h). The effect of bosentan and BQ-123 on the ET-1 induced changes to time delay **(B)**, peak normalized fluorescence **(C)** and calculated time constant **(D)** were shown. For saline, ET-1, ET-1 with bosentan, and ET-1 with BQ-123, n's equaled 4 for each condition. Significance was determined after performing one-way ANOVA and post ad hoc Tukey analysis. Calculated values were considered significant when $p < 0.05$ (*) or 0.001 (***) or were not significant (N.S.) when $p \geq 0.05$

We also assessed the ability of bosentan and BQ-123 to compete against ET-1

effects on the clearance of 40 kDa PEG-NIR. Similar to that found for 2 kDa PEG-NIR, bosentan and BQ-123 significantly prevented ET-1-induced change on time constant (Figure 11D). ET-1 shifted the time constant for 40 kDa PEG-NIR from 220.0 ± 12.8 min to 363.7 ± 17.2 min ($p < 0.001$), and with the addition of bosentan or BQ-123, the time constants were 208.7 ± 18.4 min or 219.3 ± 24.1 min, respectively ($p < 0.001$). Bosentan

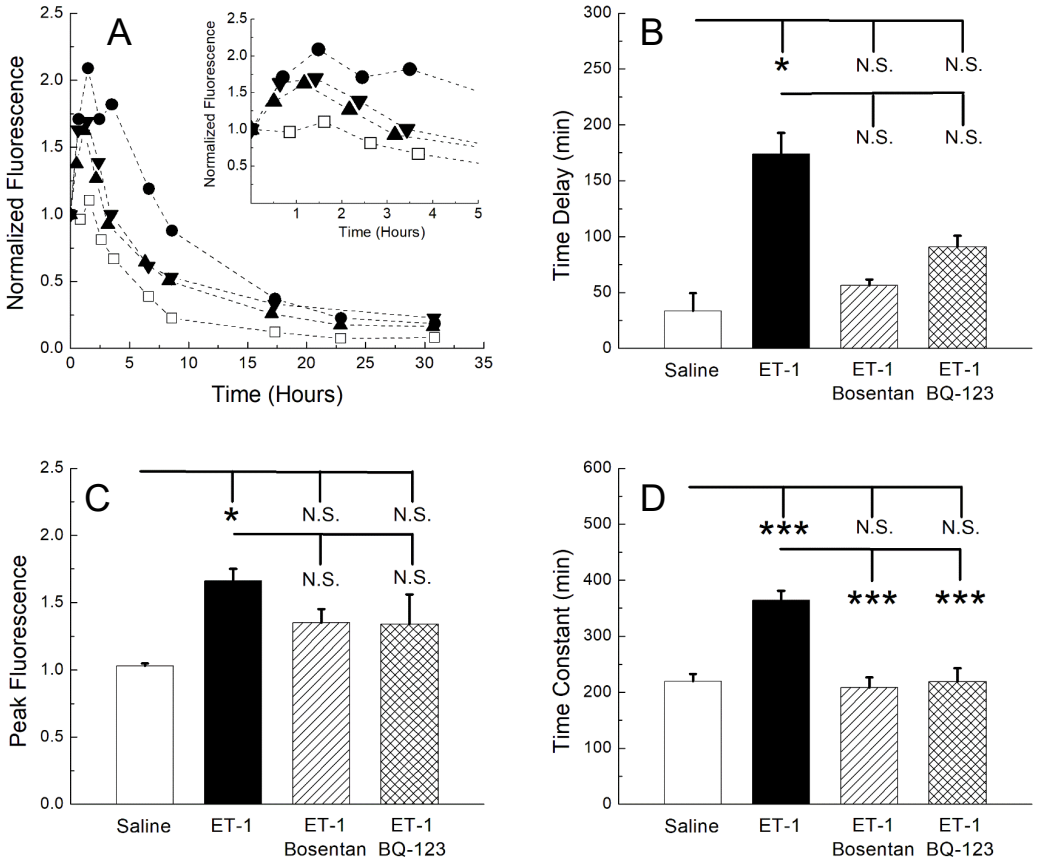

Figure 11 Bosentan and BQ-123 attenuated the effects of ET-1 inhibition of 40 kDa PEG-NIR clearance. **A:** Data points illustrated the time-dependent clearance of 40 kDa PEG-NIR without (open squares) or with ET-1 (filled circles), with ET-1 and bosentan (solid, upright triangle) and with ET-1 and BQ-123 (solid, inverted triangle). 500 ng ET-1 (0.2 nmol) were challenged with 25 µg bosentan (43.9 nmol) or 5 µg BQ-123 (8.2 nmol). Inset, the effect of ET-1 antagonists on the clearance of 2 kDa PEG-NIR with a reduced time scale (up to 5 hours). The effect of bosentan and BQ-123 on the ET-1 induced changes to time delay **(B)**, peak normalized fluorescence **(C)** and calculated time constant **(D)** were shown. For saline, ET-1, ET-1 with bosentan, and ET-1 with BQ-123, n's equaled 8, 11, 6 and 3, respectively. Significance was determined after performing one-way ANOVA and post ad hoc Tukey analysis. Calculated values were considered significant when $p < 0.05$ (*) or ≤ 0.001 (***) or were not significant (N.S.) when $p \geq 0.05$.

and BQ-123 did not have a significant effect on ET-1 induced changes to time delay and peak fluorescence.

3.4 Discussion

The clearance of materials and proteins from the knee joint is critical to normal joint homeostasis; measurement of these processes has historically been performed using radioactive tracers. However, this technique requires collecting synovial fluid samples over time, presenting technical challenges in small animal models like rats or humans where large machinery is required to obtain x-ray or MRI readings. More recently, NIR dyes and imaging techniques have enabled noninvasive longitudinal assessment of in vivo clearance kinetics on a much smaller scale[11,221,271,272]. We employed a near-infrared imaging technique to assess the clearance of nanometer-sized molecules from rat knees. In this chapter, we utilized PEGs as NIR tracking molecules because they are hydrophilic and electrostatically neutral. Thus, they are not likely to bind to ECM proteins of the joint.

Assessment of fluorescence signal from probes injected into the knee joint is an indirect measurement of knee clearance. Over time, the measured fluorescent signal is a net result of diffusion and equilibration of materials within the synovial fluid, IAP, mechanical loading, interstitial pressure due to the pressure gradient formed from the injection, and subsequent removal via the blood or lymphatic microcirculation. One finding reported in this study was the initial rise in fluorescence of either 2 kDa PEG-NIR (usually occurs within 5–10 min) or 40 kDa PEG-NIR (occurs within 30–60 min). This

increase in fluorescence is likely due to the diffusion-assisted equilibration of tracer to areas of synovium closer to the skin. The difference in the peak and time delay as a function of size also supports that this phenomenon is diffusion-driven and not due to other factors. It is unlikely that the rise in fluorescence is due to the dye's unquenching since we are using a PEG-NIR concentration within the linear range of fluorescence detection. Like our findings, Shi et al.[12] also reported a time delay of nearly an hour for ICG clearance in mice knees. ICG predominantly binds to albumin since it is an abundant soluble protein and clear through lymphatics. Also demonstrating that the peak is a size-dependent diffusion-driven process, 200 nm magnetic particles injected in the joint space present a peak intensity over 1-2 days[273].

Materials injected intra-articularly clear by a process where they diffuse through the synovial fluid, pass through the synovial lining, diffuse into the synovium, and are cleared from the joint through capillaries. These processes are effectively calculated together as a bulk parameter, given the inability to characterize each component. The calculated time constant reported herein did not include data points found in the delay (or lag) phase to minimize the initial diffusion differences of 2 kDa and 40 kDa PEG-NIR. We determined that the τ for 2 kDa PEG-NIR is about 1.4 times faster than 40 kDa PEG-NIR from rat knees. Previous studies have quantified the clearance kinetics of materials with a variety of sizes. From Shi et al.[11] published work, we approximate the τ for ICG in mice knees at about ~140 min. Singh et al.[272] calculated the half-life of 500 nm particles designed for drug delivery to be 1.9 days after intra-articular injections into rat knees.

A study recently reported joint clearance and synovial transport of different sized dextran (10 and 500 kDa) in naïve and OA rats; clearance and synovial transport were slower for 500 kDa dextran transport slowed in OA[221]. These findings are consistent with the size-based clearance that we and others have found. A separate study by Loffredo et al.[267] used heparin, a charged molecule, to retain insulin growth factors within the knee joint for a more extended period. Similarly, Bajpayee et al. [254] have shown that charged avidin conjugated to Texas Red is sequestered in articular cartilage and meniscus for days while neutral avidin is cleared within 24 hours. Further, the charged moieties were correlated to the glycosaminoglycan content of various cartilage tissues within the knee joints. The latter two studies injected similar-sized conjugates as 40 kDa PEG-NIR, but the materials had charged moieties, preventing free diffusion and clearance within the knee joint. These studies suggest that both size and charge play a critical role in retaining materials within the joint and can improve biomaterial carrier design and retention of drugs within the knee joint.

Intra-articular injections are becoming a standard minimally invasive approach to deliver various therapeutic ranging from small molecules to cells to tissue derivatives. Various formulations of PEG-based biomaterials have been used as drug carriers to improve drug retention and to increase drug concentration within a localized area[274–276]. For example, PEG hydrogel microspheres have been used to deliver compounds associated with inflammation and were retained for at least a month[275]. These data suggest that increasing the PEG size into the micron range would further influence the clearance kinetics; typically, in peripheral tissues, this size range changes clearance

mechanisms from a passive, diffusion-dominated clearance process to an active, cell-mediated clearance process. Thus, PEG-based delivery provides a platform that can be tailored to many different therapeutics, and as we show here, the retention within the joint space and the subsequent clearance route can be controlled through simple size-dependent mechanisms.

The optimal hydrodynamic diameter range for uptake into lymphatics is 10–100 nm, and anything < 5 nm is readily reabsorbed by blood capillaries[113,277,278]. Our finding in this aim is consistent with this dogma for clearance of nanosized materials into lymph nodes[279]. The 40 kDa PEG-NIR with a hydrodynamic diameter greater than 10 nm was found collected in the lymph node, while 2 kDa PEG-NIR (< 10 nm) was not present in the node. These data suggest that 40 kDa PEG-NIR is cleared by the common pathways through the lymphatic system, as demonstrated in the skin [115]. Increased fluorescence was also found in the bladder when rats were injected with 2 kDa or 40 kDa PEG-NIR, showing that these regents can clear renally.

Interestingly, a significantly higher amount of fluorescence was found from 40 kDa PEG-NIR injected animals from bladders than of 2 kDa PEG-NIR injected animals. This may be due to a higher amount of 2 kDa PEG-NIR being excreted from the animal, which we did not quantify in this study. Regardless, we did not find any free dye or fragmented 40 kDa PEG-NIR in lymph node tissues, suggesting that only intact 40 kDa PEG-NIR was collected by lymphatics.

The role of ET-1 in joint homeostasis is largely unclear. ET-1 levels have been reported to be elevated in the synovial fluid of OA patients[262], and further, the concentration of ET-1 in the synovial fluid is directly correlated to severity and stage of OA disease progression [280]. ET-1 has also been implicated in other bone-related diseases, including rheumatoid arthritis and scleroderma, and abnormalities, such as craniofacial mandible development[185]. ET-1 has been implicated in increased osteoblastic activity in cancerous bone metastases and could be involved in the development of osteophytes in OA[281]. The repeated injection of ET-1 did not appear to have any sustained effect on joint clearance in these animals as only acute changes in drainage were observed, and joints were randomized to ensure any adverse effects of ET-1, if any, would be minimized. In order to understand the effects of ET-1 administration alone on joint health, studies must be done to assess cartilage and bone morphology after acute and prolonged ET-1 exposure either endogenously via lentiviral administration to the joint or exogenously through daily injections.

These reports have led to investigations targeting ET-1 signaling as a potential therapeutic in arthritis development and progression. In an OA rat model, ET-1 antagonist BQ-123 (30 nmol via weekly intra-articular injection) was shown to attenuate OA progression[282,283]. In addition, Donate et al. [284] reported that oral administration of bosentan protected collagen-induced OA in rats. These antagonists prevent the breakdown of articular cartilage in OA since ET-1 is upregulated in chondrocytes during OA and can increase the activity of MMP's.

Our investigation in this chapter provides an alternative role for ET-1 in joint homeostasis by regulating the joint's microcirculation and clearance pathways. We demonstrated that intra-articular injection of ET-1 into rat knees dose-dependently and time-dependently inhibited the clearance of both 2 kDa and 40 kDa PEG-NIR, suggesting a modulation of both venous and lymphatic systems. Thus, it is probable that ET-1 has a general effect on the knee's microenvironment and not specific to blood or lymphatic pathways. Lymph formation itself is a function of the Starlings forces that drive capillary filtration. Thus, any factor that alters local arterial and venous pressure will likely alter lymph formation and lymphatic clearance. The data is unclear to what extent the observed changes in the clearance of the two different sized molecules result from arterial effects, venous effects, lymphatic effects, or some combination. Alterations in the local microcirculation by ET-1 reduced the clearance of both large and small molecules from the joint. Consistent with others, ET-1 can modulate isolated venous and lymphatic vessels[260,285]. Also, the effect of ET-1 is observed within minutes of intra- articular injection, suggesting that ET-1 action is within the localized knee joint. From this finding, we speculate that ET-1 may prevent clearance of inflammatory cytokines during OA, and hence, antagonists of ET-1 would improve knee clearance and thus decrease OA progression.

Similarly, Karlsen et al. [286]have also shown that ET-1 can delay lymphatic drainage from intradermal injection in mice and rats. The transient effect of ET-1 may be explained by its rapid clearance from the knee space since it is smaller than 2kDa PEG. Other factors that may contribute to the transient nature of ET-1 activity are ET receptor

internalization and desensitization[287,288]. In addition, isoflurane may influence ET-1 effectiveness in rat knee joints. We found a decreased response to ET-1 with animals continuously kept under isoflurane anesthesia. Others have reported similar findings where isoflurane can attenuate ET-1 effects on aortic contractions[289], airways of rat smooth muscle contraction [290], and calcium mobilization of cultured smooth muscle cells[290].

There are numerous small molecule inhibitors of ET-1 that are FDA-approved agents used for the treatment of hypertension. Bosentan, a small synthetic molecule, and BQ-123, a cyclic peptide, are competitive blockers of ET-1 receptors. Similar to the established pharmacodynamic profile for these antagonists, we found that bosentan was less efficacious than BQ-123, and hence, a 5.4-fold more molar amount of bosentan was needed to achieve a similar block of ET-1 induced effects as BQ-123. It is noteworthy that inhibition of ET-1 with bosentan (oral administration) ameliorates pain, inflammation, and severity of arthritis-induced cartilage deterioration in a rodent arthritis model [284]. These data suggest that bosentan may improve clearance mechanisms in arthritic knees; improved clearance could normalize joint homeostasis and prevent the accumulation of inflammatory cytokines, proteases, and other mediators of disease progression.

3.5 Conclusions

In this CHAPTER, we demonstrated the use of PEG-NIR tracers for intra-articular clearance. Clearance of PEG tracers from the joint was size-dependent, as

previously shown in the seminal joint clearance papers[111,291]. In addition, ET-1 injected into the knee had a drastic and dose-dependent overall drainage of tracers from the knee space. Given that effusions commonly manifest in OA, fluid drainage in OA may be regulated by microvascular agents and pathological changes in the synovial joint tissue structure and function. Clinical assessments are needed to understand how ET-1 secretion presents in human OA,

CHAPTER 4. MULTICHROMATIC NEAR-INFRARED IMAGING TO ASSESS INTERSTITIAL LYMPHATIC AND VENOUS UPTAKE IN VIVO

4.1 Introduction

In CHAPTER 3, we demonstrated that NIR imaging could be used to detect differences in clearance in the presence of a known effector of vascular function ET-1. In this CHAPTER, the objective was to use NIR imaging to assess venous and lymphatic clearance simultaneously. This chapter is adapted from the following manuscript, which is currently in review and can be accessed at: Bernard, F. C. et al. Multichromatic Near-Infrared Imaging to Assess Interstitial Lymphatic and Venous Uptake *In Vivo*; bioRxiv 2021.03.07.434298 (2021). doi:10.1101/2021.03.07.434298

The circulatory system maintains tissue homeostasis by delivering nutrients and oxygen to the tissue space and removing proteins and waste products. Crucial to this process is removing interstitial fluid, proteins, and lipids by the lymphatic vasculature; this fluid then returns to the circulation through absorption at the lymph nodes and delivery to the central venous system through the lymphatic ducts[128]. Generally, there are two routes of fluid clearance from tissues: 1) venous uptake and 2) lymphatic uptake. Venous return in tissue beds is passive, size-dependent, and varies based on capillary physiology[101,292]. In contrast, lymphatic capillaries originate from the tissues and have flap-like openings, which non-discriminately allow molecules of all sizes to enter. The

extrinsic motion of the surrounding tissue, combined with the intrinsic contractility of downstream lymphatics, creates transient pressure gradients that allow fluid and macromolecules to enter the vessel and be transported downstream. Impaired interstitial fluid clearance has been implicated in various diseases, including lymphedema[129], cancer[293], and arthritis[294]. Techniques to measure clearance kinetics from interstitial spaces are critical to evaluating disease states and different tissues' ability to drain molecules from the interstitial spaces. These measurements have been assessed classically via radiolabeled agents, which carry potential toxicity and require additional safety measures [295–297]. However, the advent of near-infrared (NIR) fluorescent imaging allows for cost-effective, high resolution, clinical and preclinical imaging in various applications[298–300].

NIR-based technologies have advanced considerably in the last decade—both in terms of imaging components and tracers and fluorophore-based probes—which have allowed for significant new *in vivo* capabilities. The NIR imaging window includes the visible and infrared light spectrum from 650-1300 nm, which due to longer wavelengths, penetrates tissues deeper than higher energy light[301–303]. Contrast agents like indocyanine green (ICG), polyethylene glycol (PEG) conjugated with NIR dyes, or NIR quantum dots have been used to visualize lymphatics and blood vessels *in vivo* [257,259,304–306]. Preclinical NIR imaging has also previously enabled the measurement of tracers' differential uptake as a function of size from different tissue beds[221,304]. In addition, multichromatic NIR imaging (e.g., imaging with multiple NIR fluorescent probes) empowers mapping of the drainage zones of lymph nodes in rodents[306–308]. However, this has not yet been widely

extended to differentiate between venous uptake and lymphatic uptake simultaneously in the same tissue bed.

In CHAPTER 3, the size-dependent uptake of 2 and 40 kDa NIR PEG into the venous and lymphatic circulation was validated, and we demonstrated that the intra-articular injection of endothelin-1 (ET-1), a vasoactive compound in lymphatics and veins, transiently reduced the outflow of both PEG tracers from the joint in a dose-dependent manner. Due to these experiments' monochromatic nature, we were unable to assess lymphatic and venous drainage simultaneously. The inability to differentiate clearance mechanisms and function between the venous and lymphatic systems is a critical technological gap that has broad implications for many different tissues and disease states. Coupling *in vivo* delivery with multichromatic NIR imaging could allow for the advancement of understanding how the venous and lymphatic drainage may change in the context of diseases or physical interventions. The objective of this CHAPTER was to develop a novel technological approach that couples NIR imaging with the size-dependent clearance of tracers *in vivo*. We hypothesized that a multichromatic imaging approach for differentially imaging the lymphatic and venous systems would show the technique's utility in both the mouse tail, where the superficial vessels can be visualized, and assessed in the rat knee, where joint uptake occurs slowly and in deeper tissue structures. Additionally, we perturbed the joint microenvironment by exercising the rats on a treadmill and detected venous and lymphatic clearance changes within the knee joint. We hypothesized that exercise would increase venous and lymphatic clearance from the joint in naïve animals.

4.2 Methods

4.2.1 Tracers for in vivo injection

IR Dye 800CW carboxylate (free dye) (LI-COR Biosciences) was purchased as a dry lyophilized powder. 20 nanomoles were resuspended in 100 µl of sterile saline to make a 20 mM stock solution and used within a few days of resuspension. For tail injections, 2.5 µl of the stock solution was used. For tissue phantom studies and knee injections, the stock solution was diluted to 0.4 mM in sterile saline.

40 kDa methoxy polyethylene glycol (PEG) amine (JenKem Technology) was purchased as a dry lyophilized powder for PEG tracer synthesis. To conjugate 40 kDa PEG amine to IR Dye 680RD, 16 mg of PEG amine was reacted with 30 µl of 10 mg/mL IR Dye 680RD NHS ester (diluted in dimethyl sulfoxide (DMSO)) in a total of 1 mL of Dulbecco's Phosphate-Buffered Saline (DPBS) overnight. Unreacted IR Dye, salts, and DMSO were removed via centrifugal filtration using deionized water and 10 kDa molecular weight cutoff centrifugal filters (Amicon Ultra). After centrifugation, the purified tracers were separated into ten equal volumes of 100 µl and aliquoted to 1.6 mg of tracer per aliquot, lyophilized, and kept frozen at -20°C for long term storage. For tail injections, aliquots were resuspended in 100 µl of sterile saline, and 2.5 µl of P40D680 was injected intradermally. For tissue phantom studies and knee clearance studies, aliquots were diluted to 1 mg/mL.

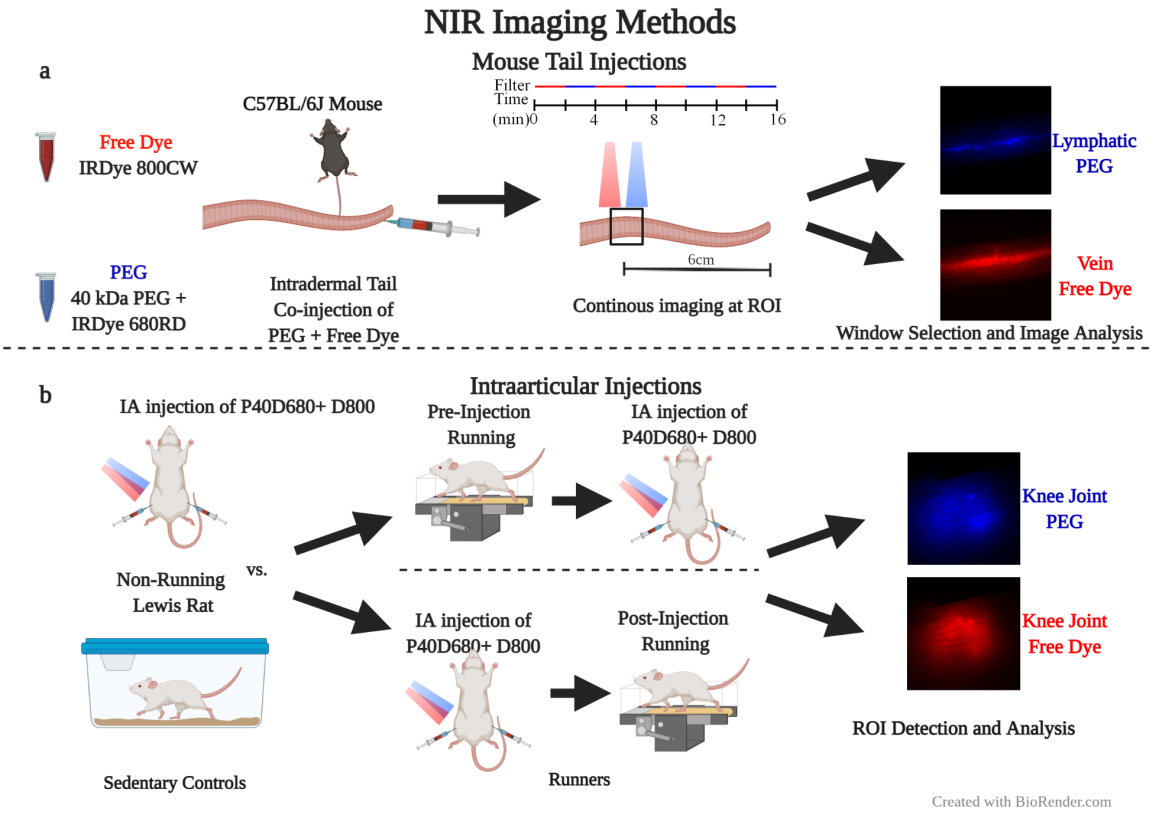

Figure 12 a. Mouse tail injection and imaging methods. **b.** Intra-articular injections for assessing the effect of exercise.

4.2.2 Optical properties of tracers

To quantify each tracer's absorbance in the visible and NIR range, 0.4 mM, 1 mg/mL of the free dye, and 1mg/mL of PEG were loaded into a standard UV/vis spectrophotometer (Ultraspec 2100, Biochrom). The emission and excitation spectra of free dye and PEG were assessed using a microplate reader with filter-based emission and detection capabilities (Synergy H4, BioTek). For PEG and free dye, fixed emission filters

of 720 and 840 nm were used while sweeping the excitation source from 400 – 700 and 400 – 820 nm, respectively, to generate excitation curves. Following the excitation sweeps, fixed excitation wavelengths of 660 and 760 nm were used to conduct an emission sweep from 680/780 – 900 nm for PEG and free dye.

4.2.3 NIR imaging setup

Multichromatic NIR imaging was carried out using a customized NIR setup[171,304]. Briefly, the system consists of a cooled EMCCD camera (Evolve eXcelon, Photometrics) attached to a stereomicroscope with adjustable zoom (MVX10, Olympus), a shutter-controlled xenon arc light source (Lambda LS, Sutter Instrument Company), and a manual filter wheel equipped with standard Cy5.5 and ICG-B filter cubes (Chroma Technology). The electronic shutter was left open during continuous imaging sessions, and images were acquired using MicroManager software[270].

4.2.4 Dye and tracer characterization and tissue phantom studies

Polydimethylsiloxane (PDMS) tissue phantoms, measuring 2 and 4 mm in thickness, were created using a previously described protocol[257]. By weight, 88.10% silicone elastomer base (Sylgard 184, Dow Corning) was mixed with 8.81% curing agent (Sylgard 184, Dow Corning), 1.76% Aluminum Oxide (Sigma Aldrich), and 1.32% cosmetic powder (Max Factor Crème Puff Deep Beige 42). PDMS phantoms were poured into plastic molds and left to cure in the oven at 60°C overnight.

To obtain reference measurements for our NIR imagine setup, stock PEG and free dye were diluted serially in two-fold dilutions in PBS. In separate 1.5 mL centrifuge

tubes, free dye and PEG were diluted using PBS to 0.4 mM and 1 mg/mL. The tissue phantoms were used to demonstrate the effect of tissue depth on tracer intensity with the previous serially diluted samples. Each centrifuge tube was imaged with no tissue phantom or a 2- or 4-mm tissue phantom to simulate increasing tissue depth. Each tracer was diluted using the stock solution of the other tracer to quantify the sensitivity to each tracer in the presence of the other NIR tracer. The 2 mm tissue phantom was used to mimic the typical depth of the superficial collecting lymphatics in rodents. All images were taken with an exposure time of 50 and 5 milliseconds, respectively, for free dye and PEG.

4.2.5 Tail injections to visualize and quantify routes of tracer clearance

To visualize the tail lymphatics and blood vessels, 20 µl of 1% (w/v) Evans blue solution was injected into the tip of the tail of an anesthetized mouse. Evans blue binds to interstitial proteins and is mainly taken up by lymphatics when injected intradermally. Post-euthanasia, the skin was removed at the base of the tail to reveal the underlying vasculature. Images of the vasculature were taken using a standard color camera to provide a comparison with NIR images. For NIR imaging through the skin, isoflurane was used to anesthetize C57Bl/6J mice, and the animal was placed in a recumbent position (on its side). A mixture containing 2.5 µl of the free dye and 2.5 µl of PEG was mixed and loaded into 1 mL insulin syringes (Becton Dickinson) and injected intradermally into the tip of the tail. After injection, standard laboratory tape was gently applied to the base and the end of the tail to minimize drift from motion artifact during imaging. Free dye and PEG signals were imaged in 2-minute increments by manually

changing the filter wheel to select the appropriate filter set every 1200 frames (**Figure 12**a). The free dye and PEG signal were evaluated at 50 and 20 milliseconds, respectively, and images were captured at ten frames per second.

Animal care and experiments were conducted under the institutional guidelines of the Georgia Institute of Technology. Experimental procedures were approved by the Georgia Institute of Technology Institutional Animal Care and Use Committee (IACUC).

4.2.6 Intra-articular injections for clearance

Male Lewis rats weighing 350-400 grams were trained to run on the treadmill over two weeks. On day one, the rats were acclimated to the treadmill for 30 minutes without running. On day two, the treadmill speed was set to 5 m/min for 5 minutes and 0 m/min for 25 minutes. The time spent running was increased by 5 minutes a day until the rats could run for 30 minutes on consecutive days after two weeks. Rats that failed to walk the targeted duration twice over the training course were excluded from the study. All other rats were randomly selected for the experimental procedure to either run or serve as controls for the study duration. Three sets of experiments were conducted with these two rat groups: 1) rats that did not run on the treadmill and were co-injected bilaterally with NIR tracers (No Running), 2) rats that were run on the treadmill for 30 minutes before injection (Pre-Injection Running), 3) rats that were run on the treadmill for 30 minutes immediately after injection (Post-Injection Running).

The day before the experiment, all rats were anesthetized, the hair was removed from the knees and lower abdomen, and background images of the knees were taken. Before imaging, each rat was induced via 5% isoflurane on the day of the experiment,

which was maintained at 2% after induction. Tracers were injected in both knees and imaged at set time intervals (approximately 0, 1, 2, 3, 5, 7 12, & 24 hours) over the course of 24 hours.

Animal care and experiments were conducted per the institutional guidelines of the Atlanta Veteran Affairs Medical Center (VAMC). Experimental procedures were approved by the Atlanta VAMC IACUC.

4.2.7 Image processing and analysis

Images captured using our custom NIR imaging system were saved in 16-bit depth 512 x 512-pixel TIF file format. For both tissue phantom experiments and *in vivo* knee joint clearance experiments, the tracer's intensity in the image was quantified using a custom MATLAB (MathWorks) script. The ROI for each image was quantified by averaging the 5% highest pixel intensities. This ROI visually corresponded with the size and position of the knee space shown in Figure 13b. Data points were fitted to a monoexponential function $f(t) = y0 + Ae^{-kt}$, where y0 is the offset, t is the time in hours, A is the normalized peak fluorescence at the maximum intensity, and k is the time constant. τ (tau) was determined as the inverse of the time constant. To compare each intervention's short-term effects, we calculated the mean change in ROI intensity over the first hour and subtracted the mean value of internal control rats. To determine each intervention's overall effects, we calculated the time constant for each runner and normalized it to the non-runner group's mean.

For mouse tail injections of NIR dyes, the filter was changed manually every 2 minutes. To remove imaging artifacts from the manual changing of the filter, 60 seconds

(600 frames) of each imaging window were cropped. Fiji software was used to crop, register, and quantify regions of interest (ROIs)[269]. An ROI was drawn on the blood and lymphatic vessels to monitor the signal of free dye and PEG over the experiment.

4.2.8 Data presentation and statistics

All clearance data are presented as mean ± SEM. A Brown-Forsythe test was used to quantify if variances were significantly different. A student's t-test with a Welch's correction was used to compare the venous and lymphatic area under the curve and tau in control rats. A one-way ANOVA with Dunnett's multiple comparison test was used to calculate statistical significance for exercise studies.

4.3 Results

4.3.1 Optimization and characterization of NIR tracers using an in vitro tissue phantom

Absorbance spectra of free dye and PEG display an absorption maximum of 765 nm and 672 nm, respectively (Figure 13a). Emission and excitation spectra for these tracers also show each tracer's expected maxima referenced to the full-width half maximum of the filter sets on the imaging system (Figure 13b). We used tissue phantoms to determine the limits of detection in our imaging system as a function of concentration and tissue depth. Individual tracers were imaged in 1.5 mL centrifuge tubes with and without 2- and 4-mm phantoms. Increasing the tissue phantom thickness decreased the fluorescent intensity, though even at 4 mm, the dyes could be detected at a concentration of 3% of the injection concentration (Figure 13c). At a thickness of 2mm, which is within

the depth of most superficial lymphatics in rodents, this detection limit was less than 1% of the injection site's intensity. Notably, mixing the tracers did not affect the sensitivity to

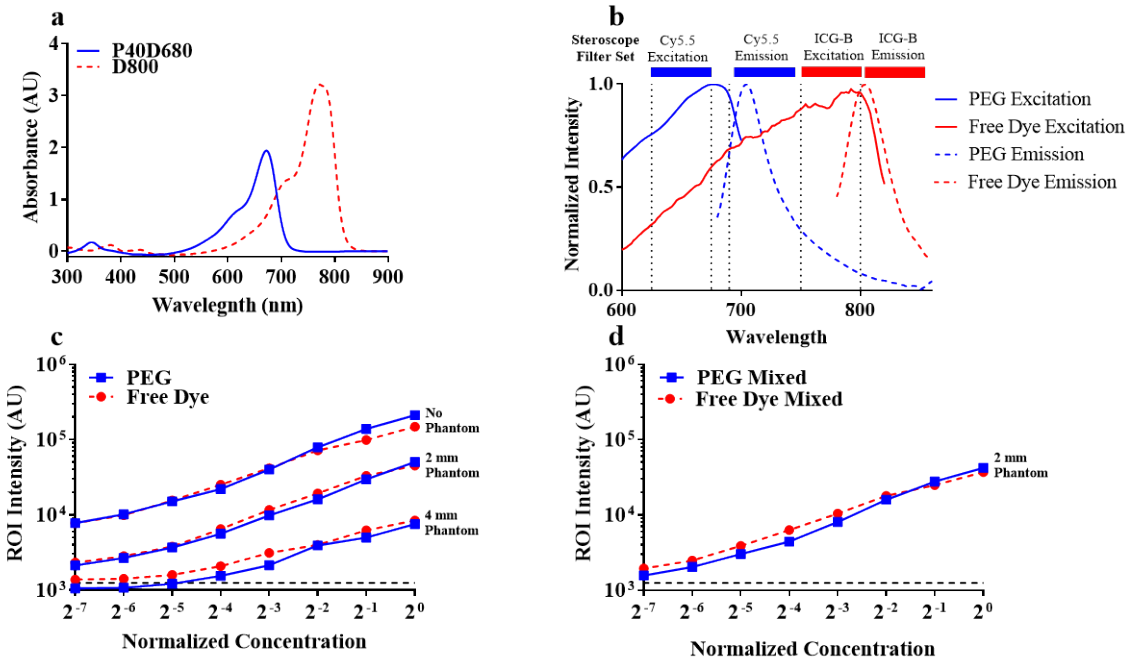

Figure 13 Sensitivity Analysis of Near-Infrared Dyes with Tissue Phantoms
a. Absorbance spectra show a unique absorption profile for each tracer. **b.** Solid and dashed lines show the excitation/emission spectra for 800CW carboxylate (free dye) and 680RD 40 kDa PEG (PEG), respectively. Our NIR stereoscope filter cube setup is represented by the bars above the graph, showing that our optical configuration is designed to read each tracer's unique signal. **c.** Tissue phantoms used to determine the effect of tissue depth on detecting free dye and PEG showed reduced intensity as a function of phantom depth and serial two-fold dilution. Consequentially, we were able to see a reduction in signal intensity below the background (dotted line) and, therefore, could reach the limit for these tracers at this tracer at 25 ms exposure and 100 ms exposure time respectively, using a 4 mm tissue phantom. **d.** Free dye was serially diluted using a stock solution of PEG and vice versa. There was no change in overall intensity and sensitivity for each tracer due to mixing and imaging in a 2 mm phantom.

detect one dye when contained in the background of the other tracer (Figure 13d).

4.3.2 NIR tracers of different size exit through spatially distinct clearance pathways

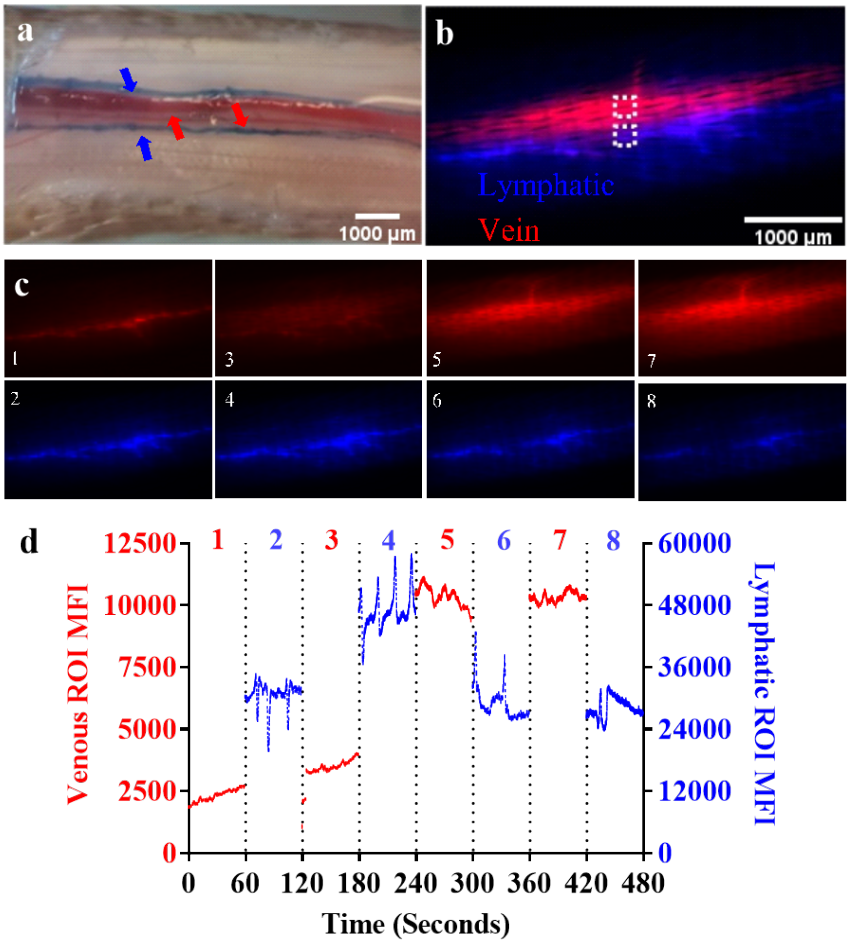

Figure 14 Co-injection of NIR tracers results in differential uptake of 800 CW Carboxylate and 680RD PEG 40 kDa Evans blue dye injected into the tail of a mouse immediately before euthanasia shows the concentration of Evans blue dye in the lymphatics (blue arrows) that flank the blood vessels (red arrows) (scale bar = 1000 um). b. Free dye and PEG show the uptake of each NIR tracer in vein and lymphatics 10 minutes post injection (scale bar = 1000um). c. Free dye can initially be seen in the lymphatic; however, over time free dye concentrates in the circulation revealing the tail vein. PEG shows the sustained uptake of PEG dye into lymphatics. d. Measurement of signal intensity over the course of the four imaging windows for each respective tracer shows large phasic lymphatic contractions for the PEG tracer and increasing free dye signal over time.

The mouse tail's unique circulatory and lymphatic vasculature was visualized via Evans blue and skin removal intradermal injection. The lymphatics immediately cleared Evans blue allowing clear visualization of the two lymphatic vessels running parallel to

the tail vein and artery (Figure 14a). To simultaneously quantify lymphatic and venous drainage, these tracers were co-injected in the mouse tail. Images for each tracer were captured during two-minute imaging windows (eight recordings per tracer). Figure 14b shows that the routes of clearance of free dye in the blood circulation (red) and PEG dye in the lymphatics (blue) 10 minutes post-injection are spatially distinct and match the expected physiology where two lymphatic vessels flank a blood vessel. The free dye was initially detected in the lymphatic within the first imaging window (Figure 14c), as the free dye is not expected to be excluded by lymphatics. The free dye intensity increased between the first, third, and fifth imaging windows and remains constant by the seventh (Figure 14). However, PEG entered the lymphatics after injection and did not appear in the bloodstream over this time interval, demonstrating the lymphatic specificity of PEG (Figure 14c). Also, the lymphatic tracer exhibited strong transient peaks in the signal intensity due to intrinsic phasic lymphatic contractions. In contrast, no such peaks were present in the tracer taken up into the blood circulation.

4.3.3 Co-injection to assess differential tracer clearance in the joint

The effect of exercise on intra-articular clearance has not been extensively studied[122,124], specifically in quantifying the change in venous and lymphatic drainage. Therefore, after confirming size-dependent uptake from the tail, we used multichromatic imaging to assess intra-articular drainage. Unlike intradermal injections, materials from the joint space clear much slower[253,286,309]; therefore, venous and lymphatic clearance from this interstitial depot was expected to occur over one day. Simultaneously injected tracer clearance PEG and free dye profiles (Figure 15a) exhibited an initial increase

followed by monoexponential clearance kinetics consistent with previously reported figures[114]. Specifically, lymphatic tracers showed a more substantial increase in intensity after the injection, whereas this increase was less pronounced for the venous tracer. By 12 hours post-injection, the intensity of the free dye was not detectable (Figure 15a). The normalized area under the curve (AUC) for free dye was calculated to be 3.59 ± 0.18 and 18.57± 1.33 for PEG ($p<0.0001$), demonstrating significant retention of the PEG in the joint space (Figure 15b). The time constant (Tau) for the clearance of free dye was calculated to be 4.28 ± 0.25 hrs, while the time constant for PEG was 7.11 ± 0.51 hrs ($p=0.0003$) (Figure 15c). A detectable amount of the PEG tracer remained in the joint space even after 24 hours (Figure 15a), likely due to some PEG tracer remaining trapped in the interstitium.

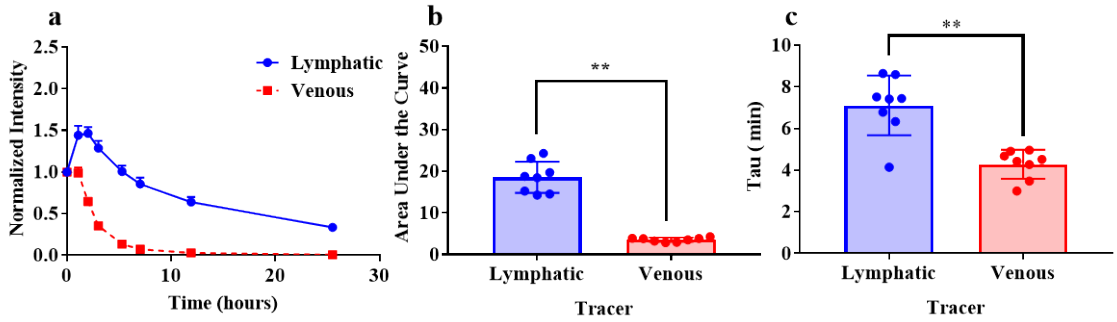

Figure 15 Co-injection of NIR tracers allows for the simultaneous detection of lymphatic and vascular mediated clearance from the joint space.
a. Clearance profiles for PEG and free dye show the characteristic lymphatic and venous clearance, respectively. **b.** The areas under the curves show a significantly lower AUC for free dye compared to the PEG. **c.** First-order clearance constant tau was calculated for each tracer and is significantly higher for the lymphatic draining PEG vs the venous draining free dye.

4.3.4 Multichromatic imaging for measuring patterns in joint clearance

Rats were exercised pre-or post-injection to demonstrate the utility and sensitivity of multichromatic imaging to evaluate differential changes in clearance mechanisms. In rats that received no running intervention, clearance curves for both lymphatic and venous tracers had clearance profiles as expected. (Figure 16a). Qualitatively, there did not appear to be differences in the traces of designated runners and control animals from the initial injections. Therefore, the normalized changes in fluorescence intensity were calculated (Figure 17a, c) and the time constant (Figure 17b, d) to quantitatively evaluate these differences.

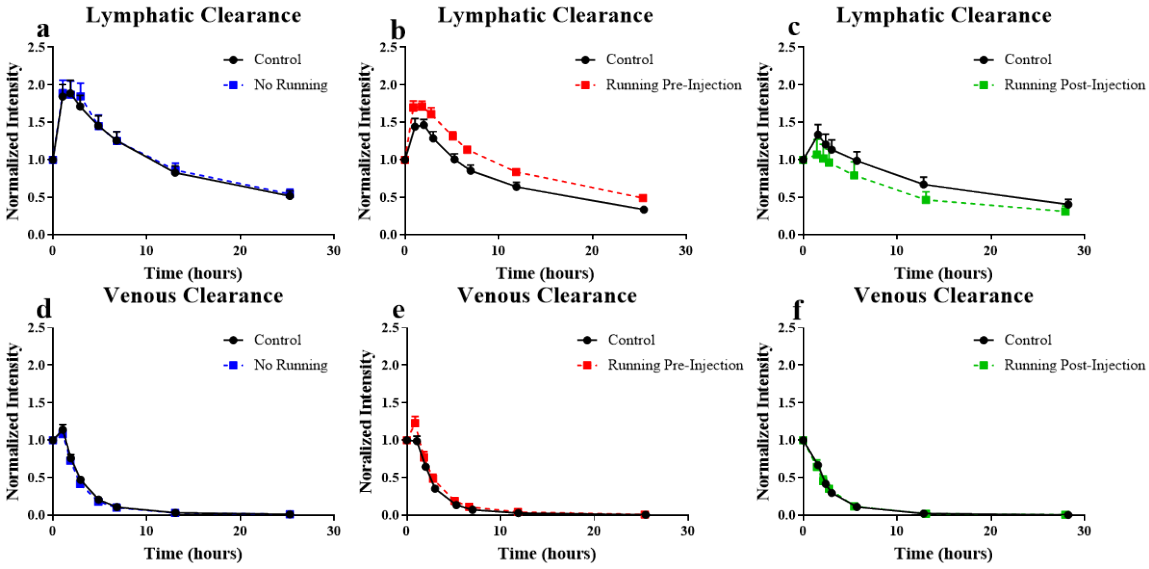

Figure 16 Clearance Profiles for PEG and free dye with running.
a-c. Clearance profile of lymphatic specific tracer (PEG) for no running, pre-injection running and post-injection running experiments. **d-f.** Clearance profile for venous draining (free dye) for No running, pre-injection running, and post-injection running experiments.

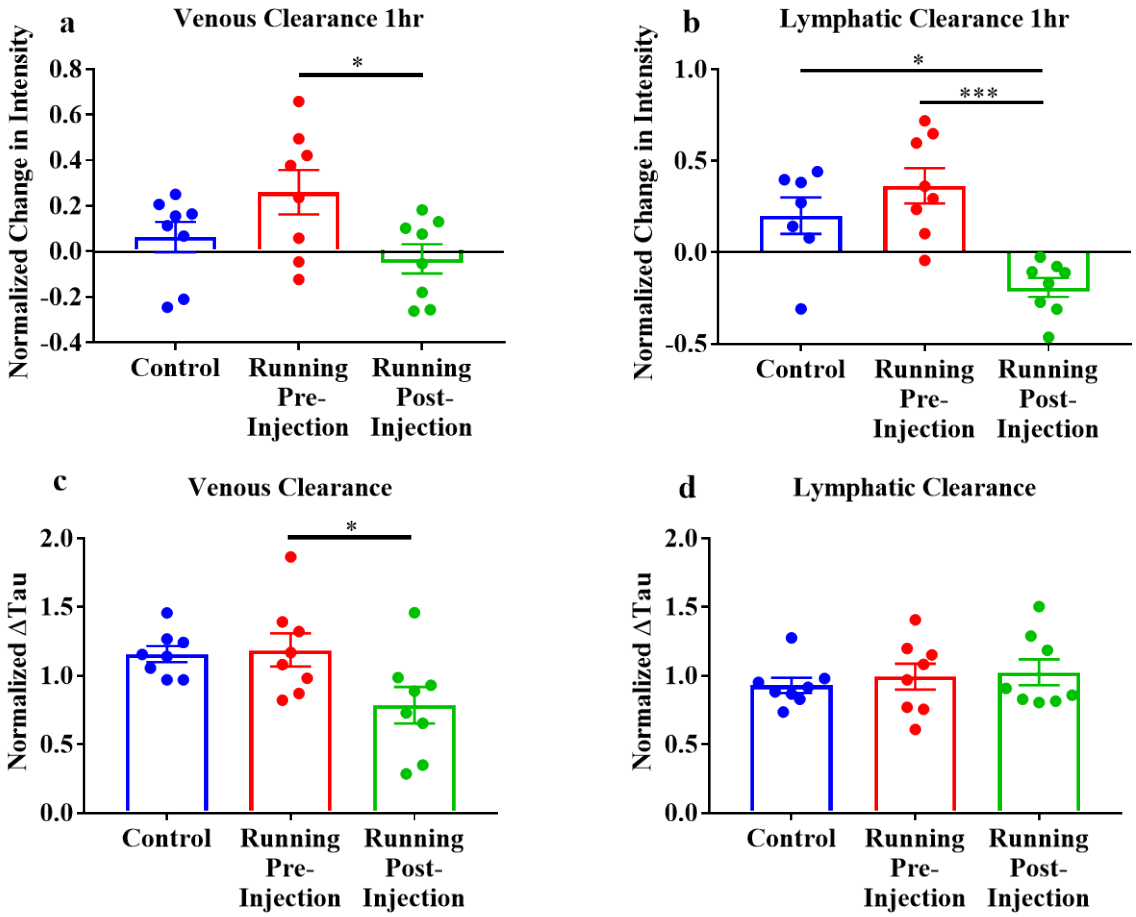

Figure 17 Effect of running on Normalized Change in Intensity and Normalized Tau. a, b. The normalized intensity was calculated to assess the transient effect of running on dye dispersion in the joint. For each experiment, all runners were normalized to the mean of non-running controls. Compared to the control experiment running pre- or post-injection did not significantly change the initial free dye intensity; however, at the second captured timepoint, post-injection normalized intensity was significantly decreased compared to pre-injection running (*, $p = 0.04$). After 1 hour, lymphatic intensity was significantly decreased compared to controls (*, $p = 0.01$) and pre-injection running (***, $p = 0.0003$) **c, d.** Time constant (tau) for each condition was normalized to the controls for each day. Compared to intraexperimental non-running controls, there are no significant differences in clearance rate for either tracer. Compared to running pre-injection, clearance rate is significantly decreased (*, $p = 0.04$).

For venous drainage, running pre-injection (0.26 ± 0.10) significantly increased ($p = 0.04$) the change in fluorescence intensity compared to running post-injection (-0.03 ± 0.06), however neither were significantly different from control (0.06 ± 0.06) (Figure 17a). Figure 17c shows the normalized tau (venous) for running post-injection was calculated to be (0.79 ± 0.13) which is significantly reduced ($p = 0.04$) the compared to pre-injection running (1.188 ± 0.12) (Figure 17c) however neither were significantly different than controls (1.16 ± 0.05).

When assessing lymphatic clearance, we observed a significant reduction ($p = 0.0003$ and $p = 0.01$) in the initial change in fluorescent intensity in running post-injection (-0.19 ± 0.05) compared to pre-injection (0.36 ± 0.1) and non-running controls (0.20 ± 0.1) (Figure 17b). however, we did not observe any significant change in tau for lymphatic tracers for the various conditions of running (Figure 17d). These data suggest the transient effect of running may be lost over the much longer timescale for which lymphatic clearance occurs.

4.4 Discussion

In this CHAPTER, we demonstrated the ability of multichromatic NIR imaging's ability to assess interstitial clearance mechanisms from multiple tissue beds. Clearance pathways and rates are essential in tissue homeostasis and dictate how biomolecules interact with their intended targets. Clearance to lymphatics or venous circulation has is understudied *in vivo*. Using tissue phantoms, we established the exposure time and tissue depth limitations required for *in vivo* multichromatic imaging and determined that sensitivity/cross talk between the dyes did not exist, confirming that the changes in signal

intensity resulted from changes in concentration or position of our tracers within our ROIs. We then used the mouse tail, a tissue drainage bed with well-defined physiology, to show that we could target lymphatic and venous circulation and quantify function. Lastly, we demonstrated the capacity to quantitatively image routes of clearance from the joint space. Given our limited understanding of how exercise regulates the clearance of materials from the joint space, we used multichromatic NIR imaging to enable technology to assess lymphatic and venous drainage in that context.

This study demonstrated the size dependence of interstitial molecules via venous and lymphatic pathways; however, the first to demonstrate this via simultaneous imaging. Proulx et al. showed that NIR tracers that clear through lymphatics have a delayed uptake into the systemic circulation compared to molecules that drain directly into the blood stream[305]. In our mouse tail study, the free dye intensity in the blood ROI is initially low. That signal intensifies in the tail vein over time, likely due to a renal clearance not surpassing the intradermal depot clearance over this total imaging window[310]. Thus, this dye's intensity in the blood circulation continuously increases as the concentration delivered to the blood over time increases. In addition, the PEG tracer signal intensity traces exhibited the characteristic phasic contractions attributed to lymphatic pumping. Therefore, our mouse tail experiment validated our two tracers' size-based partitioning to distinct routes of clearance.

The joint space is a unique interstitial space comprised of synovial fluid—hyaluronic acid, lubricin, and filtered serum—that hydrates the joint tissues and buffers the outflow of materials from the joint space[119,311]. A solute that leaves the joint space

must diffuse through the synovial fluid, then into the synovial membrane. The synovial membrane is a specialized tissue that retains the synovial fluid while also housing the venous and lymphatic fluid exchange machinery to clear solute from the joint[25,100]. Smaller materials can more easily diffuse through the synovial fluid matrix and thus exit the joint space faster[86]. Larger molecules can more easily entangle in the synovial fluid matrix and therefore have longer residence times within the joint space[312]. Using multichromatic imaging with sized tracers enables quantifying venous and lymphatic clearance kinetics in the joint, simultaneously rather than separately, as done in the previous studies[221] and furthers the ability to determine the relationship between lymphatic and venous uptake *in vivo*.

Previous studies have shown that exercise increases interstitial[125], venous[313], and lymphatic[127] flow to the muscle. In this study, we used exercise as an intervention to demonstrate the sensitivity of multichromatic NIR imaging to measure changes to venous and lymphatic clearance. In the joint space, exercise and joint loading have increased intra-articular pressure and cartilage flux. In this study, we showed that injection followed by exercise transiently increased lymphatic outflow from the joint; however, exercise did not significantly affect venous clearance. Interestingly, running pre-injection led to delayed clearance of both free dye and PEG, as exhibited by the presence of a larger peak intensity from the joint than their respective controls, which could be a consequence of altered hydrodynamic forces or delayed dye dispersion. Additionally, it must be explored whether exercise has any transient or long-term effects on clearance in OA.

Our current setup limited our temporal sampling frequency in both in vivo experiments. For running experiments, sampling frequency was limited by the time required for an animal to recover from and back under anesthesia. An ideal setup would be a wearable sensor that would go around the knee, which allows us to see the concentration in real-time without anesthesia. Similarly, in capturing the routes of clearance in the tail, we could only use one channel at a time due to our stereoscope's filter imaging limitations. Two cameras and light paths, or a computerized filter wheel, would simultaneously assess these two tracers with higher temporal frequency to quantify the relationship between vascular and lymphatic uptake *in vivo*. Additionally, the tracer sizes were designed to evaluate the particulate transport within the fluid; however, there are also cell-mediated mechanisms by which transport occurs *in vivo,* which could be imaged using these multichromatic approaches.

4.5 Conclusions

In this CHAPTER, we demonstrated the joint space is a well-regulated tissue bed that only allows for modest changes in lymphatic outflow during exercise. The observations in this CHAPTER are important because it shows that differential outcomes in lymphatic and venous clearance could be measured. Multichromatic NIR imaging can simultaneously image lymphatic and venous-mediated fluid clearance with great sensitivity and can be used to measure transient changes in clearance rates and pathways. This methodology was applied in CHAPTER 5 to assess the effects of OA venous and lymphatic drainage.

CHAPTER 5. QUANTIFYING THE ROLE OF MICROVASCULAR CLEARANCE IN OA

5.1 Introduction

CHAPTER 3 and CHAPTER 4 showed that joint transport could be modulated by exogenous stimulation with endothelin-1 and increased physical activity. In CHAPTER 5, we will apply NIR imaging in the context of OA using the MMT model in rats.

Joint clearance and biodistribution have traditionally been assessed using radiolabeled molecule tracking and fluorescence imaging[314–316]. The rate of clearance of key SF components such as proteoglycan subunits, hyaluronic acid (HA), inflammatory cytokines, and growth factors from the synovial cavity is relatively slow, clearing at rates comparable to conditions of clearance and drainage through lymphatics[317–319]. In OA, there is evidence of an increased breakdown of macromolecules like HA, potentially leading to altered clearance rates, fluid turnover, and drainage into the lymphatics[320,321].

Although lymphatics are in most tissues, their involvement in the pathogenesis of diseases has been historically understudied. More recently, lymphatic dysfunction has been implicated in the progression of various diseases, including heart disease[322], cancer, and arthritis (RA and OA)[6]. In OA, changes in lymphatic vessel density in the synovium[6] have been shown in late-stage OA. Wallis et al. looked at the differences in clearance between those with OA and RA synovial effusions and determined that radiolabelled iodine clearance was not significantly different. However, the clearance of radioiodinated

serum albumin (RISA) was significantly slower, suggesting that protein trafficking is altered in certain issues[253]. Myers et al. showed that RISA clearance was increased in canine joints with MCL transection compared to contralateral non-operated limbs 12 weeks post-surgery. Albumin is cleared mainly through the lymphatic system and albumin in normal tissues and acts as the central oncotic pressure driver[323–325]. In diseased tissues, a change in albumin clearance could signal changes in fluid transport or alternations in microvascular permeability of the venous or lymphatic system. Additionally, given that materials can exit the joint via two paths, the relationship between venous and lymphatic clearance in OA is still not well understood. Quantifying these interconnected drainage mechanisms via appropriately sized NIR tracers in a post-traumatic model of OA would allow us to better understand this missing link.

In musculoskeletal disease, walking exercise has been shown to improve patient self-reported pain and functional outcomes[17]. However, to date, minimal studies have been done to assess the effect of exercise on clearance *in vivo*. Previous research has shown that low, moderate, and high exercise regimes do not significantly impact cartilage but positively affect weight, a known modulator of OA risk[18]. Body weight-supported treadmill training has been shown to reduce cartilage degradation after PTOA development in rats suggesting that moderate exercise has beneficial effects in the development of OA[15]. Bodyweight-supported treadmill walking protected the cartilage more than treadmill walking alone; however, both significantly improve cartilage outcomes on PTOA[15,326]. However, what is unknown is how the timing or duration of exercise in the PTOA development affects the clearance of materials from the joint space.

In this CHAPTER, we will use exercise not as a treatment but as a mechanism to perturb the joint space during OA development to understand how exercise could be altering venous and lymphatic drainage clearance.

The first objective of this CHAPTER was to assess venous and lymphatic clearance as a function of time in surgically induced OA. We hypothesized that lymphatic-mediated clearance of PEG would decrease with OA progression and that venous clearance would remain unchanged. The secondary objective of this CHAPTER was to assess the contribution of exercise to venous and lymphatic clearance during the development of OA. We hypothesized that a treadmill exercise with MMT surgery would increase the overall clearance of tracers from the joint space**.**

5.2 Methods

5.2.1 Synthesis of PEG-NIR materials

40 kDa PEG IRDye 680RD (PEG) and IRDye 800CW (free dye) were synthesized and prepared as previously decreased in 4.2.1.

5.2.2 MMT and Sham surgery

The medial meniscal transection (MMT) is a surgical procedure to destabilize the rat knee joint and replicates osteoarthritis pathology in rodents (Figure 18). Briefly, animals were anesthetized via isoflurane inhalation, and the surgical site was shaved and sterilized immediately before surgery. Sustained Release buprenorphine (0.03 mg/kg) (ZooPharm, Windsor, CO) was injected subcutaneously as an analgesic. Skin and soft

tissue incision were made along with the sterile surgical site of the left medial hindlimb, along the femora-tibial joint. A blunt dissection exposed the medial collateral ligament (MCL), which was transected to expose the meniscus. For MMT animals, the meniscus was entirely cut through at the narrowest point. For Sham animals, only the MCL was transected, and the meniscus was left intact. Soft tissues were closed with 4.0 vicryl sutures, and the skin was closed with staple clips. The contralateral right hindlimbs were unoperated and served as naïve controls herein. Post-surgery, animals were rehydrated

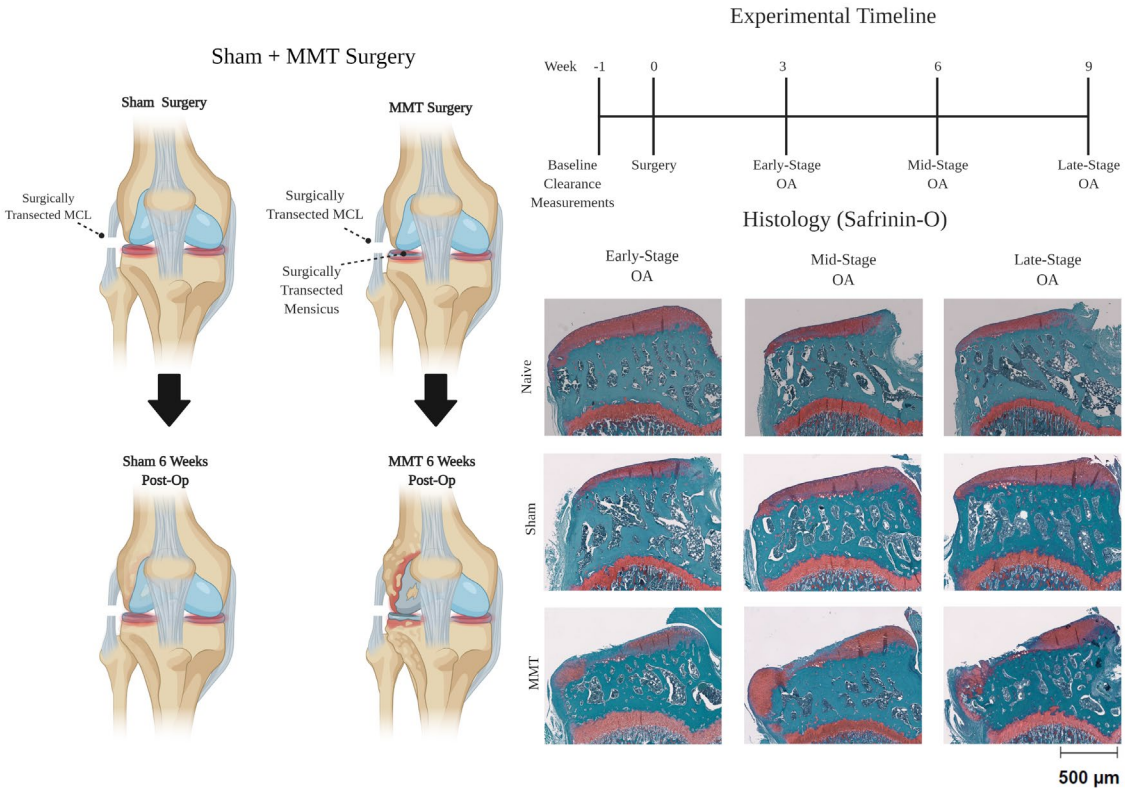

Figure 18. MMT Surgery and Histopathology during different stages. a) MMT surgery involves the transection of MCL and meniscus while the Sham surgery only involves MCL transection. **b)** Safrinin-O staining of Naïve, Sham, and MMT animals at Early, Mid, and Late Stage OA reveals progressive changes in cartilage anatomy as OA develops and progressess.

with 10 mL of Lactated Ringer's solution. All animals were monitored for three consecutive days post-surgery. Staples were removed one week after surgery when the skin had fully closed and healed. NIR Clearance was assessed at three weeks, six weeks, or nine weeks via PEG and free dye co-injection. All procedures followed institutional guidelines set by the Atlanta Veterans Affairs Medical Center (VAMC) and were approved by Institutional Animal Care and Use Committee (IACUC).

5.2.3 Exercise + MMT Surgery

Twelve-week-old male Lewis rats (Charles River) were acclimated for one week post-arrival and trained to run as previously described in section 4.2.6. On day one, the rats were acclimated to the treadmill for 30 minutes without running. Running was gradually increased to 30 minutes on consecutive days after two weeks. Rats that failed to walk the targeted duration twice over the training course were excluded from the study. All other rats were randomly selected for the experimental procedure to either run or serve as controls for the study duration. Knee joint clearance was measured at baseline (before surgery) and at weeks one, three, and six post-surgery in the rats. All rats in this experiment received MMT surgery. No rats walked on the treadmill as a daily therapeutic exercise. On each testing date, rat knees received intra-articular injections of a carboxylate modified IRDye800CW and IRDye680RD with 40 kDa polyethylene glycol. NIR images were collected immediately and out to 24 hours after injections. Rats were in two groups: sedentary or exercised. Sedentary rats remained within their cages throughout the experiments. Exercised rats underwent treadmill walking (10 m/min for 30 mins) immediately after injection. Time constants were extracted from exponential fits

of the time-intensity data. Rats designated to walk but failed to walk excluded on a particular day were excluded from that experiment's analysis.

5.2.4 Image and Data Analysis

Images were analyzed using the MATLAB code referred to in 4.2.7 to assess the top 5% most intense pixels in each image at each time point.

5.2.5 Data analysis and presentation

Each group's surgical leg was compared to its internal contralateral control in a paired t-test analysis and graphed as such to assess the effect of MMT and Sham surgeries on NIR clearance of venous and lymphatic draining tracers. This was performed at early, mid, and late-stage time points. To assess the effect of exercise vs. remaining sedentary on joint clearance post-injection in the MMT, we compared surgery legs to non-surgery legs and running legs to non-running legs using a one-way ANOVA. For running studies, clearance data are presented as mean ± SEM. A Brown-Forsythe test was used to quantify if variances were significantly different.

To understand the longitudinal effect of OA surgery on joint clearance, we performed Dunnett's test to understand the effect of Sham and MMT surgery over time in contralateral legs and surgical legs. All data were analyzed using GraphPad prism 7.0.

5.3 Results

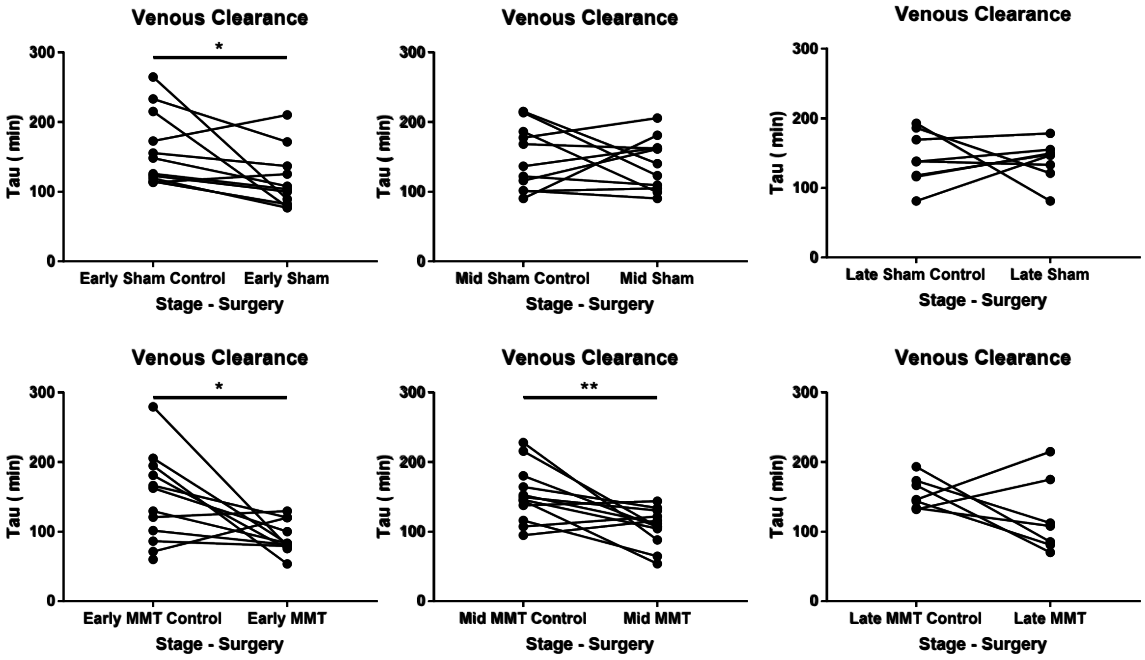

Figure 19 Venous Clearance During OA Progression. Exponential clearance of free dye was analyzed for Sham rats. Tau decrease in Sham animals at early-stage and by mid-stage and late-stage venous clearance was not signficantly different for Shams. Tau increased for MMT animals at early like the Shams however, at mid-stage OA tau remains elevated. Statistical significance was determined via a paired t-test and p-values < 0.05 (*) or ≤ 0.01 (**) were noted as significant.

5.3.1 Effect of MMT Surgery on Venous Clearance

Using the MMT and Sham models to compare the effect of surgical insult on clearance from the joint space, we either co-injected NIR tracers or tracked the tracers individually a week apart. Tau is inversely proportional to the rate of clearance, and these values are presented in Figure 19. For Sham limbs, tau significantly decreased three weeks post-surgery (162.4 ± 53.07 min vs. 116.6 ± 42.21 min, $p = 0.0330$). However, for mid and late-stage clearance, Sham clearance was not significantly different from

contralateral control legs. For MMT rats, venous clearance was also significantly increased 3-weeks post-surgery as represented by decreased tau (154.6 ± 60.74 min vs. 91.43 ± 23.3 min p = 0.0169). However, for mid-stage venous tau, MMT clearance joints remained decreased (153.1 ± 40.05 min vs. 106.9 ± 26.87 min, p = 0.0083), and by the late stage, MMT joint venous clearance was not significantly different from its respective contralateral control.

5.3.2 MMT Surgery reduces lymphatic clearance in late-stage OA

Lymphatic clearance was assessed at early, mid, and late-stage MMT (Figure 20). Tau significantly increased at mid-stage (277.1 ± 214.0 min vs. 482.1 ± 254.3 min, p = 0.0045) for Sham legs but was not significantly different at early and late-stage MMT. However, mid-stage lymphatic clearance significantly decreased compared to its

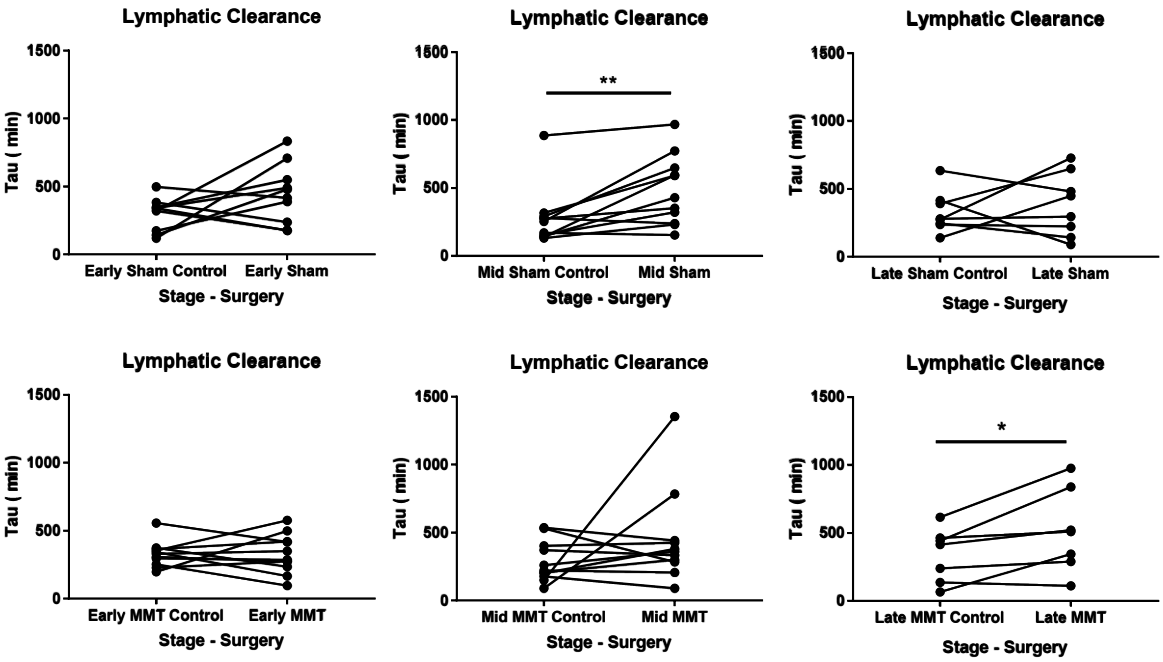

Figure 20 Lymphatic Clearance during OA Progression. Lymphatic clearance for early mid and late stage for sham. Tau increased for Sham animals at mid stage, however Tau is not significantly diffeerent at late stage for Sham. Lymphatic clearance for MMT rats compared to their respective contralateral controls shows decreased tau at late stage for MMT animals. Statistical significance was determined via a paired t-test and p-values < 0.05 (*) or ≤ 0.01 (**) were deemed significant.

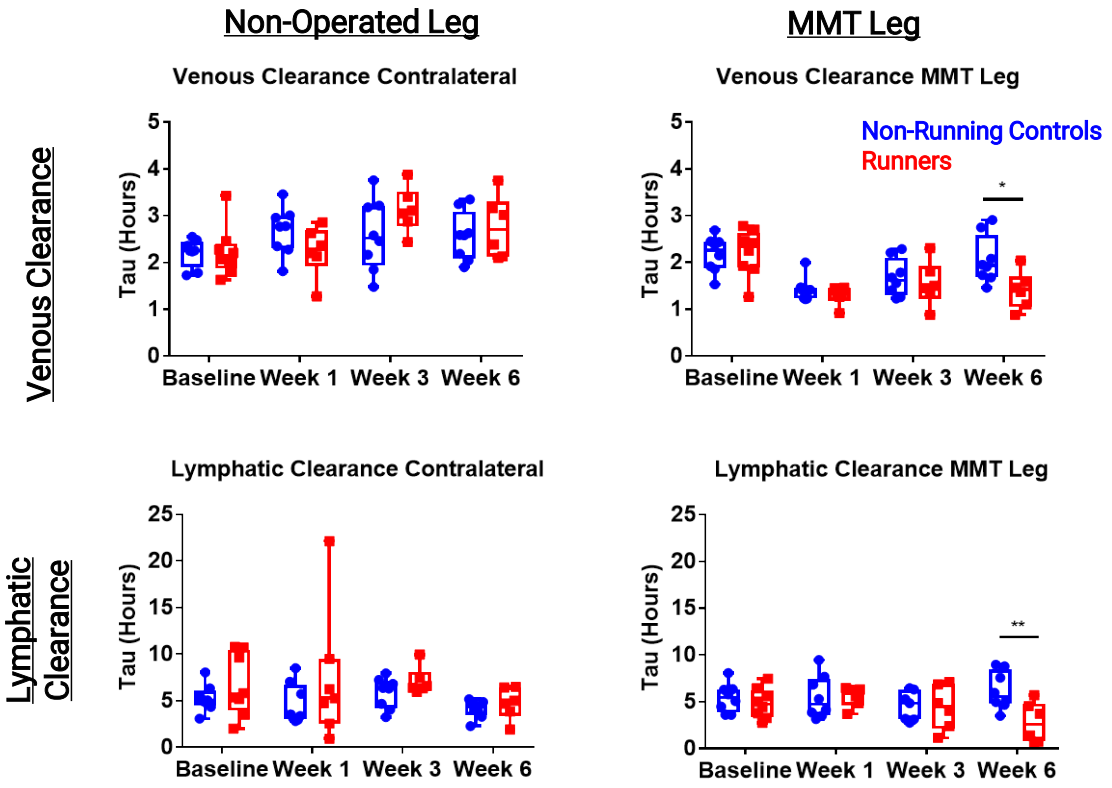

Figure 21 Exercise increases joint clearance at mid stage OA. To assess the effect of running on venous drainage during OA progression Tau was assess as a function of MMT surgery and comparisons were made between non-runners and runners. In contralateral limbs there wasn't an effect of running on Tau is previously shown in chapter 4. However for MMT animals running at week 6 decreased Tau. Lymphatic clearance shows increased PEG tracer clearance at week 6 for runners. Statistical significance was determined via two-way ANOVA with a Šidák comparison and p-values < 0.05 (*) or ≤ 0.01 (**) were deemed significant.

respective contralateral control (340.7 ± 197.7 min vs. 513.6 ± 305.7 min, p = 0.0352). Lymphatic clearance for MMT animals was not significantly different between contralateral controls at the early and mid-stage. However, at a late stage, MMT was significantly increased compared to contralateral controls.

5.3.3 Venous clearance during early, mid, and late-stage OA

To assess the effect of exercise on joint clearance, MMT animals were exercised at 1-, 3-, and 6-weeks post-surgery and before surgery, and venous and lymphatic clearance

measurements were assessed (Figure 21). Surgical and non-surgical legs were compared to their respective running or non-running controls at each time point. Running had no significant effect on clearance until week 6 for both venous (1.84 ± 0.17 hrs vs. 1.61 ± 0.21 hrs, p = 0.02) and lymphatic clearance (5.42± 0.33 hrs vs. 4.40 ± 0.58 hrs, p = 0.006).

5.4 Discussion

In this CHAPTER, we used NIR imaging to understand how intra-articular clearance changes over time in this model. We implored multichromatic imaging to assess both the changes in clearance as a function of surgical insult and then in the MMT alone to discern the effect of exercise with disease progression. We determined that surgical insult from the Sham was significant to change venous and lymphatic clearance; however, we showed the impact of MMT on lymphatic clearance developed later.

The synovial fluid is a complex biological solution composed of macromolecules, nutrients, and waste. The main constituents of synovial fluid are GAGs and proteoglycans, serum proteins, and water. The synovium reflects hyaluronic acid through size exclusion and proteoglycans and GAGs present in the extracellular spaces[75]. This helps to maintain interstitial fluid hydration and pressure. Clearance from the joint is mediated by blood and lymphatic capillaries[327]. Contained within that fluid are molecules that range in size from ~ 1 nm to ~200 nm[110]. Molecules that can escape reflection from the synovial fluid matrix are cleared through two primary paths. Molecules less than 5

nm tend to be cleared mainly through venous circulation, while molecules 10 nm and larger are cleared through lymphatic circulation[247,253,328].

Intra-articular pressure during rest and movement are vastly different. Intra-articular pressure is slightly sub-atmospheric during rest and supra-atmospheric during joint loading[329]. Hydraulic conductance through the synovium increases with increasing intra-articular pressure[330]. The relationship between intra-articular pressure and arthritis pain/severity has been explored in a few contexts, and generally, arthritis has been associated with increased IAP[329,331]. Additionally, the hydraulic conductance of the synovial membrane has been explored and has been shown to increase with increasing OA severity in a preclinical model of OA[332]. These factors combined could lead to increased flow in the context of externally applied forces during exercise in OA.

To understand the longitudinal effects of OA on clearance, we conducted Sham and MMT surgeries and quantified venous and lymphatic tau for surgical legs and non-operated contralateral controls. Sham animals had faster clearance for venous clearance at week 3, but by week 6, clearance was not significantly different. Additionally, Sham animals had slower lymphatic drainage at week 6 but not at week 9. We also demonstrated increased venous clearance at week 3 and week 6 for MMT animals and delayed lymphatic drainage at week 9. Specifically, a return to baseline for venous clearance seemed to coincide with the onset of slower lymphatic drainage. This potentially suggests that increases in venous clearance may partially offset the onset of the delay in clearance. Joint filtration and venous uptake may play a role in lymphatic function during the dynamic changes in vascularity within the joint due post-surgery.

However, after surgery, we demonstrated that regardless of treadmill running, venous clearance was increased compared to baseline values. This increase could be attributed to a variety of factors. Surgical insult via this PTOA MMT model has been shown to increase angiogenesis that peaks two weeks post-surgery and returns to baseline/control values four weeks post-surgery[333]. These values partially coincide with our measurements with increased clearance at one- and three-week post-surgery and return to baseline at 42 days[333]. Additionally, PTOA Sham surgery is associated with increased venous clearance at three weeks, returning to baseline at six weeks. Additionally, changes in IAP could result in increased outflow and hydraulic conductance through the synovium.

In contrast to venous clearance, lymphatic clearance is unchanged in contralateral joints over this study's time course. Therefore, increases in angiogenesis could counteract any increases in fluid accumulation from inflammation. In this paper, we specifically targeted materials that clear through the fluid phase. Mwangi et al. [221] showed that 500 kDa dextran clearance through the synovial was decreased in the MMT model. However, our PEG tracer is less likely to get reflected/entrapped within the extracellular matrix as the hydrodynamic radius is three times larger than our PEG construct[334]. Additionally, in that study, only the advective fluid movement was quantified, and the relationship between exercise and the movement of a larger molecule like 500 kDa Dextran has yet to be established.

Increases in angiogenesis could lead to leaky venous return or changes that could allow lymphatic-specific tracers to clear through venous uptake at week six. In this study,

we did not observe the direct uptake of tracers into the bloodstream or lymphatics. We observed the disappearance of tracers found to clear via venous and lymphatic paths in healthy tissues. However, in unhealthy tissues, there could be changes in the permeability of the vasculature that alter the traditional size partitioning effects that occur in healthy tissue. In other contexts, the chemical modification of the extracellular matrix can change the rate at which materials move without affecting the bulk mechanical properties of the tissue[108]. For example, the trans-synovial flow rate increases the clearance of hyaluronic acid from the joint space, meaning that the running intensity could potentially modulate how quickly things clear from the knee joint[108].

Our exercise study determined that exercise increased venous and lymphatic clearance at 6 weeks post-surgery, but exercise had no effect 1 and 3 weeks post-surgery. MMT surgery could modulate the protein concentration in the synovial tissues by increasing catabolism through inflammatory mediators, and these changes could drive this increased flow in the context of exercise[51]. Changes in clearance from the joint space could also dictate how injectables in the joint space perform at various stages. For example, delivering small therapeutic peptides into the joint immediately in a post-traumatic insult could result in quick clearance of the therapy. Clearance must be factored into the treatment strategy to maximize outcomes *in vivo.*

5.5 Conclusions

This study is the first investigation to assess venous and lymphatic drainage during longitudinal OA progression simultaneously. We showed that the resolution of increased

venous clearance preceded decreases in lymphatic drainage in Sham and MMT animals and that the onset of changes in lymphatic changes was offset by three weeks for MMT animals. These findings are an essential first step in understanding how post-traumatic OA could affect tracer clearance. More extended studies need to be done to understand the long-term effects of surgery on tracer clearance.

In our second study in this CHAPTER, we investigated the effect of running from joint clearance at 1, 3, and 6 weeks post-MMT and observed improved clearance of tracers 6 weeks post-surgery in surgical limbs. It is important to note that we did not assess exercise's effect as a daily intervention in this model but only exercise at well-defined points. There is a chance that exercise as a treatment could modulate inflammatory activity and restore joint homeostasis. These potential effects should be explored in future studies.

CHAPTER 6. USING EX VIVO PLATFORMS TO ASSESS LYMPHATIC CONTRACTILITY AND LYMPHANGIOGENESIS

6.1 Introduction

This CHAPTER has been modified in part from the following manuscript: Michalaki, E. *et al.* Effect of human synovial fluid from osteoarthritis patients and healthy individuals on lymphatic contractility. *bioRxiv* 2020.12.02.408294 (2020). doi:10.1101/2020.12.02.408294

In CHAPTER 5, we showed that microvascular clearance was altered in PTOA. However, it is unknown if the loss of function is simply from decreased permeability of the synovium as demonstrated by Mgawi et al. [221], changes in lymphatic vessel density, reductions in downstream lymphatic function, or a combination of all three. The extent to which the lymphatic system is affected by factors draining from the SF remains unknown. Lymphatic vessels are responsible for maintaining the joint space homeostasis; therefore, efficient transport of lymph from the joint space into lymphatics is a well-established part of joint homeostasis[149]. As joint inflammation is one of the leading drivers of OA, it is unclear what effect the OA synovial fluid may have on mature lymphatics within the synovium. As OA develops and progresses, inflammatory cytokines and by-products of the injury and degradation of articular tissues build up in the SF, providing a feedback system to exacerbate disease[318]. Thus, the lymphatic system plays a critical role in resolving inflammation and maintaining overall joint

homeostasis[335]. However, as described in earlier chapters and demonstrated in CHAPTER 5, there is stronger evidence that the lymphatics can become dysfunctional during OA[6,10,12,13]. In response to injury/inflammation, mature (precollecting and collecting)lymphatic vessels can collateralize and grow new vessels to improve flow around an obstruction or injury[182]. While a growing body of evidence implicates a critical relationship between OA and the lymphatic system, the related studies have mainly consisted of observed differences in lymph flow and the rate of fluid drainage between healthy and OA knee joints[6,11,336]. First, Wilkinson et al. demonstrated LVs in human synovial tissue, while subsequent studies showed differences in the number and size of the lymphatic vessels found in the joints[11,337]. When lymphangiogenesis was inhibited using VEGR3 neutralizing antibodies in a mouse model of OA, there was reduced synovial drainage and worsened disease progression[14]. Given the results from CHAPTER 5 and research from other groups, lymphatic dysfunction may exacerbate OA development and progression. Although there is evidence of a correlation between the lymphatic system and OA, the specific role of inflammation on lymphatic function is not fully explained.

SF is a viscous fluid found in the cavities of synovial joints functioning as a biological lubricant and a means for nutrient and cytokine transportation[94,338–340]. Multiple inflammatory and anti-inflammatory molecules secreted from joint tissues and discovered in the SF of diseased OA patients directly indicate their role in OA development[341,342]. Patients with OA have elevated prostaglandins (PGE2), leukotrienes (LKB4), cytokines, growth factors, and nitric oxide. The inflammatory cytokines, IL-1β,

IL-6, IL-15, IL-17, IL-18, and tumor necrosis factor α (TNFα), along with the anti-inflammatory cytokines, IL-4, IL-10, IL-13, can induce cartilage degradation and collagen destruction and have thus been directly implicated within the progression of OA [341,343–346]. Additionally, OA patients have shown elevated levels of the transforming growth factor β (TGFβ), fibroblast growth factors (FGFs), nerve growth factor (NGF), and vascular endothelial growth factor (VEGF) in SF, chondrocytes, subchondral bone, and serum [343,347,348]. Notably, the increased expression of VEGF, a growth factor known to regulate vascular permeability and angiogenesis, has implicated the potential involvement of both the blood and lymphatic vasculatures in OA disease[347,348]. Notably, the known effect of age on both lymphatic contractility and synovial permeability and OA disease serves as an additional indication of a potential correlation between lymphatics and OA[349–351]. As products from the joint are cleared into the lymph fluid, chemokines may affect the LVs through direct signaling or by activating immune cells. However, the direct effect of SF exposure on LV contractility still remains unknown. Recent technological development of e*x vivo* lymphatic pressurization and perfusion systems have allowed rigorous analyses of lymphatic contractile behavior under varying conditions of flow, pressure, and exposure to biochemical factors[142–144,146]. The primary objective of this chapter is to use an *ex vivo* lymphatic pressurization device to investigate how lymphatic contractility changes in response to OA development in rodents and also in response to the simulated drainage of OA synovial fluid.

While downstream pumping lymphatic capacity is important in joint homeostasis, the structure and density of lymphatics within the synovium also dictate how materials

can get transported down into the joint. Lymphangiogenesis is a complicated process by which new lymphatics grow from existing lymphatics, including the lesser-studied mature lymphatic vessels which reside within the synovium. Reduced growth from initial lymphatics, collecting lymphatics, or both may be responsible for changes in lymphatic function *in vivo*. To study lymphangiogenesis *in vitro*, two-dimension cell culture of lymphatic endothelial cells allows for specific investigations about mitosis, migration, or cell health[33,169,352]. However, 2D culture systems are limited because the LECs are not exposed to similar mechanical and cellular stimuli as *in vivo.* Additionally, without lymphatic muscle cells or fibroblasts, lymphatic endothelial cells may respond differently than they do *in vivo*[353]. Therefore, three-dimensional culture systems for lymphatic studies have been used to understand lymphatic migration, test lymphangiogenic potential, and understand what roles soluble factors play on lymphatic sprouting[37,38,354].

Recently the PEG hydrogel has been used to show the effect of biochemical and mechanical stimuli on collecting vessel segments in culture. To date, only one group has studied the *ex vivo* culture of mature lymphatic collecting vessels in hydrogel systems[38]. Bruyere et al. used a standard collagen platform to understand the biochemical factors that drive lymphangiogenesis *ex vivo*. One of the advantages of the PEG platform is the fine control over the ability to tune, mechanical properties (stiffness and diffusivity), biological signals (adhesion peptides, mitogenic factors), and degradability (enzymatic or hydrolytically 100% to 0% degradable), and these parameters are independently tunable[355–357]. In the case of the collagen gel, hydrogel stiffness cannot be uncoupled from hydrogel stiffness and adhesive ligand presentation[358]. The most common collagen

source is rat tails; therefore batch to batch variability can affect the mechanical properties between lots or vendors[359]. Given the understudied nature of mature collecting vessel lymphangiogenesis, the PEG hydrogel platform could allow us to study lymphatics in simulated pathological environments *ex vivo*.

VEGF signaling plays a critical role in lymphangiogenesis and the ability of 3D organoid systems to be used to interrogate critical regulatory components of VEGF signaling. Epsins are endocytic adaptor proteins necessary to internalize and degrade VEGF receptors during VEGF signaling[33,157,165,166,360–362]. In the contexts of diabetes, cancer atherosclerosis, three diseases with significant inflammatory components, epsin down-regulation via endothelial cell or myeloid-specific epsin 1 and 2 deletions improve disease phenotypes and improve angiogenesis and lymphangiogenesis[33,170,362]. However, given the high expression of VEGFR3 in the initial lymphatics and the low expression in collecting vessels, it is still unknown whether epsin deletion in mature vessels has a similar effect as in initial lymphatics[30].

In this CHAPTER, we utilized an *ex vivo* syringe-controlled lymphatic perfusion system device to study the effects of OA on lymphatic collecting vessel function under two conditions: 1) after MMT induction, or 2) with a simulated OA synovial fluid (OASF) drainage. We hypothesized that the pump function of lymphatic vessels draining the joint could be directly compromised in both cases due to factors within OASF and thus might present a therapeutic target in OA. Additionally, we investigated lymphangiogenesis in two contexts, 1) in the context of a simulated OA environment with OASF and 2) a tamoxifen-inducible epsin double knockout in the mouse. We

hypothesized that OA synovial fluid would decrease lymphatic growth compared to non-OA controls. Lastly, we hypothesized that epsin deletion would improve collecting lymphatic vessel sprouting and could be a suitable target for lymphangiogenesis from mature lymphatics *in vivo*.

6.2 Methods

6.2.1 Rat and Isolated Vessels Preparation

Male Lewis rats 350-400 g (Charles River Laboratories, Wilmington, MA) were used for all experiments. For isolation of segments of femoral LVs, the animals were euthanized via CO_2 gas. For the isolation of rat femoral LV (RFLV), the skin and superficial fascia layer were quickly removed to expose the area between the saphenous artery and inguinal ligament of the internal surface of the thigh (Figure 22). They were

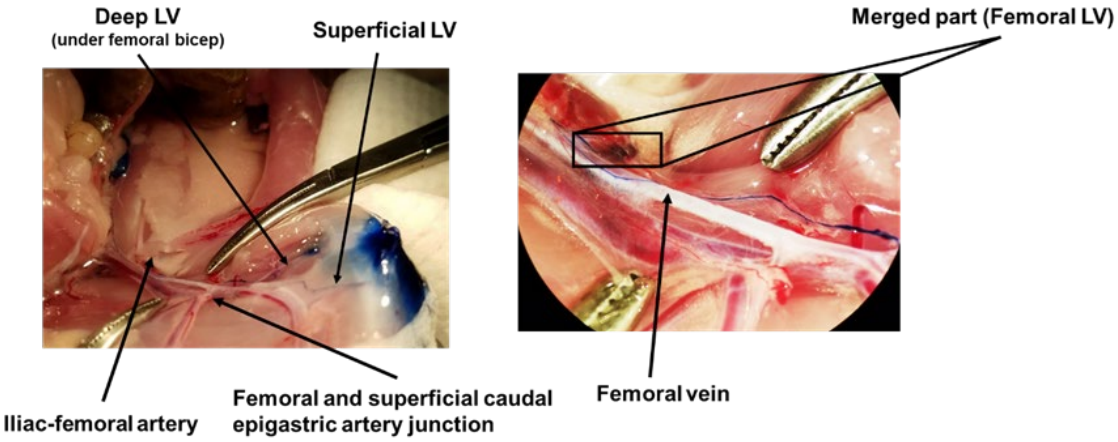

Figure 22 Rat femoral lymphatic vessel isolation. Evans blue (1% (w/v)) was injected intra-articularly into the left knee for visualization purposes. The immediate uptake of Evans blue by the lymphatics allows us to visualize the LV. The isolated RFLV is found proximal to the deep LV (LV below the femoral bicep) and superficial LV merge.

handled gently to prevent bleeding and placed aside to provide access to the femoral lymphatics, located alongside the femoral vein epigastric artery and vein was carefully teased from adjacent tissue and kept together between the femoral and superficial caudal epigastric artery junction iliac-femoral artery (Figure 22). During the dissection, the area of interest was kept moist with DPBS. Suitable LVs were found along these vessels. Sections of the RFLVs ~0.5 cm long were dissected, cleaned from connective tissue, and placed in a warm (37 °C) bath of albumin enriched physiological salt solution (APSS)[23,144] for MMT studies and DMEM/F12 for (ThermoFisher Scientific; 11039047) that was pH adjusted to 7.4 in 5% CO_2 incubator. For PEG hydrogel experiments, the lymphatic segments were stored in 10% FBS supplemented EBM and cut into roughly 300-micron long segments.

6.2.2 Epsin double knockout mice generation

The Chen group provided adult inducible epsin double knockout mice from Boston's Children Hospital. Briefly, this genetic model consists of a constitutive global deletion of Epsin 2 coupled with a lymphatic endothelial cell-specific epsin deletion driven by Prox1-Cre-ER^{T2} via the administration of 4-hydroxytamoxifen (tamoxifen). To administer tamoxifen, it was first dissolved in DMSO at 5 mg/mL and kept at -20°C. For epsin mouse studies, mice 6-16 weeks old were given 0.3mg/30gram of bodyweight 4-hydroxytamoxifen every other day for 16 days. To confirm that epsin deletion post-tamoxifen treatment, flank lymphatic vessel segments were encapsulated in PEG hydrogels and stained for epsin 1(1:50 dilution, Santa Cruz Biotechnology, Inc) using the methods described in section 6.2.12.

6.2.3 Synovial Fluid Collection

In this study, the effect of three types of SF was investigated: healthy synovial fluid (HSF), a mixture of synovial fluid derived from various OA patients (OASF-pool), and synovial fluid derived from one specific OA patient (OASF#3). HSF was purchased from Articular Engineering (Northbrook, IL; Donor ID Number: SF-1435). OASF was collected from knee OA patients receiving arthrocentesis (joint aspiration). Patients were recruited from Emory University Sports Medicine under an Institutional Review Board (IRB) OA protocol; all patients gave informed consent. OASF was directly removed from OA patients by an orthopedic physician. SF samples were kept frozen in 1 mL aliquots at -80 °C until use. For all sprouting experiments, SF was diluted in a 1:20 or 1:10 ratio with EBM, and for all the perfusion experiments, SF was diluted in 1:10 DMEM/F12.

6.2.4 Cytokine Analysis

Cytokine content of all SF samples was quantified using a bead-based multiplex immunoassay, Luminex Cytokine/Chemokine 41 Plex Kit (EMD Millipore Corporation, Burlington, MA; HCYTMAG-60K-PX41) (Figure 23). Median fluorescent intensity

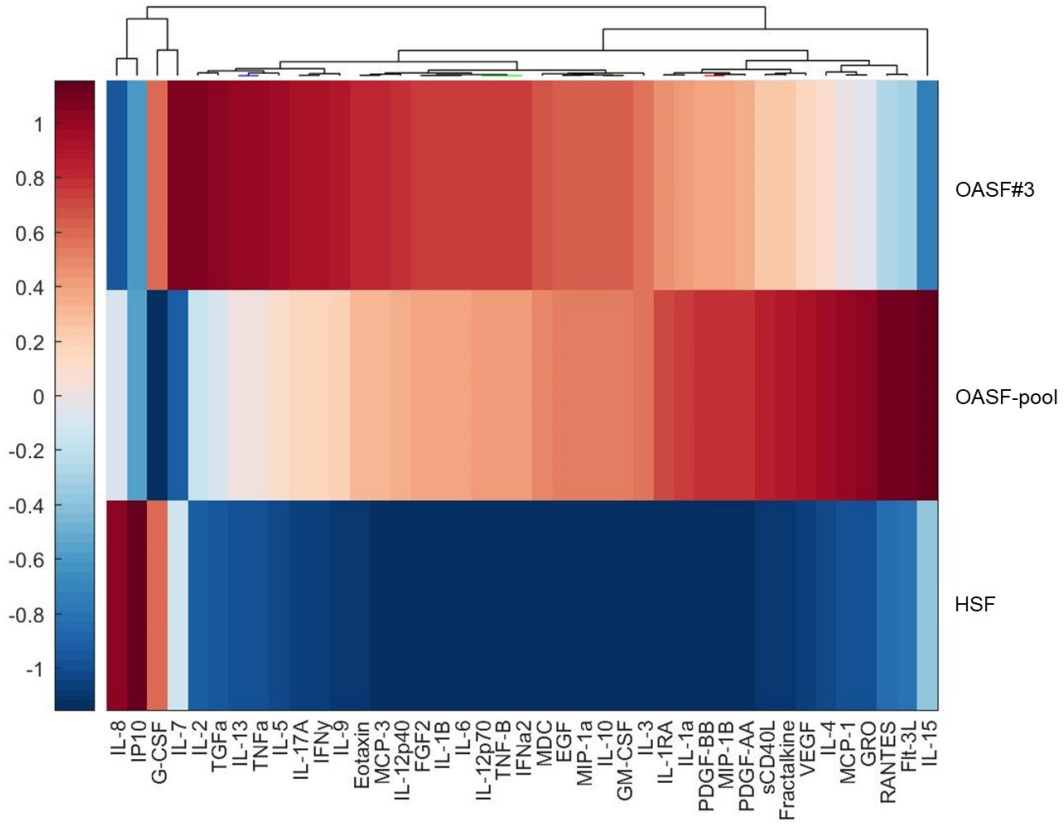

Figure 23 Cytokine profile for OASF and HSF. The relative concentration of 41 cytokines were measured in OASF#3, OASF-pool, and HSF using a multiplex immunoassay, LUMINEX. The data were normalized based on the corresponding background measurement, obtained from a LUMINEX run with only assay buffer, and presented based on a heat map where blue cells indicates a lower value while red cells indicate a higher value.

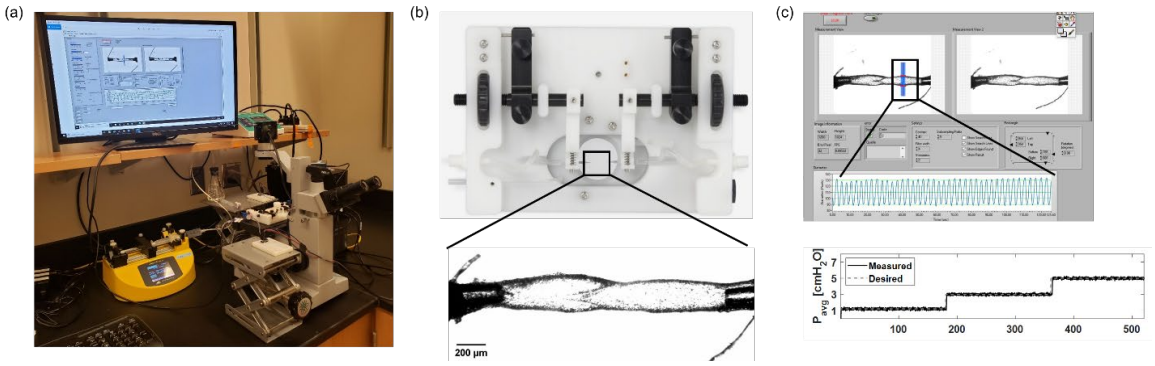

Figure 24 Ex vivo experimental set up. (a) Picture of the ex vivo lymphatic perfusion system including the computer, syringe pump, and microscope. (d) Picture of the single vessel chamber with a close-up of the cannulated RFLV. (5x objective; Scale bar = 200 µm.) (c) A custom LabView program tracks changes of the vessel diameter using data from a bright-field camera in real-time and stores this for subsequent data analysis.

values were read using Luminex xPONENT software v 4.3 in the MAGPIX system (MAGPIX-XPON4.1-CEIVD). Cytokines in both OA samples (OASF-pool and OASF#3) yield elevated levels of the majority of cytokines assessed relative to HSF. Therefore, the corresponding SF cytokines profiles were utilized along with our results to facilitate appropriate interpretation.

6.2.5 MMT Surgery for femoral lymphatic testing

Naïve, Sham, and MMT Lewis rats were purchased to determine the effect of MMT surgery on downstream lymphatic collector function. Naïve Lewis rats were tested two weeks prior and appropriately age-matched to surgical animals. Six Sham and six MMT surgeries were performed, and 8-9 weeks post-surgery, femoral lymphatic vessels were isolated from the rats.

6.2.6 Ex vivo lymphatic perfusion system setup

An *ex vivo* lymphatic perfusion system was customized to control the average transmural pressure applied to the lymphatic vessel (Figure 24). First, an LV segment without branches was cannulated on two resistance-matched glass pipettes of 150–200 μm tip diameter using the single vessel chamber (Living System Instrumentation, St Albans, VT; CH-1) (Figure 26b). After cannulation, the chamber was connected via tubing to two glass flasks containing DMEM/F12 and two syringe pumps (Genie Touch™ Syringe Pump; Kent Scientific Corporation, Torrington, CT) and immediately placed onto the microscope stage.

The syringe pumps were used to apply the same transmural pressure to the inlet and outlet of LV. Transmural pressure was adjusted using a feedback loop with two syringe pumps and pressure sensors (1 psi SSC series; Honeywell, Charlotte, NC). During the experiment, the diameter tracing was recorded in real-time via a custom LabView program, using data from a bright-field camera capturing 30 fps, as in other studies[146] (Figure 24c). Both diameter data and other sensor data were synchronized post-experiment using recorded time stamps. From the lymphatic diameter tracings, the following lymph pump parameters were calculated [364]:

$$Lymphatic\ Tone\ Index(LTI)\ or\ Tone = \frac{DD_{Ca^{2+}-free} - DD}{DD_{Ca^{2+}-free}} \cdot 100\% \quad (1)$$

$$Ejection\ Fraction\ (EF) = \frac{DD^2 - SD^2}{DD^2} \quad (2)$$

$$Fractional\ Pump\ Flow\ (FPF) = FREQ \times EF \quad (3)$$

where, $DD_{Ca^{2+}-free}$ is the completely relaxed diameter obtained post-incubation with Ca^{2+} free physiological solution, DD the diastolic diameter, SD the systolic diameter, and $FREQ$ is the contraction frequency. The tone denotes the percentage of vessel constriction at the diastolic diameter compared to the fully relaxed diameter obtained with Ca^{2+} free physiological solution. The ejection fraction (EF) indicates the fractional amount of the end-diastolic volume ejected during a lymphatic contraction. Finally, the fractional pump flow (FPF) is an index of active lymph flow that produces the fractional change in lymphatic volume per minute.

For experiments with surgery animals, the vessel was canulated in our perfusion system, and a pressure of 3 cm H2O was applied for 30 minutes to allow the vessels to re-acclimate to the application of external forces. After 30 minutes, the vessels were subjected to 5 minutes at 1.2, 3, 5, 3, and 1.2 cm H2O to precondition the vessels. After the preconditioning step, the vessels were subjected to 1.2, 3, and 5 cm of H2O. At the end of each experiment, the vessel was equilibrated in Ca^{2+}-free physiological solution containing (in mM): 119.0 NaCl, 4.7 KCl, 2.5 $CaCl_2$, 1.2 $MgSO_4$, 25.0 $NaHCO_3$, 1.2 KH_2PO_4, 0.027 EDTA, and 5.5 glucose for 20 min and subsequently exposed to an average transmural pressure of 1, 3, and 5 cm H_2O to determine the passive diameter (for calculation of tone) at each pressure.

For the experiments with SF treatment, the “inlet” side of the vessel was removed from the glass pipette, and SF was introduced to the corresponding upstream tubing and glass cannula. For the control experiments with DMEM/F12, the “inlet” side of the vessel

was removed from the glass pipette, and DMEM/F12 was introduced to the corresponding upstream tubing and glass cannula. Then, the vessel was re-cannulated, and flow with a pressure gradient of 1 cm H_2O was generated for 5 seconds (while holding the average transmural pressure to 3cm H_2O) to confirm the successful introduction of OASF, HSF, and DMEM/F12 through the vessel. Next, the vessel containing SF or DMEM/F12 was kept at 37 °C for ~1 hr at a transmural pressure of 3 cm H_2O, and the diameter was recorded to monitor changes in contractile behavior. After the 1hr-, 2hr- and overnight treatments, average transmural pressures of 1, 3, and 5 cm H_2O was applied to quantify the contractile response of RFLVs. We should note that we are the first *to our knowledge* to test the contractility of RFLVs *ex vivo* with SF. During our preliminary experiments, we demonstrated that RFLVs do not consistently contract at higher average values of transmural pressure. Thus we utilized pressures previously applied for rat cervical and thoracic duct lymphatics[145,363]. At the end of each experiment, the vessel was equilibrated in a Ca^{2+}-free physiological solution.

6.2.7 Hydrogel Preparation

To prepare PEG hydrogels, solutions were prepared for as previously described[19]. PEG-4MAL macromer (MW 22,000; Laysan Bio) was dissolved in 4-(2-hydroxyethyl)piperazine-1-ethane sulfonic acid (HEPES) buffer (20 mM HEPES in DPBS, pH 7.4) at 2.5x the final density. Adhesive and cross-linking peptides were synthesized by AAPPTec. Adhesive peptide RGD (GRGDSPC) was dissolved in HEPES at 10.0 mM (5X final ligand density) and mixed with PEG-4MAL at a 2:1 PEG-4MAL/ligand ratio to generate an RGD functionalized PEG-4MAL precursor. After a

minimum of 15 min, the functionalized PEG-4MAL precursor solution was further diluted using HEPES buffer at a 3:1 functionalized PEG-4MAL/HEPES ratio. Bis-cysteine cross-linking peptide GPQ-W (GCRDGPQG↓IWGQDRCG; ↓ denotes enzymatic cleavage site) was dissolved in HEPES at 5X the density corresponds to 1:1 maleimide/cysteine ratio after accounting for maleimide groups reacted with adhesive peptide. To assess the mechanical properties, 10 µl gels were synthesized and incubated in PBS overnight before testing. Hydrogels were crosslinked in the incubator for approximately 15 minutes before media was applied for lymphatic vessel encapsulation.

To determine whether VEGF-C could drive lymphangiogenesis through the formation of sprouts from collecting lymphatic vessels in this platform, samples were either treated for five days with control media (10% EBM), VEGF-C media (10 ng/mL),

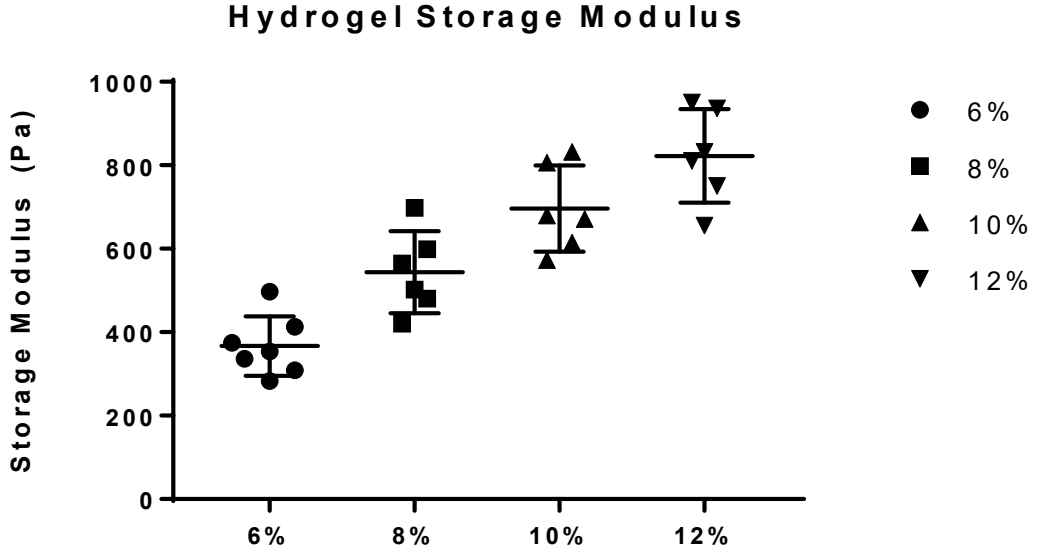

Figure 25 Storage Modulus of PEG-RGD hydrogels assessed via rheology. PEG hydrogels were mechanically tested and showed a linear correlation (Y = 75.95*X - 76.26 (R^2=0.994) between polymer density and storage modulus. 6% gels were significantly different from all other weight %.

VEGF-C + VEGFR2 + VEGFR3 (10ng/mL, 1ug/mL, 1ug/mL) to attenuate the effects fo VEGF-C. To understand the effect of pooled OASF on sprouting, samples were treated with either control media (10% FBS supplemented EBM) 10% bovine synovial fluid (BSF) or 10% pooled OASF supplemented EBM.

6.2.8 Hydrogel Characterization

The storage moduli of hydrogels of different PEG weight percentages were assessed by dynamic oscillatory strain and frequency sweeps performed on an MCR 302 stress-controlled rheometer (Anton Paar) with a 9-mm diameter, 2° cone, and plate geometry(Figure 25). Oscillatory frequency sweeps were used to examine the storage and loss moduli (ω = 1–100 rad s-1) at a strain of 2.3%.

6.2.9 Rodent Lymphatic Isolation and Encapsulation

Rat femoral lymphatic vessels were collected as previously described for

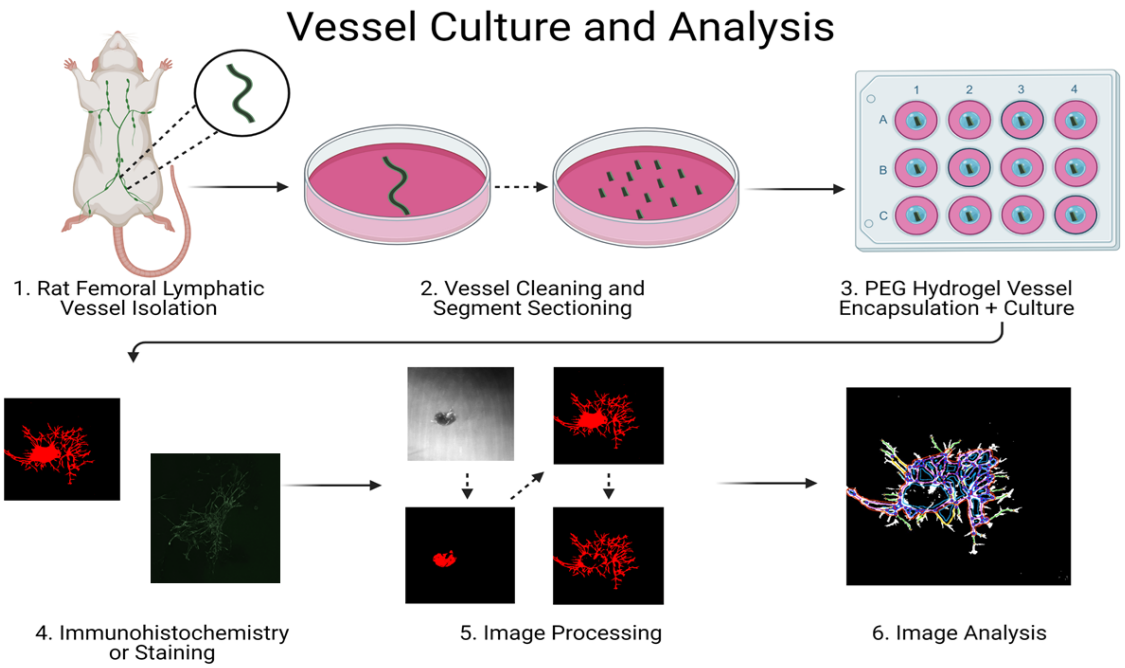

Figure 26 Ex vivo lymphatic vessel culture and image analysis.

lymphatic perfusion studies. To isolate mouse flank vessels, mice were euthanized via carbon dioxide. Flank vessels were then isolated by flaying the mice and pulling back the skin. For both vessels, after removing the vessels from the surrounding tissue, the vessel segment was removed and transported to a petri dish of EBM to remove fat and fascial tissue. Hydrogels were form hydrogels aseptically by carefully placing them into a solution of the cross-linking peptide in a 12 well plate. A solution of the adhesive peptide-functionalized PEG-4MAL macromer was then mixed in and allowed to polymerize for 15 min before the addition of the growth medium. Animal procedures were performed in compliance with procedures approved by the Georgia Institute of Technology Internal Animal Care and Use Committee (IACUC).

6.2.10 Tissue Culture

As previously described, rat and mouse vessel segments were cultured in an endothelial basal medium (EBM) formulation[353]. This consisted of EBM (Lonza,) supplemented with 10% FBS (Atlanta Biologicals), 1% penicillin-streptomycin (Gibco), 1% Glutamax (Gibco), 0.1% DBcAMP (Sigma), and 0.1% hydrocortisone acetate (Sigma). Vessel segments were cultured for a total of 5 days with no media changes. For epsin studies, vessel segments were cultured over the course of 7 days with a media change at days 3 and 5. The increased media changes were due to different limitations in terms of the availability of reagents.

6.2.11 Sprouting Analysis

Sprouting from rat vessel segments was analyzed via AngioAnalyzer (AA) software in ImageJ. Due to size variability, only the new growth from the vessel core was analyzed for complexity and normalized to the size of the core. Brightfield images taken during confocal images were converted into a maximum intensity projection, and then thresholding was used to identify the dark core, and the size of the core in pixels was calculated(Figure 26). The WGA image was then used to identify the entire network via thresholding, and the ImageJ image calculator tool was then used to subtract the core from the image. Finally, all images were converted to grayscale using the lookup table (LUT) feature in ImageJ to ensure that the images were in the proper color scheme for AA. AA was used with the following settings in batch mode: minimum object size (35), minimum branch size (25), artifactual loop size (100), isolated element size threshold (50), master segment size threshold (400), iteration number (2), show iteration (2). The only unchecked mapping setting was "suppress isolated elements," and all other options were selected. Sprouting from epsin mice was calculated by calculating the core area at day 0 and normalizing that to the day 7 area measured by actin staining.

6.2.12 Immunostaining and Imaging

RFLV samples were stained to assess morphology and cell type. Tissues were fixed for one hour with 4% PFA and washed with PBS 3 times, then stained overnight with wheat germ agglutinin (WGA) Alexa Fluor™ 633 conjugate (Invitrogen), which stains the cell membrane to assess general morphology. Samples were left to destain for at least 4 hours, then placed in a standard solution of DAPI + PBS and imaged via confocal imaging. After WGA staining, samples were then permeabilized with 0.5%

Triton-X for 20 minutes and then rinsed three times. After the third rinse, samples were blocked for 1 hour in a PBS containing 2% bovine serum albumin. The blocking solution was then removed, and samples were incubated with alpha-smooth muscle actin (eFluor570) ((αSMA, Mouse IgG2a, eBioscience) and CD31(AF488) to identify LECs (Polyclonal Goat IgG, RND Systems) suspended in a 2% BSA solution (1:200) overnight at 4C on a rocker. After a final three rinses, the samples were then imaged using confocal microscopy. Nonspecific isotype controls were incubated with samples at the same concentration as the primary antibodies to assess the extent of non-specific antibody binding. Imaging was conducted on an inverted confocal microscope (Zeiss LSM 710NLO).

6.2.13 Statistics

GraphPad Prism version 7.01 was used for statistical analysis. Student's t-tests were used when appropriate to test significance between two samples. All analyses were considered statistically significant if $p < 0.05$. Error bars on all data points are standard error. For the *ex vivo* lymphatic perfusion experiments, multiple comparisons were performed using a one-way or two-way ANOVA followed by a Dunnett multiple-comparison correction. For all cases, significance was defined as $p < 0.05$ (#, *, Ø) or $p < 0.01$ (##, **), $p < 0.001$ (###, ***), or $p < 0.0001$ (####, ****). For the *ex vivo* experiments, a # denotes a comparison with the control DMEM/F12 case, a * with the HSF case, and a Ø a comparison between the OASF-pool and the OASF#3.

6.3 Results

6.3.1 Effect of MMT surgery on lymphatic contractility

To test the effect of MMT surgery on lymphatic contractility. Lymphatic vessels from naïve, Sham, and MMT vessels were isolated 8-9 weeks after surgery or 8-9 weeks

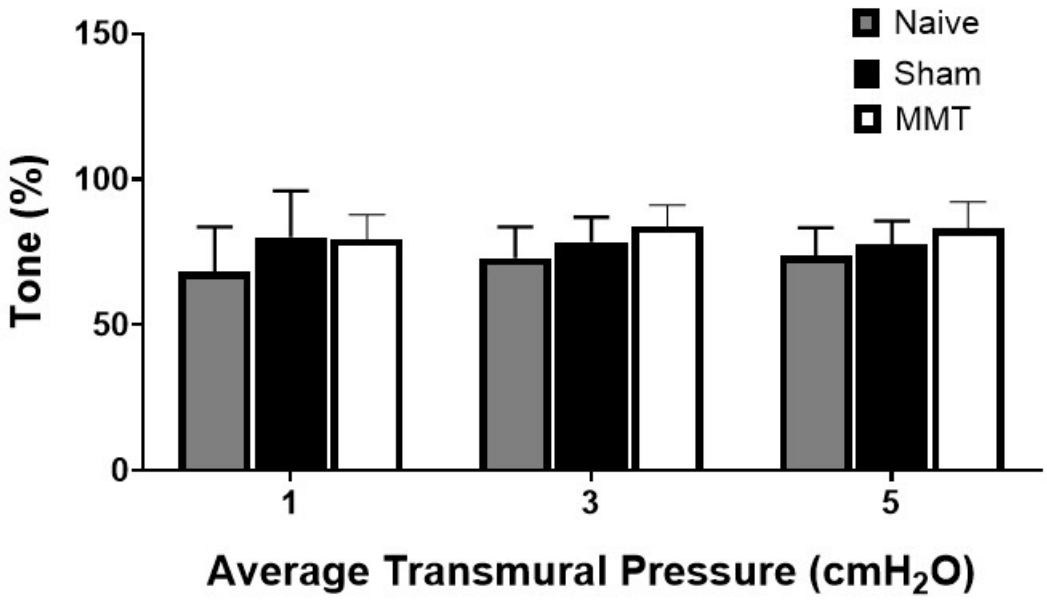

Figure 27 Tonic Contractions following MMT Surgery. Plots of tonic contractions. Tone (%) after isolation from Naïve (n=6), Sham (n=5), and MMT(n=5) animals. Each plot displays data from experiments at average transmural pressures of 1, 3, and 5 cm H2O for RFLVs in APSS. There are no significant differences to report following a two-way ANOVA with a Dunnett comparison

after the 1-week acclimation period for age match naïve controls. When the tonic activity was assessed at each pressure, there were no significant differences between Naïve, Sham, and MMT groups(Figure 27). Additionally, when we assessed the phasic lymphatic contractility metrics, frequency, fractional pump flow, and ejection fraction, we only saw a statistically significant increase in ejection fraction for MMT vessels

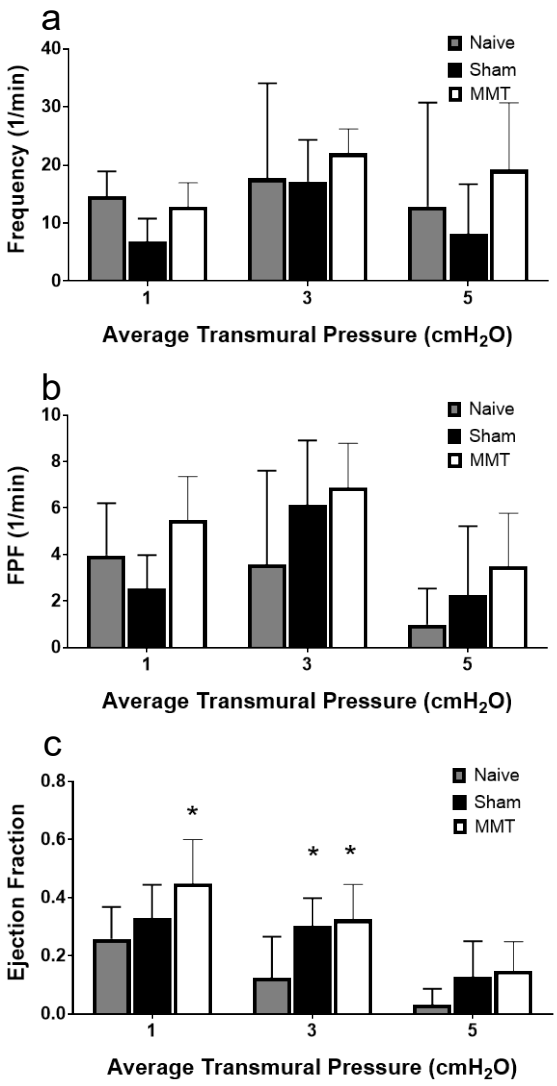

Figure 28 MMT surgery increases ejection fraction at low pressures. a) Analysis of phasic contraction frequency b) fractional pump flow and c) ejection fraction metrics for Naïve (n=6), Sham (n=5), and MMT(n=5) groups. Each plot displays data when vessels were held at average transmural pressures of 1, 3, and 5 cm H_2O. Symbols on top of error bars denote comparisons using two-way ANOVA followed by a Dunnett multiple-comparison correction with, $p < 0.05$ (*) vs Naïve.

compared to Naive at the lowest transmural pressure(Figure 28), perhaps suggesting that these vessels are in a hyperactivated contractile state, similar to what was shown in collecting lymphatic after remodeling in response to injury in the sheep[24].

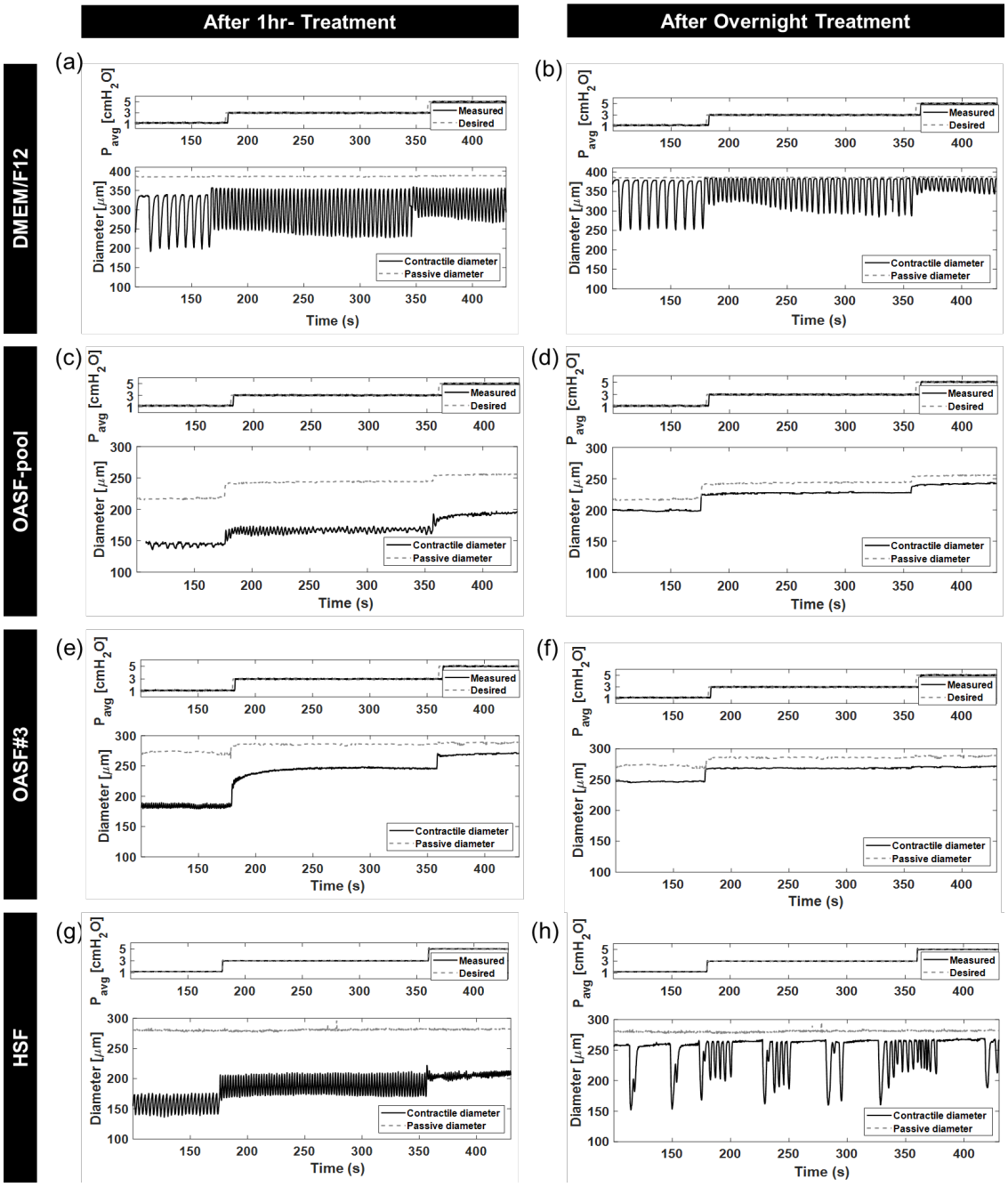

Figure 29 OASF treatment leads to the abrupt decrease in RFLV contractions. Diameter tracing: (a), (c), (e), (g) After 1hr- treatment, and (b), (d), (f), (h) After overnight treatment. Individual plots display trace diameters of RFLVs in: (a, b) DMEM/F12 (n=7), (c, d) OASF-pool (n=4), (e, f) OASF#3 (n=3), and (g, h) HSF (n=3). Average input and output pressures (cm H2O) are displayed on the top trace of each plot. They were changed simultaneously from 1 to 3 and 5 cm H2O (labelled). The outer diameter (μm) was measured continuously over time and plotted on the bottom trace (solid line). The outer diameter in Ca2+-free physiological solution (passive diameter; dashed line) was measured at the end of each experiment and plotted above the contractile diameter.

6.3.2 OA synovial fluid treatment enhances the tonic contractions in RFLVs

A single RFLV was isolated and cannulated on the *ex vivo* lymphatic perfusion system as described above. The RFLVs were treated with OASF#3 and HSF, like the *in vitro* studies, and included treatment with a mixture of pooled OASF from six people (OASF-pool).

First, we sought to investigate the effect of SF treatment on RFLV contractility qualitatively. To do so, we tracked the raw traces of RFLV contractions during the pressure step protocols after 1 hour or overnight treatment (Figure 29). We found that longer incubation times (overnight treatment) with SF led to decreased lymphatic diameter oscillations. Notably, OASF treatment (both OASF-pool and OASF#3) generated a reduction of diameter oscillations after 1-hr of treatment and a complete cessation of oscillations after an overnight treatment; HSF treatment, on the other hand, produced a gradual decrease in diameter. For the DMEM/F12 group, RFLV remained functional for the duration as indicated by the maintenance of frequent diameter oscillations with no significant change in amplitude or frequency at 1 hour or overnight timepoints.

After the pressure ramps and measurements presented above, we subsequently tested the corresponding effect of SF treatments on the tonic contractions of the isolated vessels. To do so, RFLVs were either left untreated (DMEM/F12) or treated with OASF-pool, OASF#3, and HSF for 1 hr (Figure 30a). After 1 hour, vessels treated with OASF-pool exhibited significantly increased tone at all three levels of transmural pressure compared to the untreated (DMEM/F12) case; the vessels treated with OASF#3 showed significantly increased tone only at the 1 cm H_2O pressure compared to the untreated

(DMEM/F12) case; the vessels treated with HSF showed increased tone at 1 and 3 cm H_2O compared to the untreated (DMEM/F12) case. Specifically, OASF-pool significantly elevated RFLV tonic contractions (by 25.66±5.62 at avP-1, 23.42±8.48 at avP-3, and 17.02±9.09 at avP-5; $p = 0.0005$, $p = 0.0026$, and $p = 0.013$, respectively). OASF#3 led to a significant increase of RFLV tonic contractions only for the lowest transmural pressure tested (by 21.25±6.01 at avP-1; $p = 0.0201$). Finally, HSF increased the tonic contraction of RFLVs in comparison to the control DMEM/F12 case (by 20.64±8.89 at avP-1 and 15.78±7.08 at avP-3; $p = 0.0044$ and $p = 0.0374$, respectively). Together, OASF-pool treatment was the only treatment that produced statistically significant increased tone for all applied transmural pressures.

Next, we investigated whether this enhanced tonic contraction observed during the short SF treatment (1hr- treatment) was maintained after the overnight treatment

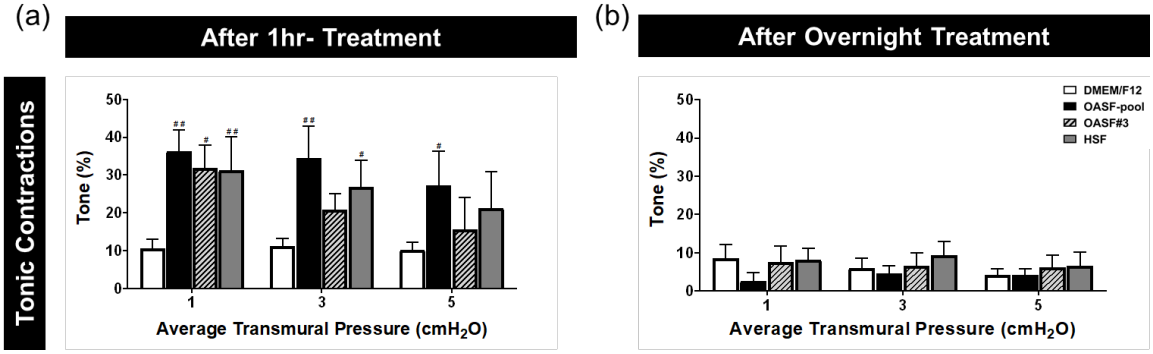

Figure 30 OASF treatment transiently enhances the RFLVs tonic contractions. Plots of tonic contractions. Tone (%) after treatment for (a) 1hr and (b) overnight. Each plot displays data from experiments at average transmural pressures of 1, 3, and 5 cm H2O for RFLVs in DMEM/F12 (n=7; white color), OASF-pool (n=4; black), OASF#3 (n=3; lined grey), and HSF (n=3; dark grey). All data represent mean values, and the error bars correspond to the standard error of the mean for each condition. Symbols on top of error bars denote comparisons using one-way ANOVA followed by a Dunnett multiple-comparison correction with, $p < 0.05$ (#) vs. control DMEM/F12.

(Figure 30b). We found that tone was still present (around 5-10%) and was within the level of untreated control conditions regardless of treatment, with no significant differences observed. Also, we found that at intermediate transmural pressure (avP-3), only OASF-pool treatment led to a significant change in tonic contractions. For low transmural pressure (avP-1), all SF treatments led to statistically significant tone index elevation compared to DMEM/F12.

6.3.3 OA synovial fluid treatment reduces the phasic contractions of rat femoral lymphatic vessels

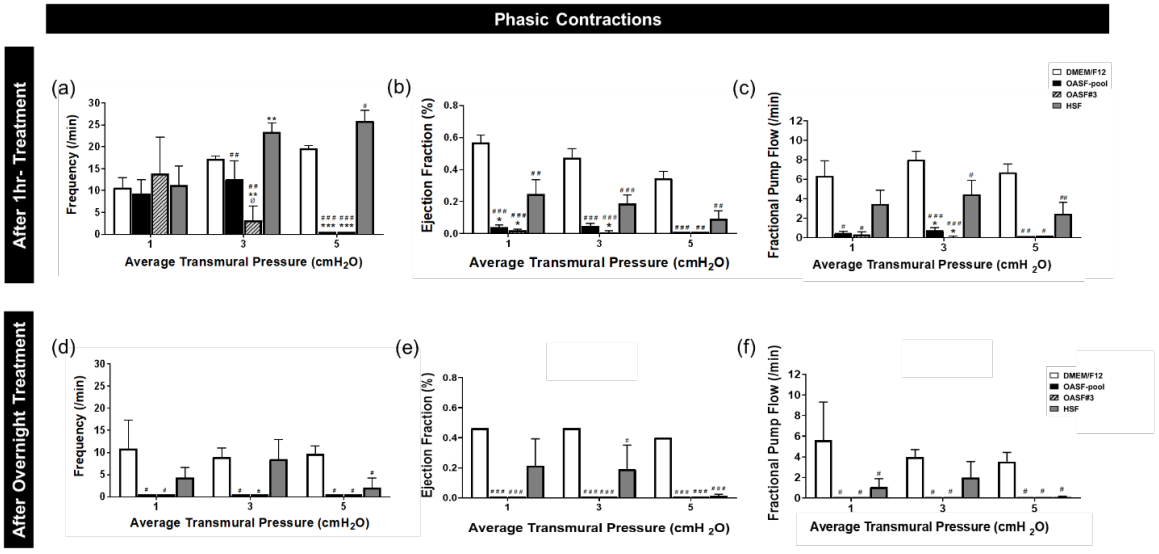

Figure 31 OASF treatment gradually reduces and eventually ceases the RFLVs phasic contractions. Analysis of phasic contraction metrics after treatment for (a-c) 1hr and (d-f) overnight: (a, d) Frequency (/min), (b, e) Ejection Fraction (%), and (c, f) Fractional Pump Flow (/min). Each plot displays data when vessels were held at average transmural pressures of 1, 3, and 5 cm H2O for RFLVs in DMEM/F12 (n=7; white color), OASF-pool (n=4; black), OASF#3 (n=3; lined grey), and HSF (n=3; dark grey). All data represent mean values, and the error bars correspond to the standard error of the mean for each condition. Symbols on top of error bars denote comparisons using one-way ANOVA followed by a Dunnett multiple-comparison correction with, $p < 0.05$ (#), $p < 0.01$ (##), $p < 0.001$ (###) vs. control DMEM/F12; $p < 0.05$ (*), $p < 0.01$ (**) vs. HSF; $p < 0.05$ (Ø) OASF-pool vs. OASF#3.

Here, we analyzed the effect of SF treatment on phasic contractions, namely the strong periodic contractions from the diastolic to the systolic diameter of the LV, as can be seen in Figure 33. After treatment for 1 hour, we found that the various SF treatments yielded different behaviors on the metrics quantifying pump function, namely frequency, ejection fraction, and fractional pump flow (Figure 31a-c). Specifically, both OASF-pool and OASF#3 significantly decreased the frequency of lymphatic contraction at the intermediate transmural pressure (by 10.78±4.27 and 14.02±3.25 at avP-3, respectively; p = 0.0088 and p = 0.0012, respectively), while it completely stopped the phasic contractions at higher transmural pressure (at avP-5). Contrarily, HSF increased the frequency of lymphatic contractions compared to the control DMEM/F12 case for intermediate and high average transmural pressures (by 6.08±2.08 at avP-3 and 6.25±2.43 at avP-5; p = 0.005 and p = 0.0218, respectively). Regarding the ejection fraction and fractional pump flow, SF treatment led to similar results. OASF-pool decreased the ejection fraction of lymphatic contractions compared to the control DMEM/F12 case (by 0.53 ±0.01 at avP-1 and 0.43±0.02 at avP-3; $p < 0.0001$ and $p < 0.0001$, respectively). In addition, OASF#3 decreased the ejection fraction of lymphatic contractions compared to the control DMEM/F12 case (by 0.55±0.02 at avP-1 and 0.46±0.01 at avP-3; $p < 0.0001$ and $p < 0.0001$, respectively). Again, OASF-pool and OASF#3 stopped phasic contractions at avP-5. Similarly, HSF lowered the ejection fraction (by 0.32±0.09 at avP-1, 0.29±0.05 at avP-3, and 0.25±0.05 at avP-5; p = 0.0006, p = 0.0007, and p = 0.0016, respectively). Notably, OASF (OASF-pool and OASF#3) treatment led to higher ejection reduction than the HSF treatment at low transmural

pressure. Finally, all SF treatments decreased fractional pump flow compared to the DMEM/F12 case (namely, OASF-pool: by 5.84 ±0.16 at avP-1 and 7.26±0.27 at avP-3; $p < 0.0111$ and $p < 0.0001$, respectively; OASF#3: by 5.97±0.27 at avP-1 and 7.94±0.09 at avP-3; $p = 0.0343$ and $p < 0.0001$, respectively, and HSF: by 3.56 ±0.05 at avP-3 and 4.28 ±0.05 at avP-5; $p = 0.0124$ and $p = 0.0035$, respectively). Notably, OASF treatment led to a lower fractional pump flow than the HSF treatment. These data together showed that short duration SF treatment (exposure) had no significant effect on the contractile frequency at low transmural pressure (avP-1); at intermediate (avP-3) and high (avP-5) pressures, OASF (OASF-pool and OASF#3) decreased while HSF increased the observed frequency. Finally, all treatments (OASF and HSF) significantly decreased fractional pump flow pressure for all applied pressures. Particularly, OASF treatment leads to a complete cease of contractions at high transmural pressure (avP-5).

Finally, we sought to determine whether these responses were maintained after a longer incubation (overnight treatment) (Figure 35d-f). OASF-pool and OASF#3 completely ceased phasic contractions at all applied transmural pressures, i.e., avP-1, avP-3, and avP-5. On the other hand, HSF significantly decreased the frequency of contractions only at high transmural pressure (by 7.55 ±2.12 at avP-5; $p = 0.0195$). HSF significantly reduced ejection fraction (by 0.27±0.16 at avP-3 and 0.39±0.01 at avP-5; $p = 0.0114$ and $p < 0.0001$, respectively), and fractional pump flow (by 4.54± at avP-1 and 3.47±0.08 at avP-5; $p = 0.05$ and $p = 0.0498$, respectively). Together, we found that overnight treatment with HSF, while having some negative effect on lymphatic

contraction, was not nearly as severe as the negative effects of OASF (OASF-pool and OASF#3) on lymphatic pump function.

6.3.4 PEG hydrogel system is tuned to assess pro and anti-lymphangiogenic factors

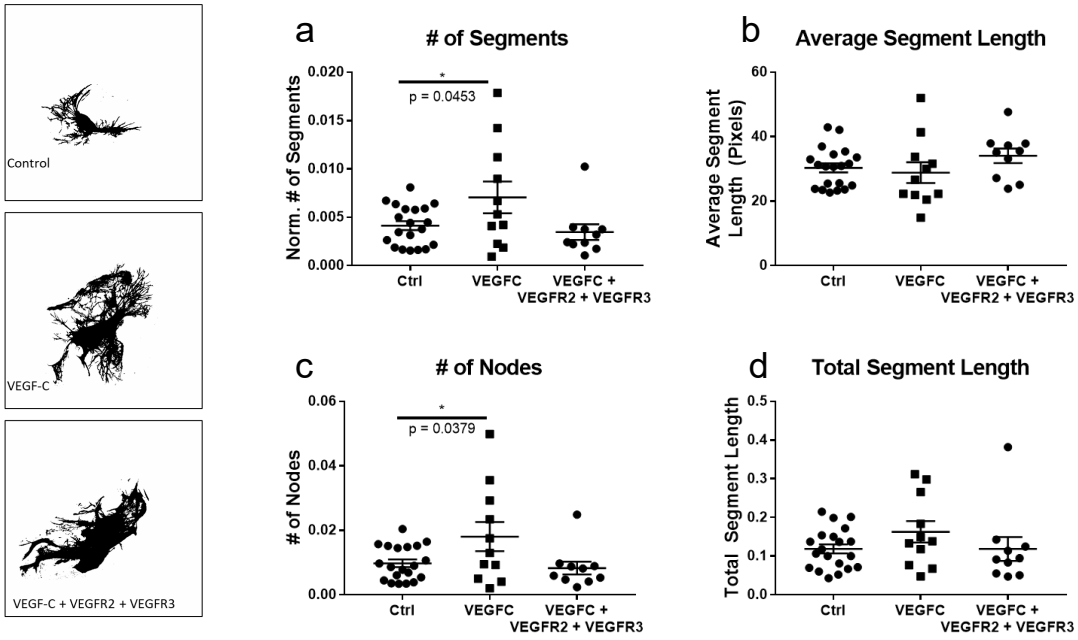

Figure 32 VEGF-C increases lymphatic growth metrics. The number of (a) segments, the (b) average segment length, (c) # of nodes and (d) total network segment length were calculated for lymphatic treated with VEGF-C or VEGF-C with soluble VEGFR3 & VEGFR2. VEGF-C treatment significantly increased the overall complexity of the network but not the overall network length. Symbols on top of error bars denote comparisons using one-way ANOVA followed by a Dunnett multiple-comparison correction vs. control (10%EBM) $p < 0.05$ (*),

RFLV segments were cultured over 5 days in either control media, VEGF-C supplemented media, or VEGF-C with soluble VEGFR2/VEGFR3 media. VEGFC significantly increased the # of segments (0.007±0.005 vs. 0.004±0.002, p=0.049) and # of nodes (0.018±0.015 vs. 0.0098±0.005, p = 0.038) while the average and total segment length was not different compared to control, indicating more branching occurred due to

VEGF-C. Blocking VEGFR2/3 signaling significantly attenuated the effect of VEGFC on sprouting. Figure 33 demonstrates that the sprouts eminating from these vessels are CD31 positive and therefore endothelial in nature.

6.3.5 OASF decreases lymphangiogenesis

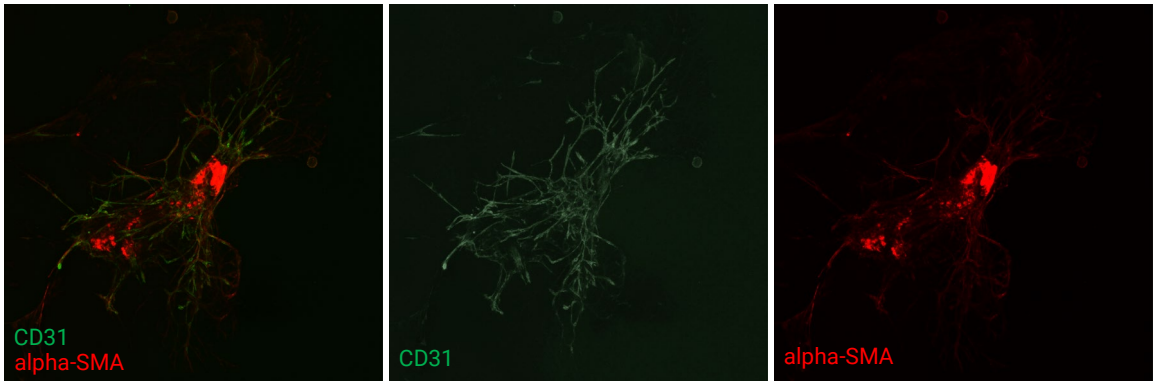

Figure 33 Lymphatic endothelial cells sprout from vessel core VEGF-C treated vessel stained for CD31 and alpha smooth muscle actin (alpha-SMA) shows that lymphatic endothelial cells sprout from the vessel core and migrate out into the ECM while the lymphatic muscle cells as stained by SMA are retained within the vessel core and do not significantly migrate and participate in the network. The same applied for vessels not treated with VEGF-C (Ctrl not pictured)

Given the ability to assess RFLV sprouting in the presence of pro-and anti-lymphangiogenic factors given the conditions, we were confident in our ability to tease

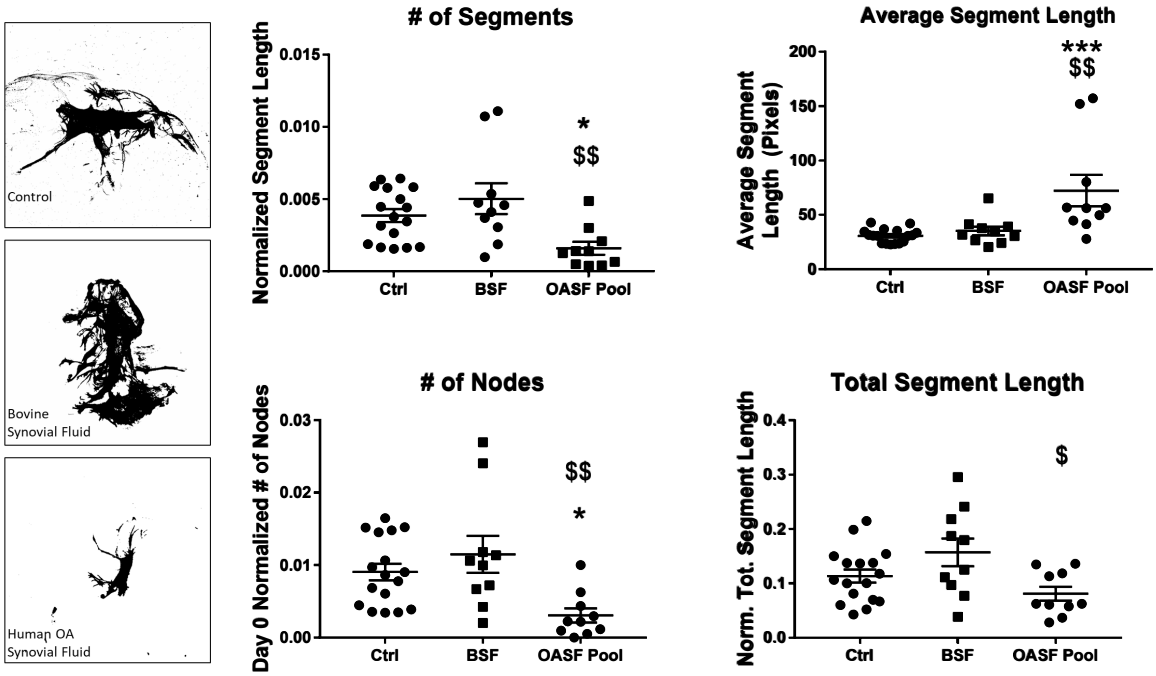

Figure 34 OA synovial fluid treatment reduces lymphatic growth. OASF decreases lymphatic growth parameters, specifically the number of segments # of nodes and average segment length compared to BSF – supplemented and 10% FBS EBM control . OASF significantly reduced complexity of the network but not the overall network length. Symbols on top of error bars denote comparisons using one-way ANOVA followed by Tukey's multiple-comparison correction vs. Ctrl (10%EBM) $p < 0.05$ (*), $p \leq 0.001$ (***), or vs BSF $p < 0.05$ ($), $p \leq 0.01$ ($$).

out the effect of OASF in lymphangiogenesis(Figure 34). OASF significantly decreased the # of segments (0.0020 ± 0.0008 vs 0.004±0.002) (p=0.002), nodes (0.005±0.002 vs 0.009±0.00, p=0.0014), and the average segment length (30.78±6.43 vs37.93±5.02 pixels, p=0.0009) compared to control samples. Total segment length, however, was not significantly different between OASF treated samples and controls. Bovine synovial fluid data

6.3.6 Epsin deletion decreases sprouting lymphangiogenesis from collecting vessel segments

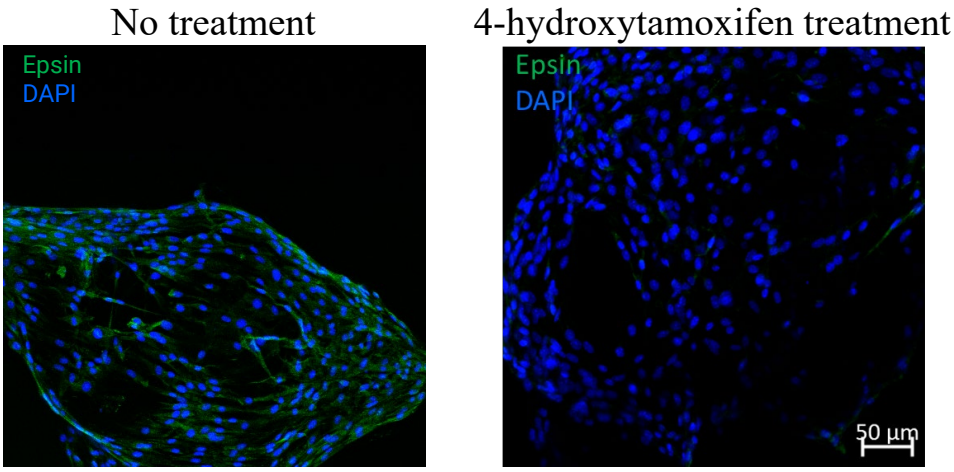

Figure 35 4-hydroxytamoxifen administration results in epsin deletion. Epsin DKO mice were generated using a course of 4-hydroxytamoxifen. Compared to mice who were not injected with tamoxifen

The in vivo deletion of epsin was assessed by encapsulating mice flank vessels from mice with and without in vivo lymphatic-specific knock-out of epsin 2 in PEG hydrogels. When epsin DKO mice were compared to control mice (Figure 35), epsin staining was significantly reduced, confirming that epsin was successfully deleted.

To quantify the effect of epsin deletion on lymphatic collecting vessel lymphangiogenesis, mouse flank vessels were encapsulated in PEG hydrogels and grown in either 1%, 5%, or 20% FBS supplemented EBM growth media. The growth was quantified by normalizing the day 0 area in brightfield to the day 7 area via confocal imaging(Figure 36) to account for slight differences in initial segment implantation size. In 1% serum, the % increase in area was significantly decreased in Epsin DKO compared

to wild type (140.5 ± 35.37 vs. 30.11 ± 18.1, p = 0.0073). However, in 5% and 20%

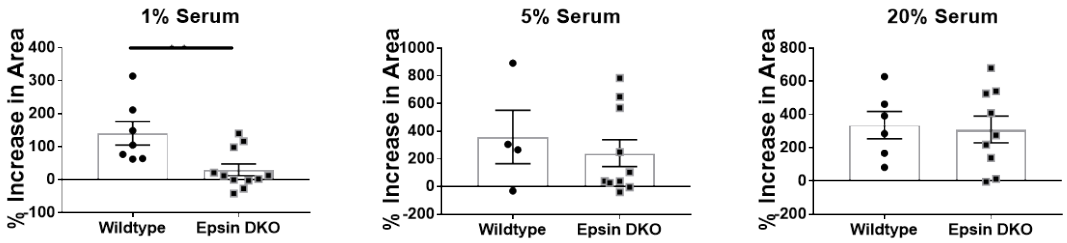

Figure 36 Epsin deletion leads to reduced growth in low serum. Wildtype mice and epsin DKO were encapsulated in PEG hydrogels with increasing concentrations of serum factors. 1% serum significantly reduced the % increase in area compared to wildtype mice. In higher percentages of serum (5% & 20%) epsin deletion did not affect sprouting. Symbols on top of error bars denote statistical comparisons using student's t-test. p ≤ 0.01 (**),

serum, there was no significant effect of epsin deletion. These results suggest that in low serum conditions, where growth factors are sparse, epsin serves to enhance collecting vessel sprouting, perhaps through its involvement in localizing the expression of VEGFR3 to tip cells and downregulating its expression elsewhere[365].

6.4 Discussion

The lymphatic system plays an essential role in maintaining joint homeostasis and may contribute to the development and progression of OA[6,11,336,337]. Previous studies have shown that lymphatics play a critical role in the clearance of different molecules from the SF of the joint. The SF acts as a lubricant in the joint and serves as a fluid to transport nutrients and waste[8]. During OA disease development and progression, the composition of the SF changes as it loses its lubricating properties, and there is a buildup of degradation by-products and inflammatory cytokines, which feedback to exacerbate the

disease process[94,338–340]. These changes in SF composition have been thought to be due mainly to the production of these factors, but studies on lymphatic function suggest that a dysfunctional lymphatic system may also impair the clearance of these factors.

Furthermore, there is an established correlation between SF clearance and progression of arthritis [318]. Thus, changes in lymphatic function and permeability in the OA disease could potentially lead to increased SF transport into the lymphatics, thus suggesting a potential future therapeutic target[366–368]. Recent studies have even established the potential utility of targeting the lymphatic system as a therapeutic modality for OA and shown that a regenerative therapy that specifically enhanced lymphangiogenesis and lymphatic function could attenuate OA disease development[369]. Despite the importance of the lymphatic system and SF in OA disease, the direct relationship between the two is poorly understood. To our knowledge, this work constitutes the first *ex vivo* investigation of how RFLVs respond to SF treatment in the case of OA.

In the first study in this chapter, we isolated RFLVs from surgery animals 9-weeks post-surgery. We observe acute changes in the contractility of MMTvessels, particularly the fractional pump flow at low pressures. These findings suggest that the vessel may be in a heightened contractile state, as demonstrated by previous lymphatic injury models[370]. In this sheep study, the lymphatic injury initiated by ligation of one of two parallel lymphatic vessels in the hind limb led to structural and functional changes in the intact, lymphatic vessel over six weeks. In *ex vivo* isolated vessel experiments, the lymphatic vessel displayed increasing intrinsic contractile frequency, force generation,

and vessel compliance, showing that injury can affect parallel or nearby lymphatic vessel contractility. One aspect of this sheep study that was not feasible in our study was the *in vivo* imaging of lymphatic contractility through the skin. Post-injury also changed the intact lymphatic vessel function *in vivo* as measured by the NIR function. Future studies in the rat could measure *in vivo* lymphatic function, knee clearance, and *ex vivo* isolated vessel function to see a relationship between the three. Future work could look for elevated oxidative stress in lymphatic muscle, and we do not know the long-term consequences of this on lymphatics. The kinetics of human disease are much longer than in the rat, and the deterioration of lymphatic muscle function may only present with age and time.

OASF treatment of isolated LVs *ex vivo* transiently enhanced the tonic contractions, while it gradually reduced and eventually ceased the RFLVs phasic contractions. Historically, it has been demonstrated that the primary mechanisms used to fill the lymphatics are: (1) for initial lymphatics, the extrinsic pump, which responds to both steady-state lymph volumes and unsteady initial lymph volumes, and (2) for collecting lymphatics, the spontaneous muscle contractions[135,141]. This intrinsic phasic contraction of the lymphatic vessels was abolished entirely after 24 hours of treatment with OASF; even though the phasic contractile function was lost, the muscle of the vessel still maintained some functional integrity as observed by the presence of vessel tone even after the overnight treatment. The loss of phasic contractility suggests that the active function of the lymphatics has been impaired while the passive flow or flow-induced through extrinsic contractile mechanisms (e.g., surrounding skeletal muscle contraction)

may still be functional; this would result in impaired and slower clearance from the joint which could exacerbate OA progression. HSF also affects the RFLV reducing the contractions; however, this effect was not nearly as severe as OASF from either the pooled SF or the SF exclusively from patient 3. In addition, the baseline contraction frequency of isolated vessels removed from their *in vivo* microenvironment is generally much higher than what has been observed *in vivo* [371]. Thus this reduction in contraction with HSF may represent a normal physiologic response.

Data from the cytokine array provides insight into elevated molecules and warrant further investigation (Figure 24). First, IFN-γ inducible protein (IP-10) levels in SF have been demonstrated to be inversely associated with the severity of knee OA [372] consistent with cytokine levels from the OASF samples in this study (high IP-10 levels *only* in HSF; Figure 23). IFN-γ has also been shown to stimulate the lymphatic endothelium facilitating the recirculation of lymphocytes during a local immune response[373]. IL-8 has been demonstrated to play an essential role in lymphatic vessel regeneration and endothelial cell growth[374,375]. Thus its elevated expression in HSF suggests a potential role of the lymphatic system as a therapeutic modality. IL-7 has been shown to play a crucial role in cartilage degradation during rheumatic diseases and correlated with the initiation and progression of OA[376–379]; it has also been suggested as a potential mediator of lymphatic drainage [36]. IL-2 has been shown to contribute to the immunopathogenesis of rheumatoid arthritis [380]. The elevated levels of IL-7 and IL-2 in OASF#3 indicate a partial OA phenotype. IL-15 is a pro-inflammatory cytokine that is increased in joint fluids of early-stage OA patients and has been associated with corresponding damage of

cartilage [381], and this is in agreement with the IL-15 elevated expression found in OASF-pool. Both IL-2 and IL-15 promote the development, homeostasis, and function of regulatory T cells in lymphoid tissues [382,383]. Their high expression in OASF#3 and OAS F-pool, respectively, suggests a potentially strong implication of the lymphatic system. The gradual diminishment of both tonic and phasic contractions was observed with the increase of SF treatment time. Furthermore, the average size of the above cytokines (~ 20 kDa) suggests clearance through draining lymph nodes after entering the interstitial fluid space [220,249]. This provides strong evidence on the importance of establishing representative *ex vivo* models for the investigation of OA.

The *ex vivo* systems are models by which we can investigate the effects of SF on collecting vessel lymphangiogenesis and RFLV function, yet as model systems, they have their limitations. To approximate the amount of SF that might end up in the lymph, we chose to dilute the SF to 10% of the volume of the media that was perfused through the lumen of the vessel contained SF. This was an approximation as it is unclear what the exact dilution of SF contents is within the pre-nodal lymph immediately draining the vessel. Furthermore, the relative concentrations of proteins and molecules between the two compartments are likely a function of the size of the individual molecule, as has been shown in other tissue beds[8,384]. In addition, as mentioned earlier, the frequency of lymphatic contractions in these idealized isolated vessel preparations is often higher than what is observed *in vivo*, suggesting that there are factors from the *in vivo* context that are not recapitulated in the isolated vessel preparation. Another limitation is the limited sample size of HSF and OASF-pool. Due to the lack of SF from healthy individuals and

the limited availability of SF from OA patients, the experimental outcome may be highly patient-dependent. Thus, the interpretation/ extrapolation of these observations should be conducted with caution. Another similar restriction is the limited amount of SF, which challenged the execution of both the *in vitro* and *ex vivo* experiments. Another limitation is the use of human-derived SF to treat rat vessel segments and rat-derived collecting vessels(*ex vivo* studies).

In this CHAPTER we also used the PEG hydrogel platform to determine the effect of OASF on lymphangiogenesis. In order to do so, we first determined the phenotype for femoral lymphatic vessels in response to VEGF-C treatment. VEGF-C treatment did not increase the network area. However, it increased the sprouting complexity as represented by more segments and decreased average branch length, which Bruyere et al. showed by quantifying the number of intersections at defined distances from the core. Additionally, as previously demonstrated in other studies, we wanted to demonstrate whether this response to VEGF-C could be attenuated by blocking VEGF-C signaling with the addition of exogenous soluble VEGFR2 and VEGFR3.

Given that n # of continuous nodes (n-1) would make up n-1# of segments or branches, the number of nodes corresponded closely with the number of branches. After demonstrating that the collecting vessel networks increase their sprouting complexity, but not overall sprout length, in response to VEGF-C, we then used pooled OASF to determine if it had a pro or anti-lymphangiogenic effect. One of the limitations of this study was that non-OA human SF was not in great abundance. Therefore, we used bovine

synovial fluid to control non-OA SF, which could be purchased in quantities comparable to that of OASF.

OASF treatment of lymphatics in the hydrogel significantly reduced lymphangiogenesis as measured by the number of segments. These samples were collected from patients with effusions. Therefore, this decreased lymphangiogenesis could indicate how synovial effusion presents *in vivo* as Walsh et al. showed that joint effusion was well correlated with reduced lymphatic vessel density[6]. While the exact molecular mechanisms responsible for this reduction in lymphatic sprouting remain unknown, future work should encompass which genes are dysregulated after treatment with OASF and which cytokines present in the synovial fluid have the most significant impact. Some of the pro-lymphangiogenic cytokines found in the pooled synovial fluid include IL-1a, VEGF, Flt-3L, while other cytokines like IL-1RA and IL-10 are directly and indirectly anti-angiogenic *in vivo.* One of the limitations of our study is that many of the factors present in synovial fluid regulate lymphangiogenesis through primary mechanisms with t-cells or macrophages; however, these support cells are not present in great quantity in our system[370,385]. A secondary limitation of our study was that bovine synovial fluid was used as our non-OA synovial fluid control. However, this is a first dive into the effect of OA on lymphangiogenesis *ex vivo*, and bovine synovial fluid has been used as a control for study synovial fluid viscosity. Additionally, in mammals, many small proteins are well conserved.

Given the demonstrated importance of epsins in regulating VEGFR3 expression in LECs, we used an inducible double knockout of epsin 1 and 2 to determine the effect

of epsin deletion on mature collecting vessels lymphangiogenesis. Epsin deletion in a variety of contexts has been shown to increase lymphangiogenesis[33,157,169]. Therefore, we hypothesized that epsin deletion in our context would also increase lymphangiogenesis from collecting vessels. However, we saw that in high serum, where growth factors were abundant, epsin deletion did not affect lymphangiogenesis. However, in reduced serum conditions, epsin DKO reduced growth from the vessel core. In vivo, the patterning of VEGFR3 receptors in lymphatics is well regulated[157,386,387]. VEGFR3 is expressed in abundance at the capillary level compared to the collecting vessels that only express VEGFR3 at the valves[365]. Thus, collecting vessels may upregulate VEGFR3 expression to induce lymphangiogenesis appropriately, and epsin dysregulation may alter that process. Future work must be conducted to tease out the differences between capillary lymphangiogenesis and collecting vessel lymphangiogenesis. This differential response with epsin deletion may be one of the first explorations into how these two tissues may differ in that way.

6.5 Conclusions

This work utilized a surgical model of OA and a simulated OA environment to investigate the potential effect of SF draining into lymph fluid on lymphatic function and contractility. MMT surgery did not significantly affect lymphatic contractility compared to sham vessels; however, it significantly affected contractility on low pressure. Finally, it is worth noting that the vessels were removed from an *in vivo* environment, demonstrating that these parameters should be tested *in vivo* as future technologies allow us to do so.

The striking effect of OASF (OASF-pool and OASF#3), which significantly attenuated and eventually completely impaired the tonic and phasic lymphatic contractions, demonstrates a critical relationship between diseased SF and the lymphatic system, which could play an essential role in the progression of OA[114,319,337,388,389]. Additionally, isolating specific factors that have the most potent effect on contractility and lymphangiogenesis could provide a new therapeutic target and would be highly beneficial when combined with other regenerative and restorative therapies in treating OA patients.

Using the PEG hydrogel system, we were able to establish two significant findings. Firstly, pooled OASF had a negative effect on lymphangiogenesis *ex vivo*. We used the synovial fluid control as bovine synovial fluid, which may not adequately simulate human synovial fluid to synovial fluid. Future synovial fluid studies should be done with human samples and genetic analysis tools that can assess which genes are dysregulated with synovial fluid treatment. Our second significant finding with the PEG hydrogel was that collecting vessel lymphangiogenesis was not significantly increased via the deletion of epsin as demonstrated in initial lymphatics and with dermal LECs[33]. Additionally, in reduced serum factors, lymphangiogenesis sensitivity was decreased, showing that lymphangiogenesis at the different hierarchal levels of lymphatic structure may occur differentially.

CHAPTER 7. CONCLUSIONS AND FUTURE DIRECTIONS

7.1 Conclusions

The work reported in this thesis supported many principal contributions.

1. We established that ET-1 could significantly decrease venous and lymphatic drainage from the joint.
2. Developed multichromatic NIR imaging to assess venous and lymphatic drainage and saw that exercise transiently increases lymphatic clearance *in vivo*.
3. We determined the dynamic effect of MMT surgery on microvascular clearance, showing that venous clearance increased at early time points and that lymphatic clearance is decreased at later stages from the joint space.
4. Using treadmill running with rats, we established an initial mechanism by which exercise may improve joint function and health by increasing clearance at later time points.
5. We established a link between reduced collecting lymphatic vessel contractility and OA synovial fluid.
6. Using a PEG hydrogel sprouting platform with collecting lymphatic vessels, we showed that:
    a. OA synovial fluid treatment significantly reduces lymphangiogenesis
    b. Epsin deletion decreases collecting vessel lymphangiogenesis in reduced serum conditions

Intra-articular clearance has been investigated in the context of rheumatic and arthritic diseases for a half-century. Particularly iodinated proteins have been used to assess lymphatic function and free radioiodine as a metric for venous clearance[111,219,253,390]. These seminal works have laid the foundation of this thesis to help establish normal and disease venous and lymphatic clearance. In addition, previously reduced lymphatic function either through downstream clearance or lymphatic vessel uptake in the joint has been considered a potential mechanism for joint dysfunction, but the *in vivo* functional effects remain understudied. The work presented in this thesis represents two technological and scientific advances in the way we can study OA. Firstly, multichannel NIR imaging can be used to assess tracer clearance from the joint space with great sensitivity, and secondly, *ex vivo* platforms to test lymphatic vessel contractility and lymphangiogenesis in the context of externally applied biochemical signals.

Through NIR imaging, we learned that the synovial fluid is very effective at retaining intra-articularly delivered biomolecules. This retention is likely one of the intentional biological functions to slow down the flow of materials from the joint space and retain water and nutrients balance. We learned that our post-traumatic OA model had a dynamic change in venous and lymphatic clearance with a contralateral control. In the context of exercise, we showed that exercise only had a modest effect on lymphatic outflow in healthy joints but substantial effects on clearance in OA joints six weeks post-surgery.

In this thesis, we determined that synovial lymphatics are sensitive to the OA environment. The use of *ex vivo* lymphatic perfusion systems has enabled us to answer complex questions in the field of lymphatic because we have more precise controls over individual factors such as pressure, flow, and biochemical environment. Additionally, we showed that synovial lymphatic collecting vessel sprouting is significantly reduced in the presence of OASF, an observation that corresponds with the observed decreases in human lymphatic vessel density. In CHAPTER 3, we showed that ET-1 could completely abrogate flow from the joint for hours only for flow to resume eventually. Similarly, in these *ex vivo* lymphatic platforms, we determined that lymphatics lost their phasic contractile activity with synovial fluid treatment. These *in vivo* and *ex vivo* studies are some additional pieces that could explain how joint clearance is altered in OA.

7.2 Future Directions

The findings in this thesis have led to several questions that should be addressed going forward. The potential research initiatives that could be explored in the future encompass the following set fundamental questions:

(1) Does the intensity and duration of exercise affect the rate of clearance of materials from the joint space?
(2) How does clearance change in spontaneously occurring or non-surgical models of OA?
(3) How do HA sieving and HA size change with OA progression?
(4) How do synovial blood and lymphatic density change in the MMT model?

(5) Can this lymphatic sprouting platform be used as a screening platform for lymphatic targeting treatments in OA?

(6) How do lymphatic collecting vessels respond to flow after treatment with OASF?

The multichannel NIR imaging approach has shown to be sensitive to detecting changes in vascular clearance *in vivo*. Given these resources, multiple approaches can be implored to elucidate further the effect of exercise, spontaneous OA, and PTOA on joint clearance. The use of larger HA tracers in these contexts could provide better information about HA diffusivity, synovial permeability, and HA catabolism, as previously shown[221]. While it is difficult to uncouple these two parameters *in vivo,* using modeling techniques, histological analysis, and NIR imaging could help elucidate fluid and macromolecule transport changes in the joint. Next-generation NIR imaging, NIR-II, could provide a deeper (imaging depth-related pun) perspective on microvascular function *in vivo,* given its ability to visualize deeper structures *in vivo*[391]. Currently, the downstream femoral lymphatic function in rats or humans has not been assessed in OA *in vivo*. That type of experiment would require surgically creating an imaging window or doing a terminal experiment where the skin is exposed.

Currently, NIR imaging is limited by the larger machinery necessary to acquired data; however, as wearable sensors become a more feasible technology in the context of NIR imaging, then this will allow us to sample data at a much higher frequency and show the instantaneous effects of interventions like exercise, PTOA, and ET-1 on microvascular clearance. One of our system's limitations was our inability to decouple trans-synovial fluid flow and trans-synovial membrane diffusion and transport. One of

the mechanisms by which we could improve our ability to differentiate the changes in OA would be to use HA as the material we are tracking. By guaranteeing that the material of interest would also participate in the synovial fluid matrix, we would be able to long-term assess the effect of PTOA on HA catabolism and HA clearance from the joint space. Lastly, to connect the dots between changes in clearance, synovial fluid integrity and to consider biochemical approaches to reducing OA's effect on joint function, there is a significant need for synovial fluid analysis and synovial membrane quantification.

One of the limitations of the MMT model used in this thesis is that it requires a major surgical insult which may affect our interpretation of the clearance data. Using a less invasive model of OA to investigate clearance could provide more usefulness about the progressive nature of microvascular changes in OA[392]. Another technical advancement that would significantly improve our understanding of how intra-articular pressure changes in the context of OA would be a wearable IAP pressure monitor. Additionally, using contrast agents to assess joint volume could help understand how IA injections and disease affect synovial fluid volume.

Using lymphatics in two *ex vivo* contexts allowed us to elucidate mechanisms that are difficult to observe *in vivo* in real-time. While the limitations of *ex vivo* systems are that the tissues are generally exposed to fewer factors (i.e., cells, mechanical forces) than they would be in vivo, in many ways, the innovative use of clinical patient samples allowed us to attempt to recapitulate the in vivo OA environment. In terms of lymphatic contractility, we know that lymphatic vessels are responsive to pressure and flow[393].

However, using our lymphatic pressurization system setups, we only modulated transmural pressure. In the future, we could determine the effect of flow on lymphatic contractility in response to the OASF treatment. Additionally, understanding if the proteome of the synovial fluid and the downstream lymph are similar could allow us to understand the proper way to model lymph from the knee joint.

Lymphangiogenesis has been classically understudied in vitro. Many advances in knowledge about lymphangiogenesis have been made studying embryonic development. However, mature collecting vessel lymphangiogenesis remains significantly understudied today, and this PEG hydrogel platform has created a tunable medium by which we can explore a variety of intrinsic and extrinsic factors that regulate lymphatic growth. In addition to using lymphatic tissues, we could only combine different cell types with lymphatic in vitro to determine what effect support cells like synoviocytes and macrophages have on lymphatic growth. Given the rat synovium structure, it could serve as a tissue to extract and culture in hydrogels. Co-culture could help explore what role synoviocytes, lymphatic, blood vessels, and resident cells within the synovium play on lymphatics. Lymphatic vessels cultured with synovial tissue from OA animals (horses, pigs, rats) and this co-culture system could explain how cellular communication between synoviocytes and lymphatics influences OA progression.

REFERENCES

1. Rat, A. C. *et al.* OAKHQOL: A new instrument to measure quality of life in knee and hip osteoarthritis. *J. Clin. Epidemiol.* **58**, 47–55 (2005).

2. Sharma, A., Kudesia, P., Shi, Q. & Gandhi, R. Anxiety and depression in patients with osteoarthritis: Impact and management challenges. *Open Access Rheumatol. Res. Rev.* **8**, 103–113 (2016).

3. Newberry, S. J., FitzGerald, J. & SooHoo, N. F. *Treatment of Osteoarthritis of the Knee: An Update Review*. *Comparative Effectiveness Review* (2017). doi:10.23970/AHRQEPCCER190

4. Kataru, R. P. *et al.* Critical role of CD11b+ macrophages and VEGF in inflammatory lymphangiogenesis, antigen clearance, and inflammation resolution. *Blood* **113**, 5650–5659 (2009).

5. Flister, M. J. *et al.* Inflammation induces lymphangiogenesis through up-regulation of VEGFR-3 mediated by NF-κB and Prox1. *Blood* **115**, 418–429 (2010).

6. Walsh, D. a. *et al.* Lymphatic vessels in osteoarthritic human knees. *Osteoarthr. Cartil.* **20**, 405–412 (2012).

7. Han, H. *et al.* Fang-Ji-Huang-Qi-Tang Attenuates Degeneration of Early-Stage KOA Mice Related to Promoting Joint Lymphatic Drainage Function. **2020**, (2020).

8. Levick, J. R. & McDonald, J. N. Fluid movement across synovium in healthy joints: Role of synovial fluid macromolecules. *Ann. Rheum. Dis.* **54**, 417–423 (1995).

9. Levick, J. R. Contributions of the lymphatic and microvascular systems to fluid absorption from the synovial cavity of the rabbit knee. *J. Physiol.* **306**, 445–61 (1980).

10. Liang, Q. qian, Shi, Q., Wood, R. W., Xing, L. ping & Wang, Y. jun. Peri-articular

lymphatic system and ‘Bi’ theory of Chinese medicine in the pathogenesis and treatment of arthritis. *Chin. J. Integr. Med.* **21**, 648–655 (2015).

11. Shi, J. *et al.* Distribution and alteration of lymphatic vessels in knee joints of normal and osteoarthritic mice. *Arthritis Rheumatol.* **66**, 657–666 (2014).

12. Shi, J. X. *et al.* Use of a whole-slide imaging system to assess the presence and alteration of lymphatic vessels in joint sections of arthritic mice. *Biotech Histochem* **88**, 428–439 (2013).

13. Xu, H. *et al.* Distribution of lymphatic vessels in normal and arthritic human synovial tissues. *Ann. Rheum. Dis.* **62**, 1227–1229 (2003).

14. Wang, W. *et al.* Attenuated Joint Tissue Damage Associated With Improved Synovial Lymphatic Function Following Treatment With Bortezomib in a Mouse Model of Experimental Posttraumatic Osteoarthritis. *Arthritis Rheumatol.* **71**, 244–257 (2019).

15. Hao, X., Wang, S., Zhang, J. & Xu, T. Effects of body weight-supported treadmill training on cartilage-subchondral bone unit in the rat model of posttraumatic osteoarthritis. *J. Orthop. Res.* 1–9 (2020). doi:10.1002/jor.24791

16. Nguyen, C., Lefèvre-Colau, M. M., Poiraudeau, S. & Rannou, F. Rehabilitation (exercise and strength training) and osteoarthritis: A critical narrative review. *Ann. Phys. Rehabil. Med.* **59**, 190–195 (2016).

17. O’Connor, S. R. *et al.* Walking exercise for chronic musculoskeletal pain: Systematic review and meta-analysis. *Arch. Phys. Med. Rehabil.* **96**, 724-734.E3 (2015).

18. Zhang, H. *et al.* The Therapeutic Effects of Treadmill Exercise on Osteoarthritis in Rats by Inhibiting the HDAC3/NF-KappaB Pathway in vivo and in vitro. *Front. Physiol.* **10**, 1–16 (2019).

19. Cruz-Acuña, R. *et al.* PEG-4MAL hydrogels for human organoid generation, culture, and in vivo delivery. *Nat. Protoc.* **13**, 2102–2119 (2018).

20. García, A. J. PEG-maleimide hydrogels for protein and cell delivery in regenerative medicine. *Ann. Biomed. Eng.* **42**, 312–322 (2014).

21. Quick, C. M., Ngo, B. L., Venugopal, A. M. & Stewart, R. H. Lymphatic pump-conduit duality: Contraction of postnodal lymphatic vessels inhibits passive flow. *Am. J. Physiol. - Hear. Circ. Physiol.* **296**, 662–668 (2009).

22. Telinius, N. *et al.* Human thoracic duct in vitro: Diameter-tension properties, spontaneous and evoked contractile activity. *Am. J. Physiol. - Hear. Circ. Physiol.* **299**, 811–818 (2010).

23. Gashiev, A. A., Davis, M. J., Delp, M. D. & Zawieja, D. C. Regional variations of contractile activity in isolated rat lymphatics. *Microcirculation* **11**, 477–492 (2004).

24. Razavi, M. S., Nelson, T. S., Nepiyushchikh, Z., Gleason, R. L. & Dixon, J. B. The relationship between lymphangion chain length and maximum pressure generation established through in vivo imaging and computational modeling. *Am. J. Physiol. - Hear. Circ. Physiol.* **313**, H1249–H1260 (2017).

25. Nelson, T. S. *et al.* Minimally invasive method for determining the effective lymphatic pumping pressure in rats using near-infrared imaging. *Am. J. Physiol. - Regul. Integr. Comp. Physiol.* **306**, (2014).

26. Bove, S. E. *et al.* Surgically induced osteoarthritis in the rat results in the development of both osteoarthritis-like joint pain and secondary hyperalgesia. *Osteoarthr. Cartil.* **14**, 1041–1048 (2006).

27. Willett, N. J. *et al.* Intra-articular injection of micronized dehydrated human amnion/chorion membrane attenuates osteoarthritis development. *Arthritis Res. Ther.* **16**, R47 (2014).

28. García, J. R., Clark, A. Y. & García, A. J. Integrin-specific hydrogels functionalized with VEGF for vascularization and bone regeneration of critical-size bone defects. *J. Biomed. Mater. Res. Part A* **104**, 889–900 (2016).

29. Phelps, E. a, Landázuri, N., Thulé, P. M., Taylor, W. R. & García, A. J. Bioartificial matrices for therapeutic vascularization. *Proc. Natl. Acad. Sci. U. S.*

A. **107**, 3323–3328 (2010).

30. Davis, J. A. *et al.* ETS transcription factor Etsrp / Etv2 is required for lymphangiogenesis and directly regulates vegfr3 / flt4 expression. *Dev. Biol.* **440**, 40–52 (2018).

31. Wang, Y. *et al.* Ephrin-B2 controls VEGF-induced angiogenesis and lymphangiogenesis. *Nature* **465**, 483–486 (2010).

32. Yan, H. *et al.* CD146 is required for VEGF-C-induced lymphatic sprouting during lymphangiogenesis. *Sci. Rep.* **7**, 1–12 (2017).

33. Wu, H. *et al.* Epsin deficiency promotes lymphangiogenesis through regulation of VEGFR3 degradation in diabetes. *J. Clin. Invest.* **128**, (2018).

34. Gordon, E. J. *et al.* Macrophages define dermal lymphatic vessel calibre during development by regulating lymphatic endothelial cell proliferation (Development 137, (3899-3910)). *Development* **138**, 797 (2011).

35. Wang, Y. *et al.* Smooth muscle cell recruitment to lymphatic vessels requires PDGFB and impacts vessel size but not identity. *Dev.* **144**, 3590–3601 (2017).

36. Iolyeva, M. *et al.* Interleukin-7 is produced by afferent lymphatic vessels and supports lymphatic drainage. *Blood* **122**, 2271–2281 (2013).

37. Detry, B. *et al.* Digging deeper into lymphatic vessel formation in vitro and in vivo. *BMC Cell Biol.* **12**, (2011).

38. Bruyère, F. *et al.* Modeling lymphangiogenesis in a three-dimensional culture system. *Nat. Methods* **5**, 431–437 (2008).

39. Maertens, L. *et al.* Bone marrow-derived mesenchymal stem cells drive lymphangiogenesis. *PLoS One* **9**, e106976 (2014).

40. Chen, D. *et al.* Osteoarthritis: Toward a comprehensive understanding of pathological mechanism. *Bone Res.* **5**, 1–13 (2016).

41. Cucchiarini, M. *et al.* Basic science of osteoarthritis. *J. Exp. Orthop.* **3**, 1–18 (2016).

42. Arden, N. & Nevitt, M. C. Osteoarthritis: Epidemiology. *Best Pract. Res. Clin. Rheumatol.* **20**, 3–25 (2006).

43. Iolascon, G. *et al.* Early osteoarthritis: How to define, diagnose, and manage. A systematic review. *Eur. Geriatr. Med.* **8**, 383–396 (2017).

44. Berenbaum, F., Wallace, I. J., Lieberman, D. E. & Felson, D. T. Modern-day environmental factors in the pathogenesis of osteoarthritis. *Nat. Rev. Rheumatol.* **14**, 674–681 (2018).

45. Maricar, N., Callaghan, M. J., Parkes, M. J., Felson, D. T. & O'Neill, T. W. Clinical assessment of effusion in knee osteoarthritis-A systematic review. *Semin. Arthritis Rheum.* **45**, 556–563 (2016).

46. Bortoluzzi, A., Furini, F. & Scirè, C. A. Osteoarthritis and its management - Epidemiology, nutritional aspects and environmental factors. *Autoimmun. Rev.* **17**, 1097–1104 (2018).

47. Shu, C. C. *et al.* The relationship between synovial inflammation, structural pathology, and pain in post-traumatic osteoarthritis: Differential effect of stem cell and hyaluronan treatment. *Arthritis Res. Ther.* **22**, 1–13 (2020).

48. Mathiessen, A. & Conaghan, P. G. Synovitis in osteoarthritis: Current understanding with therapeutic implications. *Arthritis Res. Ther.* **19**, 1–9 (2017).

49. O'Neill, T. W. & Felson, D. T. Mechanisms of osteoarthritis (OA) pain. *Current Osteoporosis Reports* **16**, 611–616 (2018).

50. Wang, X., Hunter, D. J., Jin, X. & Ding, C. The importance of synovial inflammation in osteoarthritis: Current evidence from imaging assessments and clinical trials. *Osteoarthr. Cartil.* **26**, 165–174 (2018).

51. Robinson, W. H. *et al.* Low-grade inflammation as a key mediator of the pathogenesis of osteoarthritis. *Nat. Rev. Rheumatol.* **12**, 580–592 (2016).

52. Felson, D. T. *et al.* The prevalence of knee osteoarthritis in the elderly. the framingham osteoarthritis study. *Arthritis Rheum.* **30**, 914–918 (1987).

53. Hernborg, J. & Nilsson, B. E. the Relationship Between Osteophytes in the Knee Joint, Osteoarthritis and Aging. *Acta Orthop.* **44**, 69–74 (1973).

54. Cameron, K. L., Driban, J. B. & Svoboda, S. J. Osteoarthritis and the tactical athlete: A systematic review. *J. Athl. Train.* **51**, 952–961 (2016).

55. Nazarinasab, M., Motamedfar, A. & Moqadam, A. E. Investigating mental health in patients with osteoarthritis and its relationship with some clinical and demographic factors. *Reumatologia* **55**, 183–188 (2017).

56. Lee, Y., Lee, S. H., Lim, S. M., Baek, S. H. & Ha, I. H. Mental health and quality of life of patients with osteoarthritis pain: The sixth Korea National Health and Nutrition Examination Survey (2013–2015). *PLoS One* **15**, 1–17 (2020).

57. Murray, C. J. L. *et al.* Disability-adjusted life years (DALYs) for 291 diseases and injuries in 21 regions, 1990-2010: A systematic analysis for the Global Burden of Disease Study 2010. *Lancet* **380**, 2197–2223 (2012).

58. Losina, E. *et al.* Lifetime risk and age at diagnosis of symptomatic knee osteoarthritis in the US. *Arthritis Care Res.* **65**, 703–711 (2013).

59. Øiestad, B. E., Engebretsen, L., Storheim, K. & Risberg, M. A. Knee osteoarthritis after anterior cruciate ligament injury: A systematic review. *Am. J. Sports Med.* **37**, 1434–1443 (2009).

60. Thomas, A. C., Hubbard-turner, T., Wikstrom, E. A. & Palmieri-smith, R. M. Epidemiology of Posttraumatic Osteoarthritis. **52**, 491–496 (2017).

61. Bhattaram, P. & Chandrasekharan, U. The joint synovium: A critical determinant of articular cartilage fate in inflammatory joint diseases. *Semin. Cell Dev. Biol.* **62**, 86–93 (2017).

62. Juneja, P., Munjal, A. & Hubbard, J. B. Anatomy, Joints. in (2021).

63. Moriyama, H. *et al.* Effects of aging and exercise training on the histological and mechanical properties of articular structures in knee joints of male rat. *Biogerontology* **13**, 369–381 (2012).

64. Bali, R. & Shukla, A. K. Rheological effects of synovial fluid on nutritional transport. *Tribol. Lett.* **9**, 233–239 (2001).

65. Chahine, N. O., Chen, F. H., Hung, C. T. & Ateshian, G. A. Direct measurement of osmotic pressure of glycosaminoglycan solutions by membrane osmometry at room temperature. *Biophys. J.* **89**, 1543–1550 (2005).

66. Gilchrist, C. L., Witvoet-Braam, S. W., Guilak, F. & Setton, L. a. Measurement of intracellular strain on deformable substrates with texture correlation. *J. Biomech.* **40**, 786–94 (2007).

67. Simkin, P. a. A biography of the chondrocyte. *Ann. Rheum. Dis.* **67**, 1064–8 (2008).

68. Makris, E. A., Hadidi, P. & Athanasiou, K. A. The knee meniscus: Structure-function, pathophysiology, current repair techniques, and prospects for regeneration. *Biomaterials* **32**, 7411–7431 (2011).

69. Nakamura, S. *et al.* Changes in viscoelastic properties of articular cartilage in early stage of osteoarthritis, as determined by optical coherence tomography-based strain rate tomography. *BMC Musculoskelet. Disord.* **20**, 1–4 (2019).

70. Desrochers, J., Amrein, M. W. & Matyas, J. R. Viscoelasticity of the articular cartilage surface in early osteoarthritis. *Osteoarthr. Cartil.* **20**, 413–421 (2012).

71. Bonnet, C. S. & Walsh, D. A. Osteoarthritis, angiogenesis and inflammation. *Rheumatology* **44**, 7–16 (2005).

72. Onyekwelu, I., Goldring, M. B. & Hidaka, C. Chondrogenesis, joint formation, and articular cartilage regeneration. *J. Cell. Biochem.* **107**, 383–392 (2009).

73. Komdeur, P., Pollo, F. E. & Jackson, R. W. Dynamic knee motion in anterior cruciate impairment: a report and case study. *Proc. (Bayl. Univ. Med. Cent).* **15**,

257–259 (2002).

74. Edwards, J. C. W. Synovial intimal fibroblasts. *Ann. Rheum. Dis.* **54**, 395–397 (1995).

75. Revell, P. A., Al-Saffar, N., Fish, S. & Osei, D. Extracellular matrix of the synovial intimal cell layer. *Ann. Rheum. Dis.* **54**, 404–7 (1995).

76. Tiwari, N. *et al.* Imaging of normal and pathologic joint synovium using nonlinear optical microscopy as a potential diagnostic tool. *J. Biomed. Opt.* **15**, 056001 (2010).

77. Tamer, T. M. Hyaluronan and synovial joint: Function, distribution and healing. *Interdiscip. Toxicol.* **6**, 111–125 (2013).

78. Ralphs, J. R. & Benjamin, M. The joint capsule: structure, composition, ageing and disease. *J. Anat.* **184 (Pt 3**, 503–509 (1994).

79. Levick, J. R. & McDonald, J. N. Ultrastructure of transport pathways in stressed synovium of the knee in anaesthetized rabbits. *J. Physiol.* **419**, 493–508 (1989).

80. D. Smith, M. The Normal Synovium. *Open Rheumatol. J.* **5**, 100–106 (2012).

81. Momberger, T. S., Levick, J. R. & Mason, R. M. Hyaluronan secretion by synoviocytes is mechanosensitive. *Matrix Biol.* **24**, 510–519 (2005).

82. Schmidt, T. A., Gastelum, N. S., Nguyen, Q. T., Schumacher, B. L. & Sah, R. L. Boundary lubrication of articular cartilage: Role of synovial fluid constituents. *Arthritis Rheum.* **56**, 882–891 (2007).

83. Jay, G. D. & Waller, K. A. The biology of Lubricin: Near frictionless joint motion. *Matrix Biol.* **39**, 17–24 (2014).

84. Ingram, K. R., Wann, a K. T., Angel, C. K., Coleman, P. J. & Levick, J. R. Cyclic movement stimulates hyaluronan secretion into the synovial cavity of rabbit joints. *J. Physiol.* **586**, 1715–29 (2008).

85. Chubinskaya, S. *et al.* Articular cartilage injury and potential remedies. *J. Orthop. Trauma* **29**, S47–S52 (2015).

86. Hadler, N. M. Synovial fluids facilitate small solute diffusivity. *Ann. Rheum. Dis.* **39**, 580–585 (1980).

87. Flannery, C. R. *et al.* Articular cartilage superficial zone protein (SZP) is homologous to megakaryocyte stimulating factor precursor and is a multifunctional proteoglycan with potential growth-promoting, cytoprotective, and lubricating properties in cartilage metabolism. *Biochem. Biophys. Res. Commun.* **254**, 535–541 (1999).

88. Marcelino, J. *et al.* CACP, encoding a secreted proteoglycan, is mutated in camptodactyly- arthropathy-coxa vara-pericarditis syndrome. *Nat. Genet.* **23**, 319–322 (1999).

89. Purbach, B., Hills, B. A. & Wroblewski, B. M. Surface-active phospholipid in total hip arthroplasty. *Clin. Orthop. Relat. Res.* 115–118 (2002). doi:10.1097/00003086-200203000-00020

90. Petelska, A. D., Kazimierska-Drobny, K., Janicka, K., Majewski, T. & Urbaniak, W. Understanding the unique role of phospholipids in the lubrication of natural joints: An interfacial tension study. *Coatings* **9**, (2019).

91. Schwarz, I. M. & Hills, B. A. Surface-active phospholipid as the lubricating component of lubricin. *Br. J. Rheumatol.* **37**, 21–26 (1998).

92. Whicher, J. T. *Abnormalities of Plasma Proteins*. *Scientific Foundations of Biochemistry in Clinical Practice* (D. L. Williams and V. Marks, 1994). doi:10.1016/b978-0-7506-0167-2.50033-9

93. Dobbie, J. W. *et al.* Lamellar body secretion: ultrastructural analysis of an unexplored function of synoviocytes. *Br. J. Rheumatol.* **34**, 13–23 (1995).

94. Knox, P., Levick, J. R. & McDonald, J. N. Synovial fluid--its mass, macromolecular content and pressure in major limb joints of the rabbit. *Q. J. Exp. Physiol.* **73**, 33–45 (1988).

95. Levick, J. R. Flow through interstitium and other fibrous matrices. *Q. J. Exp. Physiol.* **72**, 409–437 (1987).

96. Scott, D., Coleman, P. J., Mason, R. M. & Levick, J. R. Direct evidence for the partial reflection of hyaluronan molecules by the lining of rabbit knee joints during trans-synovial flow. *J. Physiol.* **508**, 619–623 (1998).

97. Chen, H. *et al.* Molecular interaction, chain conformation, and rheological modification during electrospinning of hyaluronic acid aqueous solution. *Membranes (Basel).* **10**, 1–13 (2020).

98. Dongaonkar, R. M., Laine, G. A., Stewart, R. H. & Quick, C. M. Balance point characterization of interstitial fluid volume regulation. *Am. J. Physiol. - Regul. Integr. Comp. Physiol.* **297**, 6–16 (2009).

99. Wiig, H. & Swartz, M. A. Interstitial fluid and lymph formation and transport: Physiological regulation and roles in inflammation and cancer. *Physiol. Rev.* **92**, 1005–1060 (2012).

100. Simkin, P. a. & Bassett, J. E. Pathways of microvascular permeability in the synovium of normal and diseased human knees. *J. Rheumatol.* **38**, 2635–2642 (2011).

101. Hemant, S. Physiologic upper limits of pore size of different blood capillary types and another perspective on the dual pore theory of microvascular permeability. *J. Angiogenes. Res.* **2**, 1–19 (2010).

102. Kwan, M. K., Michael Lai, W. & Van Mow, C. Fundamentals of fluid transport through cartilage in compression. *Ann. Biomed. Eng.* **12**, 537–558 (1984).

103. Maroudas, A., Bullough, P., Swanson, S. A. & Freeman, M. A. The permeability of articular cartilage. *J. Bone Joint Surg. Br.* **50**, 166–177 (1968).

104. DiDomenico, C. D., Xiang Wang, Z. & Bonassar, L. J. Cyclic Mechanical Loading Enhances Transport of Antibodies Into Articular Cartilage. *J. Biomech. Eng.* **139**, (2016).

105. Graham, B. T., Moore, A. C., Burris, D. L. & Price, C. Sliding enhances fluid and solute transport into buried articular cartilage contacts. *Osteoarthr. Cartil.* **25**, 2100–2107 (2017).

106. Zhang, L., Gardiner, B. S., Smith, D. W., Pivonka, P. & Grodzinsky, A. The effect of cyclic deformation and solute binding on solute transport in cartilage. *Arch. Biochem. Biophys.* **457**, 47–56 (2007).

107. Kang, J. Y. *et al.* Novel porous matrix of hyaluronic acid for the three-dimensional culture of chondrocytes. *Int. J. Pharm.* **369**, 114–120 (2009).

108. Sabaratnam, S., Coleman, P. J., Mason, R. M. & Levick, J. R. Interstitial matrix proteins determine hyaluronan reflection and fluid retention in rabbit joints: Effect of protease. *J. Physiol.* **578**, 291–299 (2007).

109. Sabaratnam, S., Mason, R. M. & Levick, J. R. Filtration rate dependence of hyaluronan reflection by joint-to-lymph barrier: Evidence for concentration polarisation. *J. Physiol.* **557**, 909–922 (2004).

110. Sabaratnam, S., Arunan, V., Coleman, P. J., Mason, R. M. & Levick, J. R. Size selectivity of hyaluronan molecular sieving by extracellular matrix in rabbit synovial joints. *J. Physiol.* **567**, 569–581 (2005).

111. Simkin, P. A. & Benedict, R. S. Iodide and albumin kinetics in normal canine wrists and knees. *Arthritis Rheum.* **33**, 73–9 (1990).

112. Simkin, P. A. The human knee: A window on the microvasculature. *Tissue barriers* **3**, e970465 (2015).

113. Bagby, T. R. *et al.* Impact of molecular weight on lymphatic drainage of a biopolymer-based imaging agent. *Pharmaceutics* **4**, 276–295 (2012).

114. Doan, T. N., Bernard, F. C., McKinney, J. M., Dixon, J. B. & Willett, N. J. Endothelin-1 inhibits size dependent lymphatic clearance of PEG-based conjugates after intra-articular injection into the rat knee. *Acta Biomater.* **93**, 270–281 (2019).

115. Proulx, S. T. *et al.* Quantitative imaging of lymphatic function with liposomal

indocyanine green. *Cancer Res.* **70**, 7053–7062 (2010).

116. Levick, J. R. An investigation into the validity of subatmospheric pressure recordings from synovial fluid and their dependence on joint angle. *J. Physiol.* **289**, 55–67 (1979).

117. McDonald, J. N. & Levick, J. R. Morphology of surface synoviocytes in situ at normal and raised joint pressure, studied by scanning electron microscopy. *Ann. Rheum. Dis.* **47**, 232–240 (1988).

118. Scott, D., Coleman, P. J., Mason, R. M. & Levick, J. R. Concentration dependence of interstitial flow buffering by hyaluronan in synovial joints. *Microvasc. Res.* **59**, 345–53 (2000).

119. Coleman, P. J., Scott, D., Mason, R. M. & Levick, J. R. Role of hyaluronan chain length in buffering interstitial flow across synovium in rabbits. *J. Physiol.* **526 Pt 2**, 425–434 (2000).

120. Simkin, P. A., Huang, A. & Benedict, R. S. Effects of exercise on blood flow to canine articular tissues. *J. Orthop. Res.* **8**, 297–303 (1990).

121. Sabaratnam, S., Mason, R. M. & Levick, J. R. Inside-out cannulation of fine lymphatic trunks used to quantify coupling between transsynovial flow and lymphatic drainage from rabbit knees. *Microvasc. Res.* **64**, 1–13 (2002).

122. Dulin, J. A. *et al.* Influence of exercise on the distribution of technetium Tc 99m medronate following intra-articular injection in horses. *Am. J. Vet. Res.* **73**, 418–425 (2012).

123. Fam, A. G. *et al.* Effect of joint motion on experimental calcium pyrophosphate dihydrate crystal induced arthritis. *J. Rheumatol.* **17**, 644–55 (1990).

124. James, M. J., Cleland, L. G., Gaffney, R. D., Proudman, S. M. & Chatterton, B. E. Effect of exercise on 99mTc-DTPA clearance from knees with effusions. *J. Rheumatol.* **21**, 501–4 (1994).

125. Schütze, H., Hildebrandt, W. & Stegemann, J. The interstitial fluid content in

working muscle modifies the cardiovascular response to exercise. *Eur. J. Appl. Physiol. Occup. Physiol.* **62**, 332–6 (1991).

126. Lane, K. N., Dolan, L. B., Worsley, D. & McKenzie, D. C. Upper extremity lymphatic function at rest and during exercise in breast cancer survivors with and without lymphedema compared with healthy controls. *J. Appl. Physiol.* **103**, 917–925 (2007).

127. Havas, E. *et al.* Lymph flow dynamics in exercising human skeletal muscle as detected by scintography. *J. Physiol.* **504**, 233–239 (1997).

128. Miller, L. M. & Gal, A. Cardiovascular System and Lymphatic Vessels. in *Pathologic Basis of Veterinary Disease* 561-616.e1 (Elsevier, 2017). doi:10.1016/B978-0-323-35775-3.00010-2

129. Olszewski, W. L. The lymphatic system in body homeostasis: physiological conditions. *Lymphat. Res. Biol.* **1**, (2003).

130. Kupper, T. S. & Fuhlbrigge, R. C. Immune surveillance in the skin: Mechanisms and clinical consequences. *Nat. Rev. Immunol.* **4**, 211–222 (2004).

131. Babcock, D. T. *et al.* Circulating blood cells function as a surveillance system for damaged tissue in Drosophila larvae. *Proc. Natl. Acad. Sci. U. S. A.* **105**, 10017–10022 (2008).

132. GABE, I. T. *et al.* Measurement of Instantaneous Blood Flow Velocity and Pressure in Conscious Man with a Catheter-Tip Velocity Probe. *Circulation* **40**, 603–614 (1969).

133. Ivanov, K. P., Kalinina, M. K. & Levkovich, Y. I. Blood flow velocity in capillaries of brain and muscles and its physiological significance. *Microvasc. Res.* **22**, 143–155 (1981).

134. Sandoo, A., Veldhuijzen van Zanten, J. J. C. ., Metsios, G. S., Carroll, D. & Kitas, G. D. The Endothelium and Its Role in Regulating Vascular Tone. *Open Cardiovasc. Med. J.* **4**, 302–312 (2015).

135. Schmid-Schönbein, G. W. Mechanisms causing initial lymphatics to expand and compress to promote lymph flow. *Arch. Histol. Cytol.* **53**, 107–114 (1990).

136. Asano, K. *et al.* Pre-collecting lymphatic vessels form detours following obstruction of lymphatic flow and function as collecting lymphatic vessels. *PLoS One* **15**, 1–13 (2020).

137. Suami, H., Chang, D. W., Matsumoto, K. & Kimata, Y. Demonstrating the lymphatic system in rats with microinjection. *Anat. Rec.* **294**, 1566–1573 (2011).

138. Levick, J. R. & Michel, C. C. Microvascular fluid exchange and the revised Starling principle. *Cardiovasc. Res.* **87**, 198–210 (2010).

139. Willard-Mack, C. L. Normal Structure, Function, and Histology of Lymph Nodes. *Toxicol. Pathol.* **34**, 409–424 (2006).

140. Niu, G. & Chen, X. Lymphatic imaging: Focus on imaging probes. *Theranostics* **5**, 686–697 (2015).

141. Ohhashi, T., Azuma, T. & Sakaguchi, M. Active and passive mechanical characteristics of bovine mesenteric lymphatics. *Am. J. Physiol. - Hear. Circ. Physiol.* **8**, 88–95 (1980).

142. Dixon, J. B. *et al.* Lymph flow, shear stress, and lymphocyte velocity in rat mesenteric prenodal lymphatics. *Microcirculation* **13**, 597–610 (2006).

143. Gashev, A. A. & Zawieja, D. C. Hydrodynamic regulation of lymphatic transport and the impact of aging. *Pathophysiology* **17**, 277–287 (2010).

144. Gashev, A. A., Davis, M. J. & Zawieja, D. C. Inhibition of the active lymph pump by flow in rat mesenteric lymphatics and thoracic duct. *J. Physiol.* **540**, 1023–37 (2002).

145. Wang, W. *et al.* Inhibition of myosin light chain phosphorylation decreases rat mesenteric lymphatic contractile activity. *Am. J. Physiol. - Hear. Circ. Physiol.* **297**, H734 (2009).

146. Gashev, A. A., Davis, M. J., Delp, M. D. & Zawieja, D. C. Regional variations of contractile activity in isolated rat lymphatics. *Microcirculation* **11**, 477–492 (2004).

147. Castorena-gonzalez, J. A., Li, M. & Davis, M. J. Effects of elevated downstream pressure and the role of smooth muscle cell coupling through connexin45 on lymphatic pacemaking. *Biomolecules* **10**, 1–21 (2020).

148. Benoit, J. N., Zawieja, D. C., Goodman, A. H. & Granger, H. J. Characterization of intact mesenteric lymphatic pump and its responsiveness to acute edemagenic stress. *Am. J. Physiol.* **257**, H2059-69 (1989).

149. Scallan, J. P., Zawieja, S. D., Castorena-Gonzalez, J. A. & Davis, M. J. Lymphatic pumping: mechanics, mechanisms and malfunction. *J. Physiol.* **594**, 5749–5768 (2016).

150. Adams, R. H. & Alitalo, K. Molecular regulation of angiogenesis and lymphangiogenesis. *Nat. Rev. Mol. Cell Biol.* **8**, 464–478 (2007).

151. Ucuzian, A. A., Gassman, A. A., East, A. T. & Greisler, H. P. Molecular mediators of angiogenesis. *J. Burn Care Res.* **31**, 158–175 (2010).

152. Morfoisse, F., Renaud, E., Hantelys, F., Prats, A. C. & Garmy-Susini, B. Role of hypoxia and vascular endothelial growth factors in lymphangiogenesis. *Mol. Cell. Oncol.* **1**, 1–8 (2014).

153. Nagy, J. A. *et al.* Vascular permeability factor/vascular endothelial growth factor induces lymphangiogenesis as well as angiogenesis. *J. Exp. Med.* **196**, 1497–1506 (2002).

154. Davis, G. E. & Bayless, K. J. An integrin and Rho GTPase-dependent pinocytic vacuole mechanism controls capillary lumen formation in collagen and fibrin matrices. *Microcirculation* **10**, 27–44 (2003).

155. Karkkainen, M. J. *et al.* Vascular endothelial growth factor C is required for sprouting of the first lymphatic vessels from embryonic veins. *Nat. Immunol.* **5**, 74–80 (2004).

156. Petrova, T. V. *et al.* Lymphatic endothelial reprogramming of vascular endothelial cells by the Prox-1 homeobox transcription factor. *EMBO J.* **21**, 4593–4599 (2002).

157. Liu, X. *et al.* Temporal and spatial regulation of epsin abundance and VEGFR3 signaling are required for lymphatic valve formation and function. *Sci. Signal.* **7**, ra97 (2014).

158. Sabine, A. *et al.* FOXC2 and fluid shear stress stabilize postnatal lymphatic vasculature. *J. Clin. Invest.* **125**, 3861–3877 (2015).

159. Norrmén, C. *et al.* FOXC2 controls formation and maturation of lymphatic collecting vessels through cooperation with NFATc1. *J. Cell Biol.* **185**, 439–457 (2009).

160. Lutter, S., Xie, S., Tatin, F. & Makinen, T. Smooth muscle-endothelial cell communication activates Reelin signaling and regulates lymphatic vessel formation. *J. Cell Biol.* **197**, 837–849 (2012).

161. Witte, M. H. *et al.* Lymphangiogenesis and hemangiogenesis: Potential targets for therapy. *J. Surg. Oncol.* **103**, 489–500 (2011).

162. Enholm, B. *et al.* Adenoviral expression of vascular endothelial growth factor-C induces lymphangiogenesis in the skin. *Circ. Res.* **88**, 623–629 (2001).

163. Rissanen, T. T. *et al.* VEGF-D is the strongest angiogenic and lymphangiogenic effector among VEGFs delivered into skeletal muscle via adenoviruses. *Circ. Res.* **92**, 1098–1106 (2003).

164. Wong, W. T. *et al.* A protein-binding domain, EH, identified in the receptor tyrosine kinase substrate Eps15 and conserved in evolution. *Proc. Natl. Acad. Sci. U. S. A.* **92**, 9530–9534 (1995).

165. Chen, H. *et al.* Epsin is an EH-domain-binding protein implicated in clathrin-mediated endocytosis. *Nature* **394**, 793–7 (1998).

166. Rosenthal, J. A. *et al.* The epsins define a family of proteins that interact with

components of the clathrin coat and contain a new protein module. *J. Biol. Chem.* **274**, 33959–33965 (1999).

167. Gleisner, M. *et al.* Epsin N-terminal homology domain (ENTH) Activity as a function of membrane tension. *J. Biol. Chem.* **291**, 19953–19961 (2016).

168. Ford, M. G. J. *et al.* Curvature of clathrin-coated pits driven by epsin. *Nature* **419**, 361–366 (2002).

169. Tessneer, K. L. *et al.* Genetic reduction of vascular endothelial growth factor receptor 2 rescues aberrant angiogenesis caused by epsin deficiency. *Arterioscler. Thromb. Vasc. Biol.* **34**, 331–337 (2014).

170. Brophy, M. L. *et al.* Myeloid-Specific Deletion of Epsins 1 and 2 Reduces Atherosclerosis by Preventing LRP-1 Downregulation. *Circ. Res.* **124**, e6–e19 (2019).

171. Weiler, M. J., Cribb, M. T., Nepiyushchikh, Z., Nelson, T. S. & Dixon, J. B. A novel mouse tail lymphedema model for observing lymphatic pump failure during lymphedema development. *Sci. Rep.* **9**, 1–15 (2019).

172. Kwon, S., Agollah, G. D., Wu, G. & Sevick-Muraca, E. M. Spatio-temporal changes of lymphatic contractility and drainage patterns following lymphadenectomy in mice. *PLoS One* **9**, (2014).

173. Bruna, J. Collateral lymphatic circulation. *Eur. J. Plast. Surg.* **23**, 321–325 (2000).

174. Kuyinu, E. L., Narayanan, G., Nair, L. S. & Laurencin, C. T. Animal models of osteoarthritis: Classification, update, and measurement of outcomes. *J. Orthop. Surg. Res.* **11**, 1–27 (2016).

175. Jimenez, P. A., Glasson, S. S., Trubetskoy, O. V & Haimes, H. B. Spontaneous osteoarthritis in Dunkin Hartley guinea pigs: histologic, radiologic, and biochemical changes. *Lab. Anim. Sci.* **47**, 598–601 (1997).

176. Bapat, S., Hubbard, D., Munjal, A., Hunter, M. & Fulzele, S. Pros and cons of mouse models for studying osteoarthritis. *Clin. Transl. Med.* **7**, (2018).

177. Lampropoulou-Adamidou, K. *et al.* Useful animal models for the research of osteoarthritis. *Eur. J. Orthop. Surg. Traumatol.* **24**, 263–271 (2014).

178. Custers, R. J. H. *et al.* Reliability, reproducibility and variability of the traditional Histologic/Histochemical Grading System vs the new OARSI Osteoarthritis Cartilage Histopathology Assessment System. *Osteoarthr. Cartil.* **15**, 1241–1248 (2007).

179. Vaienti, E., Scita, G., Ceccarelli, F. & Pogliacomi, F. Understanding the human knee and its relationship to total knee replacement. *Acta Biomed.* **88**, 6–16 (2017).

180. Janusz, M. J. *et al.* Induction of osteoarthritis in the rat by surgical tear of the meniscus: Inhibition of joint damage by a matrix metalloproteinase inhibitor. *Osteoarthr. Cartil.* **10**, 785–791 (2002).

181. Willett, N. J. *et al.* Intra-articular injection of micronized dehydrated human amnion/chorion membrane attenuates osteoarthritis development. *Arthritis Res. Ther.* **16**, 1–10 (2014).

182. Allen, K. D. *et al.* Kinematic and dynamic gait compensations resulting from knee instability in a rat model of osteoarthritis. *Arthritis Res. Ther.* **14**, R78 (2012).

183. Monfort, J. & Benito, P. Hyaluronic acid in the treatment of osteoarthritis. *Reumatol. Clin.* **2**, 36–43 (2006).

184. Lieberthal, J., Sambamurthy, N. & Scanzello, C. R. Inflammation in joint injury and post-traumatic osteoarthritis. *Osteoarthr. Cartil.* **23**, 1825–1834 (2015).

185. Sin, A., Tang, W., Wen, C. Y., Chung, S. K. & Chiu, K. Y. The emerging role of endothelin-1 in the pathogenesis of subchondral bone disturbance and osteoarthritis. *Osteoarthr. Cartil.* **23**, 516–524 (2015).

186. Wang, X., Hunter, D. J., Jin, X. & Ding, C. The importance of synovial inflammation in osteoarthritis: current evidence from imaging assessments and clinical trials. *Osteoarthr. Cartil.* **26**, 165–174 (2018).

187. Franco, R. N. *et al.* Correlation between inflammatory cells and sulfated

glycosaminoglycan concentration in synovial fluid of subjects with secondary knee osteoarthritis. *J. Rheumatol.* **35**, 1096–1101 (2008).

188. Wood, M. J. *et al.* Macrophage proliferation distinguishes 2 subgroups of knee osteoarthritis patients. *JCI Insight* **4**, 0–12 (2019).

189. Barreto, G. *et al.* Lumican is upregulated in osteoarthritis and contributes to TLR4-induced pro-inflammatory activation of cartilage degradation and macrophage polarization. *Osteoarthr. Cartil.* **28**, 92–101 (2020).

190. McNulty, A. L., Rothfusz, N. E., Leddy, H. A. & Guilak, F. Synovial fluid concentrations and relative potency of interleukin-1 alpha and beta in cartilage and meniscus degradation. *J. Orthop. Res.* **31**, 1039–1045 (2013).

191. Orlowsky, E. W. & Kraus, V. B. The Role of Innate Immunity in Osteoarthritis: When Our First Line of Defense Goes On the Offensive. *J. Rheumatol.* **42**, 363–371 (2015).

192. McKinney, J. M. *et al.* Therapeutic efficacy of intra-articular delivery of encapsulated human mesenchymal stem cells on early stage osteoarthritis. *Eur. Cell. Mater.* **37**, 42–59 (2019).

193. Willett, N. J. *et al.* Quantitative pre-clinical screening of therapeutics for joint diseases using contrast enhanced micro-computed tomography. *Osteoarthr. Cartil.* 1–9 (2016). doi:10.1016/j.joca.2016.04.021

194. Grenier, S., Bhargava, M. M. & Torzilli, P. A. An in vitro model for the pathological degradation of articular cartilage in osteoarthritis. *J. Biomech.* **47**, 645–652 (2014).

195. Lee, J. H., Fitzgerald, J. B., DiMicco, M. A. & Grodzinsky, A. J. Mechanical injury of cartilage explants causes specific time-dependent changes in chondrocyte gene expression. *Arthritis Rheum.* **52**, 2386–2395 (2005).

196. Maldonado, M. & Nam, J. The role of changes in extracellular matrix of cartilage in the presence of inflammation on the pathology of osteoarthritis. *Biomed Res. Int.* **2013**, (2013).

197. Manacu, C. A. *et al.* Endothelin-1 in osteoarthritic chondrocytes triggers nitric oxide production and upregulates collagenase production. *Arthritis Res. Ther.* **7**, R324-32 (2005).

198. de Sousa, E. B. *et al.* Osteoarthritic synovial fluid modulates cell phenotype and metabolic behavior in vitro. *Stem Cells Int.* **2019**, (2019).

199. Wojdasiewicz, P., Poniatowski, Ł. A. & Szukiewicz, D. The role of inflammatory and anti-inflammatory cytokines in the pathogenesis of osteoarthritis. *Mediators Inflamm.* **2014**, (2014).

200. Cohen, N. P., Foster, R. J. & Mow, V. C. Composition and dynamics of articular cartilage: Structure, function, and maintaining healthy state. *J. Orthop. Sports Phys. Ther.* **28**, 203–215 (1998).

201. Benito, M. J., Veale, D. J., FitzGerald, O., Van Den Berg, W. B. & Bresnihan, B. Synovial tissue inflammation in early and late osteoarthritis. *Ann. Rheum. Dis.* **64**, 1263–1267 (2005).

202. Haywood, L. *et al.* Inflammation and angiogenesis in osteoarthritis. *Arthritis Rheum.* **48**, 2173–2177 (2003).

203. Haseeb, A. & Haqqi, T. M. Immunopathogenesis of osteoarthritis. *Clin. Immunol.* **146**, 185–196 (2013).

204. Ioan-facsinay, A. & Kloppenburg, M. An emerging player in knee osteoarthritis : the infrapatellar fat pad. (2013).

205. Wallis, W. J., Simkin, P. A. & Nelp, W. B. Low synovial clearance of iodide provides evidence of hypoperfusion in chronic rheumatoid synovitis. *Arthritis Rheum.* **28**, 1096–1104 (1985).

206. Rhodes, L. A. *et al.* The validation of simple scoring methods for evaluating compartment-specific synovitis detected by MRI in knee osteoarthritis. *Rheumatology* **44**, 1569–1573 (2005).

207. Guermazi, A. *et al.* Assessment of synovitis with contrast-enhanced MRI using a

whole-joint semiquantitative scoring system in people with, or at high risk of, knee osteoarthritis: the MOST study. *Ann. Rheum. Dis.* **70**, 805–811 (2011).

208. D'Agostino, M. A. *et al.* Scoring ultrasound synovitis in rheumatoid arthritis: A EULAR-OMERACT ultrasound taskforce - Part 1: Definition and development of a standardised, consensus-based scoring system. *RMD Open* **3**, 1–9 (2017).

209. Kaeley, G. S., Bakewell, C. & Deodhar, A. The importance of ultrasound in identifying and differentiating patients with early inflammatory arthritis: A narrative review. *Arthritis Res. Ther.* **22**, 1–10 (2020).

210. Manferdini, C. *et al.* From osteoarthritic synovium to synovial-derived cells characterization: synovial macrophages are key effector cells. *Arthritis Res. Ther.* **18**, 83 (2016).

211. Temple-Wong, M. M. *et al.* Hyaluronan concentration and size distribution in human knee synovial fluid: variations with age and cartilage degeneration. *Arthritis Res. Ther.* **18**, 18 (2016).

212. Dahl, L. B., Dahl, I. M. S., Engstrom-Laurent, A. & Granath, K. Concentration and molecular weight of sodium hyaluronate in synovial fluid from patients with rheumatoid arthritis and other arthropathies. *Ann. Rheum. Dis.* **44**, 817–822 (1985).

213. Jay, G. D. *et al.* Lubricating ability of aspirated synovial fluid from emergency department patients with knee joint synovitis. *J. Rheumatol.* **31**, 557–64 (2004).

214. Engstrom-Laurent, A. Hyaluronan in joint disease. *J. Intern. Med.* **242**, 57–60 (1997).

215. Criscione, L. G. *et al.* Variation of serum hyaluronan with activity in individuals with knee osteoarthritis. *Osteoarthr. Cartil.* **13**, 837–840 (2005).

216. Smith, J., Mickler, E. A., Myers, S. L. & Brandt, K. D. Effect of intraarticular hyaluronan injection on synovial fluid hyaluronan in the early stage of canine post-traumatic osteoarthritis. *J. Rheumatol.* **28**, 1341–1346 (2001).

217. Cai, Z., Zhang, H., Wei, Y., Wu, M. & Fu, A. Shear-thinning hyaluronan-based

fluid hydrogels to modulate viscoelastic properties of osteoarthritis synovial fluids. *Biomater. Sci.* **7**, 3143–3157 (2019).

218. Wallis, W. J., Simkin, P. a & Nelp, W. B. Protein traffic in human synovial effusions. *Arthritis Rheum.* **30**, 57–63 (1987).

219. Myers, S. L., O'Connor, B. L. & Brandt, K. D. Accelerated clearance of albumin from the osteoarthritic knee: implications for interpretation of concentrations of 'cartilage markers' in synovial fluid. *J. Rheumatol.* **23**, 1744–8 (1996).

220. Rodnan, G. P. & Maclachlan, M. J. The absorption of serum albumin and gamma globulin from the knee joint of man and rabbit. *Arthritis Rheum.* **3**, 152–157 (1960).

221. Mwangi, T. K. *et al.* Intra-articular clearance of labeled dextrans from naive and arthritic rat knee joints. *J. Control. Release* **283**, 76–83 (2018).

222. Murphy, L. B., Cisternas, M. G., Pasta, D. J., Helmick, C. G. & Yelin, E. H. Medical Expenditures and Earnings Losses Among US Adults With Arthritis in 2013. *Arthritis Care Res.* **70**, 869–876 (2018).

223. Palazzo, C., Nguyen, C., Lefevre-Colau, M.-M., Rannou, F. & Poiraudeau, S. Risk factors and burden of osteoarthritis. *Ann. Phys. Rehabil. Med.* **59**, 134–138 (2016).

224. Turner, M. N. *et al.* The Role of Resistance Training Dosing on Pain and Physical Function in Individuals With Knee Osteoarthritis: A Systematic Review. *Sports Health* **12**, 200–206 (2020).

225. Dai, W. L., Zhou, A. G., Zhang, H. & Zhang, J. Efficacy of Platelet-Rich Plasma in the Treatment of Knee Osteoarthritis: A Meta-analysis of Randomized Controlled Trials. *Arthrosc. - J. Arthrosc. Relat. Surg.* **33**, 659-670.e1 (2017).

226. Pelletier, J. P., Martel-Pelletier, J., Rannou, F. & Cooper, C. Efficacy and safety of oral NSAIDs and analgesics in the management of osteoarthritis: Evidence from real-life setting trials and surveys. *Semin. Arthritis Rheum.* **45**, S22–S27 (2016).

227. Ma, X. long *et al.* Efficacy and safety of intraarticular hyaluronic acid and

corticosteroid for knee osteoarthritis: A meta-analysis. *Int. J. Surg.* **39**, 95–103 (2017).

228. Zhang, W., Ouyang, H., Dass, C. R. & Xu, J. Current research on pharmacologic and regenerative therapies for osteoarthritis. *Bone Res.* **4**, (2016).

229. Brown, T., Laurent, U. & Fraser. Turnover of hyaluronan in synovial joints: elimination of labelled hyaluronan from the knee joint of the rabbit. *Exp. Physiol.* **76**, 125–134 (1991).

230. Fraser, J. R. E., Kimpton, W. G., Pierscionek, B. K. & Cahill, R. N. P. The kinetics of hyaluronan in normal and acutely inflamed synovial joints: Observations with experimental arthritis in sheep. *Semin. Arthritis Rheum.* **22**, 9–17 (1993).

231. Bhadra, A. K. *et al.* Appropriate Use Criteria for Hyaluronic Acid in the Treatment of Knee Osteoarthritis in the United States. *Cartilage* **8**, 234–254 (2017).

232. Gupta, R. C., Lall, R., Srivastava, A. & Sinha, A. Hyaluronic Acid: Molecular Mechanisms and Therapeutic Trajectory. *Front. Vet. Sci.* **6**, 192 (2019).

233. Santilli, V., Paoloni, M., Mangone, M., Alviti, F. & Bernetti, A. Hyaluronic acid in the management of osteoarthritis: injection therapies innovations. *Clin. Cases Miner. Bone Metab.* **13**, 131–134 (2016).

234. Regan, E. a., Bowler, R. P. & Crapo, J. D. Joint fluid antioxidants are decreased in osteoarthritic joints compared to joints with macroscopically intact cartilage and subacute injury. *Osteoarthr. Cartil.* **16**, 515–521 (2008).

235. Leighton, R. *et al.* Systematic clinical evidence review of NASHA (Durolane hyaluronic acid) for the treatment of knee osteoarthritis. *Open Access Rheumatol. Res. Rev.* **10**, 43–54 (2018).

236. Velasco, E., Ribera, M. V. & Pi, J. Single-arm open-label study of Durolane (NASHA nonanimal hyaluronic acid) for the treatment of osteoarthritis of the thumb. *Open Access Rheumatol. Res. Rev.* **9**, 61–66 (2017).

237. Zhang, H. *et al.* Comparison of two hyaluronic acid formulations for safety and

efficacy (CHASE) study in knee osteoarthritis: A multicenter, randomized, double-blind, 26-week non-inferiority trial comparing Durolane to Artz. *Arthritis Res. Ther.* **17**, 1–10 (2015).

238. Mautner, K., Bowers, R., Easley, K., Fausel, Z. & Robinson, R. Functional Outcomes Following Microfragmented Adipose Tissue Versus Bone Marrow Aspirate Concentrate Injections for Symptomatic Knee Osteoarthritis. *Stem Cells Transl. Med.* **8**, 1149–1156 (2019).

239. Bayliss, L. E. *et al.* The effect of patient age at intervention on risk of implant revision after total replacement of the hip or knee: a population-based cohort study. *Lancet* **389**, 1424–1430 (2017).

240. Siviero, P. *et al.* Quality of life outcomes in patients undergoing knee replacement surgery: longitudinal findings from the QPro-Gin study. *BMC Musculoskelet. Disord.* **21**, 1–11 (2020).

241. McQueen, D. A., Long, M. J., Algotar, A. M., Schurman, J. R. & Bangalore, V. G. The effect of obesity on quality-of-life improvement after total knee arthroplasty. *Am. J. Orthop. (Belle Mead. NJ).* **36**, (2007).

242. Konopka, J. F., Lee, Y., Su, E. P. & McLawhorn, A. S. Quality-Adjusted Life Years After Hip and Knee Arthroplasty. *JBJS Open Access* **3**, e0007 (2018).

243. Kaushik, P. & Kaushik, R. Diagnosis and Management of Rheumatoid Arthritis. *Am. J. Med.* **121**, 1245–1252 (2008).

244. Xia, Z. Bin *et al.* Inhibition of NF-κB signaling pathway induces apoptosis and suppresses proliferation and angiogenesis of human fibroblast-like synovial cells in rheumatoid arthritis. *Med. (United States)* **97**, (2018).

245. van der Heijden, J. W. *et al.* The proteasome inhibitor bortezomib inhibits the release of NFκB-inducible cytokines and induces apoptosis of activated T cells from rheumatoid arthritis patients. *Clin. Exp. Rheumatol.* **27**, 92–98 (2009).

246. Zhou, Q. *et al.* Vascular endothelial growth factor C attenuates joint damage in chronic inflammatory arthritis by accelerating local lymphatic drainage in mice. *Arthritis Rheum.* **63**, 2318–2328 (2011).

247. Simkin, P. A. & Pizzorno, J. E. Synovial permeability in rheumatoid arthritis. *Arthritis Rheum.* **22**, 689–696 (1979).

248. Kuehl, C. *et al.* Hyaluronic Acid Molecular Weight Determines Lung Clearance and Biodistribution after Instillation. *Mol. Pharm.* **13**, 1904–1914 (2016).

249. Brown, D. L., Cooper, A. G. & Bluestone, R. Exchange of IgM and albumin between plasma and synovial fluid in rheumatoid arthritis. *Ann. Rheum. Dis.* 644–651 (1969). doi:10.1136/ARD.28.6.644

250. Albuquerque, M. & de Lima, J. P. Articular lymphoscintigraphy in human knees using radiolabeled dextran. *Lymphology* **23**, 215–8 (1990).

251. Simkin, P. a. Assessing biomarkers in synovial fluid: consider the kinetics of clearance. *Osteoarthritis Cartilage* **21**, 7–9 (2013).

252. Larsen, N. E., Dursema, H. D., Pollak, C. T. & Skrabut, E. M. Clearance kinetics of a hylan-based viscosupplement after intra-articular and intravenous administration in animal models. *J. Biomed. Mater. Res. - Part B Appl. Biomater.* **100 B**, 457–462 (2012).

253. Wallis, W. J., Simkin, P. A., Nelp, W. B. & Foster, D. M. Intraarticular volume and clearance in human synovial effusions. *Arthritis Rheum.* **28**, 441–9 (1985).

254. Bajpayee, A. G., Scheu, M., Grodzinsky, A. J. & Porter, R. M. Electrostatic interactions enable rapid penetration, enhanced uptake and retention of intra-articular injected avidin in rat knee joints. *J. Orthop. Res.* **32**, 1044–1051 (2014).

255. Sharma, R. *et al.* Quantitative imaging of lymph function. *Am. J. Physiol. - Hear. Circ. Physiol.* **292**, 3109–3118 (2007).

256. Gompels, L. L., Lim, N. H., Vincent, T. & Paleolog, E. M. In vivo optical imaging in arthritis-an enlightening future? *Rheumatology* **49**, 1436–1446 (2010).

257. Weiler, M., Kassis, T. & Dixon, J. B. Sensitivity analysis of near-infrared functional lymphatic imaging. *J. Biomed. Opt.* **17**, 066019 (2012).

258. Sevick-Muraca, E. M., Kwon, S. & Rasmussen, J. C. Emerging lymphatic imaging technologies for mouse and man. *J. Clin. Invest.* **124**, 905–914 (2014).

259. Weiler, M. & Dixon, J. B. Differential transport function of lymphatic vessels in the rat tail model and the long-term effects of indocyanine green as assessed with near-infrared imaging. *Front. Physiol.* **4 AUG**, 1–10 (2013).

260. Fortes, Z. B., Scivoletto, R. & Garcia-Leme, J. Endothelin-1 induces potent constriction of lymphatic vessels in situ. *Eur. J. Pharmacol.* **170**, 69–73 (1989).

261. Spinella, F. *et al.* Endothelin axis induces metalloproteinase activation and invasiveness in human lymphatic endothelial cells. *Can. J. Physiol. Pharmacol.* **88**, 782–787 (2010).

262. Miyasaka, N. *et al.* Increased production of endothelin-1 in patients with inflammatory arthritides. *Arthritis Rheum.* **35**, 397–400 (1992).

263. Wharton, J. *et al.* Autoradiographic localization and analysis of endothelin-1 binding sites in human synovial tissue. *Arthritis Rheum.* **35**, 894–899 (1992).

264. Yoshida, H., Ohhara, M. & Ohsumi, K. Production of endothelin-1 by cultured human synoviocytes. *Clin. Chim. Acta* **259**, 187–189 (1997).

265. Messai, H., Panasyuk, A., Khatib, A. M., Barbara, A. & Mitrovic, D. R. Endothelin-1 receptors on cultured rat articular chondrocytes: Regulation by age, growth factors, and cytokines, and effect on cAMP production. *Mech. Ageing Dev.* **122**, 519–531 (2001).

266. Barrett-O'Keefe, Z. *et al.* Endothelin-A-mediated vasoconstriction during exercise with advancing age. *J. Gerontol. A. Biol. Sci. Med. Sci.* **70**, 554–65 (2015).

267. Andersson, S. E., Lexmüller, K., Alving, K. & Ekström, G. M. Periarticular tissue levels of cytokine- and endothelin-1-like immunoreactivity during the course of antigen-induced arthritis in the rat. *Inflamm. Res.* **48**, 491–496 (1999).

268. Roy-Beaudry, M. *et al.* Endothelin 1 Promotes Osteoarthritic Cartilage Degradation Via Matrix Metalloprotease 1 and Matrix Metalloprotease 13

Induction. *Arthritis Rheum.* **48**, 2855–2864 (2003).

269. Schindelin, J. *et al.* Fiji: An open-source platform for biological-image analysis. *Nat. Methods* **9**, 676–682 (2012).

270. Edelstein, A. D. *et al.* Advanced methods of microscope control using μManager software. *J. Biol. Methods* **1**, 10 (2014).

271. Wang, X. *et al.* Associations between knee effusion-synovitis and joint structural changes in patients with knee osteoarthritis. *J. Rheumatol.* **44**, 1644–1651 (2017).

272. Singh, A. *et al.* Nanoengineered particles for enhanced intra-articular retention and delivery of proteins. *Adv. Healthc. Mater.* **3**, 1562–1567 (2014).

273. Partain, B. D., Unni, M., Rinaldi, C. & Allen, K. D. The clearance and biodistribution of magnetic composite nanoparticles in healthy and osteoarthritic rat knees. *J. Control. Release* **321**, 259–271 (2020).

274. Puebla, P., Pastoriza, P., Barcia, E. & Fernández-Carballido, A. PEG-derivative effectively modifies the characteristics of indomethacin-PLGA microspheres destined to intra-articular administration. *J. Microencapsul.* **22**, 793–808 (2005).

275. Bédouet, L. *et al.* Intra-articular fate of degradable poly(ethyleneglycol)-hydrogel microspheres as carriers for sustained drug delivery. *Int. J. Pharm.* **456**, 536–544 (2013).

276. Somack, R., Saifer, M. G. & Williams, L. D. Preparation of long-acting superoxide dismutase using high molecular weight polyethylene glycol (41,000-72,000 daltons). *Free Radic. Res. Commun.* **12-13 Pt 2**, 553–562 (1991).

277. Nune, S. K., Gunda, P., Majeti, B. K., Thallapally, P. K. & Forrest, M. L. Advances in lymphatic imaging and drug delivery. *Adv. Drug Deliv. Rev.* **63**, 876–885 (2011).

278. Reddy, S. T. *et al.* Exploiting lymphatic transport and complement activation in nanoparticle vaccines. *Nat. Biotechnol.* **25**, 1159–1164 (2007).

279. Thomas, S. N. & Schudel, A. Overcoming transport barriers for interstitial-, lymphatic-, and lymph node-targeted drug delivery. *Curr. Opin. Chem. Eng.* **7**, 65–74 (2015).

280. Zhao, Z., Li, E., Cao, Q., Sun, J. & Ma, B. Endothelin-1 concentrations are correlated with the severity of knee osteoarthritis. *J. Investig. Med.* **64**, 872–874 (2016).

281. Yin, J. J. *et al.* A causal role for endothelin-1 in the pathogenesis of osteoblastic bone metastases. *Proc. Natl. Acad. Sci. U. S. A.* **100**, 10954–10959 (2003).

282. Kaufman, G. N., Zaouter, C., Valteau, B., Sirois, P. & Moldovan, F. Nociceptive tolerance is improved by bradykinin receptor B1 antagonism and joint morphology is protected by both endothelin type A and bradykinin receptor B1 antagonism in a surgical model of osteoarthritis. *Arthritis Res. Ther.* **13**, R76 (2011).

283. Warner, T. D. & Klemm, P. What turns on the endothelins? *Inflamm. Res.* **45**, 51–53 (1996).

284. Donate, P. B. *et al.* Bosentan, an endothelin receptor antagonist, ameliorates collagen-induced arthritis: The role of TNF-α in the induction of endothelin system genes. *Inflamm. Res.* **61**, 337–348 (2012).

285. Houde, M., Desbiens, L. & D'Orléans-Juste, P. Endothelin-1: Biosynthesis, Signaling and Vasoreactivity. *Adv. Pharmacol.* **77**, 143–175 (2016).

286. Karlsen, T. V, McCormack, E., Mujic, M., Tenstad, O. & Wiig, H. Minimally invasive quantification of lymph flow in mice and rats by imaging depot clearance of near-infrared albumin. *Am. J. Physiol. Heart Circ. Physiol.* **302**, H391-401 (2012).

287. Bremnes, T. *et al.* Regulation and intracellular trafficking pathways of the endothelin receptors. *J. Biol. Chem.* **275**, 17596–17604 (2000).

288. Gärtner, F., Seidel, T., Schulz, U., Gummert, J. & Milting, H. Desensitization and internalization of endothelin receptor a; Impact of g protein-coupled receptor kinase 2 (GRK2)-mediated phosphorylation. *J. Biol. Chem.* **288**, 32138–32148 (2013).

289. Boillot, A., Vallet, B., Marty, J., Auclerc, A. & Barale, F. Effects of halothane, enflurane and isoflurane on contraction of rat aorta induced by endothelin-1. *Br. J. Anaesth.* **75**, 761–767 (1995).

290. Akhtar, S. & Brull, S. J. Effect of isoflurane on endothelin-1 mediated airway smooth muscle contraction. *Pulm. Pharmacol. Ther.* **11**, 227–230 (1998).

291. Levick, J. R. A method for estimating macromolecular reflection by human synovium, using measurements of intra-articular half lives. *Ann. Rheum. Dis.* **57**, 339–44 (1998).

292. Pappenheimer, J. R., Renkin, E. M. & Borrero, L. M. Filtration, Diffusion and Molecular Sieving Through Peripheral Capillary Membranes. *Am. J. Physiol. Content* **167**, 13–46 (1951).

293. Zhao, J., Salmon, H. & Sarntinoranont, M. Effect of heterogeneous vasculature on interstitial transport within a solid tumor. *Microvasc. Res.* **73**, 224–236 (2007).

294. Bouta, E. M. *et al.* The role of the lymphatic system in inflammatory-erosive arthritis. *Semin. Cell Dev. Biol.* **38**, 90–97 (2015).

295. Frush, D. P. & Applegate, K. Computed tomography and radiation: Understanding the issues. *J. Am. Coll. Radiol.* **1**, 113–119 (2004).

296. Goodman, T. R. Understanding the Cancer-CT Conundrum. **44**, 469–474 (2010).

297. Kim, S. J. & Kim, K. A. Safety issues and updates under MR environments. *Eur. J. Radiol.* **89**, 7–13 (2017).

298. Moreno, M. J., Ling, B. & Stanimirovic, D. B. In vivo near-infrared fluorescent optical imaging for CNS drug discovery. *Expert Opin. Drug Discov.* **15**, 903–915 (2020).

299. Tian, Y., Qiang, S. & Wang, L. Gold Nanomaterials for Imaging-Guided Near-Infrared in vivo Cancer Therapy. *Front. Bioeng. Biotechnol.* **7**, (2019).

300. Zeng, H. C., Hu, J. L., Bai, J. W. & Zhang, G. J. Detection of Sentinel Lymph Nodes with Near-Infrared Imaging in Malignancies. *Mol. Imaging Biol.* **21**, 219–227 (2019).

301. Stolik, S., Delgado, J. A., Pérez, A. & Anasagasti, L. Measurement of the penetration depths of red and near infrared light in human ″ex vivo″ tissues. *J. Photochem. Photobiol. B Biol.* **57**, 90–93 (2000).

302. Ash, C., Dubec, M., Donne, K. & Bashford, T. Effect of wavelength and beam width on penetration in light-tissue interaction using computational methods. *Lasers Med. Sci.* **32**, 1909–1918 (2017).

303. Jagdeo, J. R., Adams, L. E., Brody, N. I. & Siegel, D. M. Transcranial Red and Near Infrared Light Transmission in a Cadaveric Model. *PLoS One* **7**, 1–10 (2012).

304. Proulx, S. T. *et al.* Use of a PEG-conjugated bright near-infrared dye for functional imaging of rerouting of tumor lymphatic drainage after sentinel lymph node metastasis. *Biomaterials* **34**, 5128–5137 (2013).

305. Proulx, S. T., Ma, Q., Andina, D., Leroux, J.-C. & Detmar, M. Quantitative measurement of lymphatic function in mice by noninvasive near-infrared imaging of a peripheral vein. *JCI Insight* **2**, 1–13 (2017).

306. Kobayashi, H. *et al.* Simultaneous multicolor imaging of five different lymphatic basins using quantum dots. *Nano Lett.* **7**, 1711–1716 (2007).

307. Hama, Y., Koyama, Y., Urano, Y., Choyke, P. L. & Kobayashi, H. Simultaneous two-color spectral fluorescence lymphangiography with near infrared quantum dots to map two lymphatic flows from the breast and the upper extremity. *Breast Cancer Res. Treat.* **103**, 23–28 (2007).

308. Ruddell, A. *et al.* Dynamic contrast-enhanced magnetic resonance imaging of tumor-induced lymph flow. *Neoplasia* **10**, 706–713 (2008).

309. Modi, S., Stanton, A. W. B., Mortimer, P. S. & Levick, J. R. Clinical Assessment of Human Lymph Flow Using Removal Rate Constants of Interstitial Macromolecules: A Critical Review of Lymphoscintigraphy. *Lymphat. Res. Biol.*

5, 183–202 (2007).

310. Carr, J. A. *et al.* Shortwave infrared fluorescence imaging with the clinically approved near-infrared dye indocyanine green. *Proc. Natl. Acad. Sci. U. S. A.* **115**, 4465–4470 (2018).

311. Coleman, P. J., Scott, D., Ray, J., Mason, R. M. & Levick, J. R. Hyaluronan secretion into the synovial cavity of rabbit knees and comparison with albumin turnover. *J. Physiol.* **503**, 645–656 (1997).

312. Kohlhof, H. *et al.* Single Molecule Microscopy Reveals an Increased Hyaluronan Diffusion Rate in Synovial Fluid from Knees Affected by Osteoarthritis. *Sci. Rep.* **6**, (2016).

313. Joyner, M. J. & Casey, D. P. Regulation of increased blood flow (Hyperemia) to muscles during exercise: A hierarchy of competing physiological needs. *Physiol. Rev.* **95**, 549–601 (2015).

314. Whitmire, R. E. *et al.* Self-assembling nanoparticles for intra-articular delivery of anti-inflammatory proteins. *Biomaterials* **33**, 7665–7675 (2012).

315. Pradal, J. *et al.* Effect of particle size on the biodistribution of nano- and microparticles following intra-articular injection in mice. *Int. J. Pharm.* **498**, 119–129 (2016).

316. Kim, S. R. *et al.* Cationic PLGA/Eudragit RL nanoparticles for increasing retention time in synovial cavity after intra-articular injection in knee joint. *Int. J. Nanomedicine* **10**, 5263–5271 (2015).

317. Bard, D., King, B. & Dingle, J. T. Clearance of proteoglycan from joint cavities. *Ann. Rheum. Dis.* **46**, 934–937 (1987).

318. Simkin, P. A. Assessing biomarkers in synovial fluid: Consider the kinetics of clearance. *Osteoarthr. Cartil.* **21**, 7–9 (2013).

319. Simkin, P. A. The human knee: A window on the microvasculature. *Tissue Barriers* **3**, e970465 (2015).

320. Bowman, S., Awad, M. E., Hamrick, M. W., Hunter, M. & Fulzele, S. Recent advances in hyaluronic acid based therapy for osteoarthritis. *Clin. Transl. Med.* **7**, 1–11 (2018).

321. Gupta, R. C., Lall, R., Srivastava, A. & Sinha, A. Hyaluronic acid: Molecular mechanisms and therapeutic trajectory. *Front. Vet. Sci.* **6**, 1–24 (2019).

322. Milasan, A., Ledoux, J. & Martel, C. Lymphatic network in atherosclerosis: the underestimated path. *Futur. Sci. OA* **1**, FSO61 (2015).

323. Levick, J. R. & McDonald, J. N. Viscous and osmotically mediated changes in fluid movement across synovium in response to intraarticular albumin. *Microvasc. Res.* **47**, 68–89 (1994).

324. Levick, J. R., McDonald, J. N. & Knight, A. D. Asymmetrical effects of albumin on transsynovial fluid movement. *Semin. Arthritis Rheum.* **21**, 184–190 (1991).

325. Levick, J. R. An analysis of the interaction between interstitial plasma protein, interstitial flow, and fenestral filtration and its application to synovium. *Microvasc. Res.* **47**, 90–125 (1994).

326. Iijima, H. *et al.* Effects of short-term gentle treadmill walking on subchondral bone in a rat model of instability-induced osteoarthritis. *Osteoarthr. Cartil.* **23**, 1563–1574 (2015).

327. Influence of Exercise on the Distribution of. (2011).

328. Simkin, P. A. & Benedict, R. S. Hydrostatic and oncotic determinants of microvascular fluid balance in normal canine joints. *Arthritis Rheum.* **33**, 80–86 (1990).

329. Wood, L., Ferrell, W. R. & Baxendale, R. H. Pressures in Normal and Acutely Distended Human Knee Joints and Effects on Quadriceps Maximal Voluntary Contractions. *Q. J. Exp. Physiol.* **73**, 305–314 (1988).

330. Knight, A. D. & Levick, J. R. Effect of fluid pressure on the hydraulic conductance of interstitium and fenestrated endothelium in the rabbit knee. *J. Physiol.* **360**,

311–332 (1985).

331. Goddard, N. J. & Gosling, P. T. Intra-articular fluid pressure and pain in osteoarthritis of the hip. *J. Bone Jt. Surg. - Ser. B* **70**, 52–55 (1988).

332. Hwang, J. *et al.* Increased hydraulic conductance of human articular cartilage and subchondral bone plate with progression of osteoarthritis. *Arthritis Rheum.* **58**, 3831–3842 (2008).

333. Mapp, P. I. *et al.* Angiogenesis in two animal models of osteoarthritis. *Osteoarthr. Cartil.* **16**, 61–69 (2008).

334. Armstrong, J. K., Wenby, R. B., Meiselman, H. J. & Fisher, T. C. The hydrodynamic radii of macromolecules and their effect on red blood cell aggregation. *Biophys. J.* **87**, 4259–70 (2004).

335. Alitalo, K. The lymphatic vasculature in disease. *Nat. Med.* **17**, 1371–1380 (2011).

336. Reimann, I., Vittas, D., Nielsen, S. L. & Svalastoga, E. Lymphatic transport from normal and synovitic knees in rabbits. *Acta Orthop.* **60**, 185–187 (1989).

337. Wilkinson, L. S. & Edwards, J. C. W. Demonstration of lymphatics in human synovial tissue. *Rheumatol. Int.* **11**, 151–155 (1991).

338. Blewis, M. E., Nugent-Derfus, G. E., Schmidt, T. A., Schumacher, B. L. & Sah, R. L. A model of synovial fluid lubricant composition in normal and injured joints. *Eur. Cells Mater.* **13**, 26–38 (2007).

339. Levick, J. R. & McDonald, J. N. Fluid movement across synovium in healthy joints: Role of synovial fluid macromolecules. *Ann. Rheum. Dis.* **54**, 417–423 (1995).

340. Luisa Calich, A. G., Domiciano, D. S. & Fuller, R. Osteoarthritis: Can anti-cytokine therapy play a role in treatment? *Clin. Rheumatol.* **29**, 451–455 (2010).

341. Wojdasiewicz, P., Poniatowski, Ł. A. & Szukiewicz, D. The role of inflammatory

and anti-inflammatory cytokines in the pathogenesis of osteoarthritis. *Mediators Inflamm.* **2014**, 1–19 (2014).

342. Grissom, M. J. *et al.* Synovial fluid lubricant properties are transiently deficient after arthroscopic articular cartilage defect repair with platelet-enriched fibrin alone and with mesenchymal stem cells. *Orthop. J. Sport. Med.* **2**, 1–10 (2014).

343. Mora, J. C., Przkora, R. & Cruz-Almeida, Y. Knee osteoarthritis: Pathophysiology and current treatment modalities. *J. Pain Res.* **11**, 2189–2196 (2018).

344. Farahat, M. N., Yanni, G., Poston, R. & Panayi, G. S. Cytokine expression in synovial membranes of patients with rheumatoid arthritis and osteoarthritis. *Ann. Rheum. Dis.* **52**, 870–875 (1993).

345. Melchiorri, C. *et al.* Enhanced and coordinated in vivo expression of inflammatory cytokines and nitric oxide synthase by chondrocytes from patients with osteoarthritis. *Arthritis Rheum.* **41**, 2165–2174 (1998).

346. Massicotte, F. *et al.* Can altered production of interleukin-1β, interleukin-6, transforming growth factor-β and prostaglandin E2 by isolated human subchondral osteoblasts identity two subgroups of osteoarthritic patients. *Osteoarthr. Cartil.* **10**, 491–500 (2002).

347. Nagao, M. *et al.* Vascular endothelial growth factor in cartilage development and osteoarthritis. *Sci. Rep.* **7**, 1–16 (2017).

348. Hamilton, J. L. *et al.* Targeting VEGF and its receptors for the treatment of osteoarthritis and associated pain. *Journal of Bone and Mineral Research* **31**, 911–924 (2016).

349. Zolla, V. *et al.* Aging-related anatomical and biochemical changes in lymphatic collectors impair lymph transport, fluid homeostasis, and pathogen clearance. *Aging Cell* **14**, 582–594 (2015).

350. Kushner, I. & Somerville, J. A. Permeability of human synovial membrane to plasma proteins. Relationship to molecular size and inflammation. *Arthritis Rheum.* **14**, 560–570 (1971).

351. Pasquali-Ronchetti, I. *et al.* Aging of the human synovium: An in vivo and ex vivo morphological study. *Semin. Arthritis Rheum.* **21**, 400–414 (1992).

352. Qin, T.-T. *et al.* Tumour necrosis factor superfamily member 15 (Tnfsf15) facilitates lymphangiogenesis via up-regulation of *Vegfr3* gene expression in lymphatic endothelial cells. *J. Pathol.* **237**, 307–318 (2015).

353. Kassis, T., Skelton, H. M., Lu, I. M., Moorhead, A. R. & Dixon, J. B. An Integrated In Vitro Imaging Platform for Characterizing Filarial Parasite Behavior within a Multicellular Microenvironment. *PLoS Negl. Trop. Dis.* **8**, (2014).

354. Gibot, L. *et al.* Tissue-engineered 3D human lymphatic microvascular network for in vitro studies of lymphangiogenesis. *Nat. Protoc.* **12**, 1077–1088 (2017).

355. Phelps, E. a., Headen, D. M., Taylor, W. R., Thulé, P. M. & García, A. J. Vasculogenic bio-synthetic hydrogel for enhancement of pancreatic islet engraftment and function in type 1 diabetes. *Biomaterials* **34**, 4602–4611 (2013).

356. Phelps, E. a., Templeman, K. L., Thul??, P. M. & Garc??a, A. J. Engineered VEGF-releasing PEG???MAL hydrogel for pancreatic islet vascularization. *Drug Deliv. Transl. Res.* **5**, 125–136 (2015).

357. Phelps, E. A. *et al.* Maleimide cross-linked bioactive PEG hydrogel exhibits improved reaction kinetics and cross-linking for cell encapsulation and in situ delivery. *Adv. Mater.* **24**, 64–70 (2012).

358. Yamamura, N., Sudo, R., Ikeda, M. & Tanishita, K. Effects of the mechanical properties of collagen gel on the in vitro formation of microvessel networks by endothelial cells. *Tissue Eng.* **13**, 1443–1453 (2007).

359. WU, C.-C., Ding, S.-J., Wang, Y.-H., Tang, M.-J. & Chang, H.-C. Mechanical properties of collagen gels derived from rats of different ages. *J. Biomater. Sci. Polym. Ed.* **16**, 1261–1275 (2005).

360. Dong, Y. *et al.* Motif mimetic of epsin perturbs tumor growth and metastasis. *J. Clin. Invest.* **125**, 4349–4364 (2015).

361. Song, K. *et al.* Endothelial epsins as regulators and potential therapeutic targets of tumor angiogenesis. *Cell. Mol. Life Sci.* **74**, 393–398 (2017).

362. Pasula, S. *et al.* Endothelial epsin deficiency decreases tumor growth by enhancing VEGF signaling. *J. Clin. Invest.* **122**, 4424–4438 (2012).

363. Nepiyushchikh, Z. V. *et al.* Differential effects of myosin light chain kinase inhibition on contractility, force development and myosin light chain 20 phosphorylation of rat cervical and thoracic duct lymphatics. *J. Physiol.* **589**, 5415–5429 (2011).

364. Scallan, J. P. & Davis, M. J. Genetic removal of basal nitric oxide enhances contractile activity in isolated murine collecting lymphatic vessels. *J. Physiol.* **591**, 2139–2156 (2013).

365. Zhang, Y. *et al.* Heterogeneity in VEGFR3 levels drives lymphatic vessel hyperplasia through cell-autonomous and non-cell-autonomous mechanisms. *Nat. Commun.* **9**, (2018).

366. Wallis, W. J., Simkin, P. a & Nelp, W. B. Protein traffic in human synovial effusions. *Arthritis Rheum.* **30**, 57–63 (1987).

367. Partain, B. D., Unni, M., Rinaldi, C. & Allen, K. D. The clearance and biodistribution of magnetic composite nanoparticles in healthy and osteoarthritic rat knees. *J. Control. Release* **321**, 259–271 (2020).

368. Mwangi, T. K. *et al.* Intra-articular clearance of labeled dextrans from naive and arthritic rat knee joints. *J. Control. Release* **283**, 76–83 (2018).

369. Han, H. *et al.* Fang-Ji-Huang-Qi-Tang attenuates degeneration of early-stage KOA mice related to promoting joint lymphatic drainage function. *Evidence-Based Complement. Altern. Med.* **2020**, 1–10 (2020).

370. Watari, K. *et al.* Tumor-derived interleukin-1 promotes lymphangiogenesis and lymph node metastasis through M2-type macrophages. *PLoS One* **9**, 1–15 (2014).

371. Zawieja, S. D., Castorena-Gonzalez, J. A., Dixon, B. & Davis, M. J. Experimental

models used to assess lymphatic contractile function. *Lymphat. Res. Biol.* **15**, 331–342 (2017).

372. Saetan, N. *et al.* Association of plasma and synovial fluid interferon-γ inducible protein-10 with radiographic severity in knee osteoarthritis. *Clin. Biochem.* **44**, 1218–1222 (2011).

373. Seabrook, T. J., Borron, P. J., Dudler, L., Hay, J. B. & Young, A. J. A novel mechanism of immune regulation: Interferon-γ regulates retention of CD4 + T cells during delayed type hypersensitivity. *Immunology* **116**, 184–192 (2005).

374. Shi, J., Li, Y. J., Yan, B. & Wei, P. K. Interleukin-8: A potent promoter of human lymphatic endothelial cell growth in gastric cancer. *Oncol. Rep.* **33**, 2703–2710 (2015).

375. Choi, I. *et al.* Interleukin-8 reduces post-surgical lymphedema formation by promoting lymphatic vessel regeneration. *Angiogenesis* **16**, 29–44 (2013).

376. Van Roon, J. A. & Lafeber, F. P. Role of interleukin-7 in degenerative and inflammatory joint diseases. *Arthritis Res. Ther.* **10**, 1–2 (2008).

377. Zhang, H. X., Wang, Y. G., Lu, S. Y., Lu, X. X. & Liu, J. Identification of IL-7 as a candidate disease mediator in osteoarthritis in Chinese Han population: A case-control study. *Rheumatology* **55**, 1681–1685 (2016).

378. Van Roon, J. A. G., Glaudemans, K. A. F. M., Bijilsma, J. W. J. & Lafeber, F. P. J. G. Interleukin 7 stimulates tumour necrosis factor α and Th 1 cytokine production in joints of patients with rheumatoid arthritis. *Ann. Rheum. Dis.* **62**, 113–119 (2003).

379. Ponchel, F. *et al.* Interleukin-7 deficiency in rheumatoid arthritis: Consequences for therapy-induced lymphopenia. *Arthritis Res. Ther.* **7**, R80–R92 (2005).

380. Combe, B. *et al.* Interleukin-2 in rheumatoid arthritis: production of and response to interleukin-2 in rheumatoid synovial fluid, synovial tissue and peripheral blood. *Clin. Exp. Immunol.* **59**, 528 (1985).

381. Warner, S. C. *et al.* IL-15 and IL15RA in osteoarthritis: Association with symptoms and protease production, but not structural severity. *Front. Immunol.* **11**, 1–10 (2020).

382. Owen, D. L. *et al.* Identification of cellular sources of IL-2 needed for regulatory T cell development and homeostasis. *J. Immunol.* **200**, 3926–3933 (2018).

383. Lodolce, J. P. *et al.* IL-15 receptor maintains lymphoid homeostasis by supporting lymphocyte homing and proliferation. *Immunity* **9**, 669–676 (1998).

384. Miller, N. E. *et al.* Secretion of adipokines by human adipose tissue in vivo: Partitioning between capillary and lymphatic transport. *Am. J. Physiol. - Endocrinol. Metab.* **301**, E659–E667 (2011).

385. Hos, D. *et al.* IL-10 Indirectly Regulates Corneal Lymphangiogenesis and Resolution of Inflammation via Macrophages. *Am. J. Pathol.* **186**, 159–171 (2016).

386. Srinivasan, R. S. *et al.* The Prox1–Vegfr3 feedback loop maintains the identity and the number of lymphatic endothelial cell progenitors. *Genes Dev.* **28**, 2175–2187 (2014).

387. Mäkinen, T., Norrmén, C. & Petrova, T. V. Molecular mechanisms of lymphatic vascular development. *Cell. Mol. Life Sci.* **64**, 1915–1929 (2007).

388. Bouta, E. M. *et al.* The role of the lymphatic system in inflammatory-erosive arthritis. *Semin. Cell Dev. Biol.* **38**, 90–97 (2015).

389. Yoshida, H., Fujita, S., Nishida, M. & Iizuka, T. Immunohistochemical distribution of lymph capillaries and blood capillaries in the synovial membrane in cases of internal derangement of the temporomandibular joint. *J. Oral Pathol. Med.* **26**, 356–361 (1997).

390. Myers, S. L., Brandt, K. D. & Eilam, O. Even low-grade synovitis significantly accelerates the clearance of protein from the canine knee. Implications for measurement of synovial fluid 'markers' of osteoarthritis. *Arthritis Rheum.* **38**, 1085–91 (1995).

391. Hong, G. *et al.* Through-skull fluorescence imaging of the brain in a new near-infrared window. *Nat. Photonics* **8**, 723–730 (2014).

392. Brown, S. B. *et al.* Characterization of Post-Traumatic Osteoarthritis in Rats Following Anterior Cruciate Ligament Rupture by Non-Invasive Knee Injury (NIKI). *J. Orthop. Res.* **38**, 356–367 (2020).

393. Mukherjee, A., Hooks, J., Nepiyushchikh, Z. & Dixon, J. B. Entrainment of Lymphatic Contraction to Oscillatory Flow. *Sci. Rep.* **9**, 1–14 (2019).